



**Dottorato di Ricerca in Ingegneria Civile ed Edile/Architettura**

Graduate School in Civil and Architectural Engineering

DICAr – Dipartimento di Ingegneria Civile ed Architettura

Facoltà di Ingegneria, Università degli Studi di Pavia

Faculty of Engineering, University of Pavia

XXIX cycle – XV new series

# Numerical model for framed structures with thin-walled cross-section members

PhD thesis

Giammaria Gabbianelli

Advisor

Prof. Armando Gobetti

Revisor

Prof.ssa Lucia Faravelli

December 2016



Dottorato di Ricerca in Ingegneria Civile ed Edile/Architettura  
*Graduate School in Civil and Architectural Engineering*

XXIX Ciclo/*Cycle* (XV Nuova Serie/*New Series*)

Settore: <i>Field:</i>	Ingegneria <i>Engineering</i>
Sede Amministrativa non consortile: <i>Administrative location:</i>	Università degli Studi di Pavia <i>University of Pavia</i>
Durata: <i>Duration:</i>	3 anni <i>3 years</i>
Periodo formativo estero: <i>Period in foreign organizations:</i>	come previsto dal regolamento del dottorato di ricerca <i>as required by the School rules</i>
Numero minimo di corsi: <i>Minimum number of courses:</i>	6 corsi <i>6 courses</i>

## Recapiti/*Contact numbers and address*



via Ferrata 3 - 27100 Pavia - Italy

Tel. 0382/985450-51 Fax 0382/528422

## Coordinatore/*Coordinator*

CASCIATI Fabio

Professore Ordinario (ICAR/08)

Dipartimento di Ingegneria Civile e Architettura

via Ferrata 3 - 27100 Pavia - Italia Tel. 0382/985787

e-mail: [fabio.casciati@unipv.it](mailto:fabio.casciati@unipv.it)

## Collegio dei docenti/*Scientific Board*

BERIZZI Carlo	Ricercatore (ICAR/14)
CASCIATI Fabio	Professore Ordinario (ICAR/08)
CASELLA Vittorio	Professore Associato (ICAR/06)
CINQUINI Carlo	Professore Ordinario (ICAR/08)
CIAPONI Carlo	Professore Ordinario (ICAR/02)
COLLIVIGNARELLI Maria Cristina	Ricercatore (ICAR/03)
DE LOTTO Roberto	Professore Associato (ICAR/20)
DEL GROSSO Andrea Enrico	Professore (ICAR/09) in quiescenza dal 01/11/2015
FARAVELLI Lucia	Professore Ordinario (ICAR/08)
GALLATI Mario	Professore (ICAR/01) in quiescenza dal 01/11/2015
GHILARDI Paolo	Professore Associato (ICAR/01)
GOBETTI Armando	Professore Associato (ICAR/08)
GRECO Alessandro	Professore Associato (ICAR/10)
MAGRINI Anna	Professore Ordinario (ING-IND/11)
MARCELLINI Alberto	Dirigente CNR Milano in quiescenza dal 01/11/2014
MOISELLO Ugo	Professore (ICAR/02) in quiescenza dal 01/11/2015

MORANDOTTI Marco

Professore Associato (ICAR/10)

PAPIRI Sergio

Professore Associato (ICAR/02)

SALA Roberto

Professore (ING-IND/08)

in quiescenza dal 01/11/2014

## Organizzazione del corso

Il dottorato di ricerca in *Ingegneria Civile ed Edile/Architettura* presso la Facoltà di Ingegneria dell'Università degli Studi di Pavia è stato istituito nell'anno accademico 2010/11 (XXVI ciclo; XII ciclo Nuova Serie).

L'obiettivo formativo peculiare del dottorato è addestrare giovani laureati allo svolgimento di attività di ricerca e viene perseguito nell'ambito dei settori disciplinari di Ingegneria Civile ed Architettura (ICAR), senza tralasciare alcune interdisciplinarietà, in via di consolidamento, con discipline strumentali o complementari. Il corso consente al dottorando di scegliere tra sei distinti curricula: compositivo, idraulico, sanitario, sismico, strutturale e tecnologico.

In particolare, le tematiche di ricerca sono quelle che caratterizzano i raggruppamenti disciplinari ICAR/01, ICAR/02, ICAR/03, ICAR/06, ICAR/08, ICAR/09, ICAR/10, ICAR/14, ICAR/18, ICAR/20, tutte di pertinenza dell'ingegneria civile e architettura. A questi si aggiungono ING-IND/11 (fisica tecnica ambientale) e ING-IND/08 (macchine a fluido).

L'attività di ricerca si svolge soprattutto presso il Dipartimento di Ingegneria Civile e Architettura (DICAr) dell'Università degli Studi di Pavia.

Durante i primi due anni sono previsti almeno sei corsi, seguiti da prove finali che il dottorando è tenuto a sostenere.

Il Collegio dei Docenti organizza i corsi con lo scopo di fornire allo studente di dottorato opportunità di approfondimento su alcune delle discipline di base per i settori componenti, ingegneria idraulica, strutturale ed edile/architettura. Corsi e seminari vengono tenuti da docenti di università nazionali ed estere.

Alla fine di ogni anno i dottorandi devono presentare una relazione sull'attività svolta. Al termine del primo anno viene richiesta una presentazione orale, al contrario al termine del secondo anno il dottorando è tenuto a scrivere una tesina su un argomento pertinente alla propria ricerca di dottorato.

Sulla base di tali relazioni il Collegio dei Docenti, previa valutazione dell'assiduità e dell'operosità dimostrata dall'iscritto, può proporre al Rettore l'esclusione del candidato dal corso o non approvarne il passaggio all'anno successivo.

Il dottorando può svolgere attività di ricerca di tipo teorico, numerico e sperimentale, grazie ai laboratori di cui il Dipartimento dispone.

## *Course Organization*

*The Graduate School in Civil and Architectural Engineering at the School of Engineering of the University of Pavia, was established in the academic year 2010/2011 (XXVI cycle, XII new series cycle). Its peculiar educational aim is to train young graduates to conduct research activities and it is pursued by the disciplinary fields of Civil Engineering and Architecture (ICAR), without omitting some interdisciplinary, which are consolidating, with supporting or complementary disciplines. The course allows the PhD student to choose between six different curricula: composition, hydraulic, sanitary, seismic, structural and technological.*

*The research themes are chosen from the disciplinary areas ICAR/01, ICAR/02, ICAR/03, ICAR/06, ICAR/08, ICAR/09, ICAR/10, ICAR/14, ICAR/18, ICAR/20 belonging to civil engineering and architecture. In addition, there are ING-IND/11 (environmental technical physics) and ING-IND/08 (fluid machines).*

*The research activity takes place mainly at the Department of Civil Engineering and Architecture (DICAr) of the University of Pavia. During the first two years, at least 6 courses are required, followed by final examination that the PhD student has to take. The Teaching Staff organizes courses with the aim of providing the PhD student the opportunity to deepen some basic disciplines in the components fields, such as hydraulic engineering, structural, and building engineering and architecture. Courses and seminars are held by professor of national and foreign universities.*

*At the end of each year, the PhD students have to present an activity report. At the end of the first year, an oral presentation is requested, at the end of the second year the PhD student is required to write a term paper about a topic connected to the doctoral research. On the basis of these reports, the Teaching Staff, after the evaluation of the demonstrated regularity and hard work of the PhD student, may propose to the Rector the exclusion of the candidate from the course or not to approve to the next year. The PhD student can carry out research activities both theoretical and experimental, thanks to the laboratories owned by the Department.*

## Elenco delle tesi/*Theses List*

1. Valentina Giacometti (XXVI Ciclo, XII Ciclo Nuova Serie), Cultura dell'accessibilità e Accessibilità della Cultura: uno strumento di valutazione per l'edilizia universitaria storica, relatore: Prof. A. Greco, ottobre 2013.
2. Enrico Murari (XXVI Ciclo, XII Ciclo Nuova Serie), Adattamento dei sistemi idropotabili a scenari di carenza idrica, relatore: Prof. C. Ciaponi, ottobre 2013.
3. Emanuele Zamperini (XXVI Ciclo, XII Ciclo Nuova Serie), Evoluzione tecnologica e tipologica delle coperture lignee in Italia nel periodo 1800-1950, relatore: Prof. M. Morandotti, ottobre 2013.
4. Cecilia Morelli di Popolo (XXVI Ciclo, XII Ciclo Nuova Serie), La città flessibile. Le dimensioni della flessibilità nella città contemporanea e futura, relatore: Prof. R. De Lotto, aprile 2014.
5. Umut Yıldırım (XXVI Ciclo, XII Ciclo Nuova Serie), System identification towards diagnosis to prognosis, relatore: Prof. F. Casciati, aprile 2014.
6. Daniele Bortoluzzi (XXVII Ciclo, XIII Ciclo Nuova Serie), Control systems for the mitigation of footbridge vibrations, relatore: Prof. L. Faravelli, ottobre 2014.
7. Federico Castagnola (XXVII Ciclo, XIII Ciclo Nuova Serie), Applicazione di una tecnologia MBR termofila funzionante in condizioni aerate/non aerate per la minimizzazione di fanghi di depurazione civili ed industriali, relatore: Prof. M.C. Collivignarelli, ottobre 2014.
8. Valentina Cinieri (XXVII Ciclo, XIII Ciclo Nuova Serie), Patrimonio edificato diffuso. Un approccio sostenibile alla conservazione e alla gestione, relatori: Proff. M. Morandotti, D. Besana, ottobre 2014.
9. Kan Liu (XXVII Ciclo, XIII Ciclo Nuova Serie), Cultural transfer and architecture. Foreign architectural practice in Shanghai after 1949, relatore: Prof. Z. Shiling, ottobre 2014.
10. Edoardo Gino Macchi (XXVII Ciclo, XIII Ciclo Nuova Serie), Experimental and numerical studies on RF ablation: advances on physical understanding and efficiency, relatore: Prof. M. Gallati, ottobre 2014
11. Daniele Molognoni (XXVII Ciclo, XIII Ciclo Nuova Serie), Microbial Fuel Cells Application to Wastewater Treatment: laboratory experience and controlling strategies, relatore: Prof. A. Capodaglio, ottobre 2014.

12. Marco Sordi (XXVII Ciclo, XIII Ciclo Nuova Serie), Applicazione di un sistema MBR termofilo aerobico per il trattamento di rifiuti liquidi ad elevata concentrazione di COD, tensioattivi, solventi e cloruri, relatore: Prof. M.C. Collivignarelli, ottobre 2014.
13. Andrea Fenocchi (XXVII Ciclo, XIII Ciclo Nuova Serie), Circulation dynamics in a shallow fluvial lake - The case of the Superior Lake of Mantua, relatore: Prof. S. Sibilla, giugno 2015.
14. Nawal Benabdelkader (XXVII Ciclo, XIII Ciclo Nuova Serie), The restoration and enhancement. The historical site of Mansourah - Tlemcen, relatore: Prof. M. Morandotti, ottobre 2015.
15. Giovanni Anselmo (XXVIII Ciclo, XIV Ciclo Nuova Serie), Effetti idrologici e idraulici dell'urbanizzazione e possibili interventi di mitigazione, relatori: Proff. S. Papiri e G. Barbero, ottobre 2015.
16. Lorenzo Elia (XXVIII Ciclo, XIV Ciclo Nuova Serie), Metaheuristic optimization tools for structural monitoring, relatore: Prof. L. Faravelli, ottobre 2015.
17. Emanuele Giorgi (XXVIII Ciclo, XIV Ciclo Nuova Serie), Man and environment: looking for the future, relatori: Proff. Z. Shiling e F. Casciati, ottobre 2015.
18. Elena Romano (XXVIII Ciclo, XIV Ciclo Nuova Serie), Uno strumento per il miglioramento prestazionale dell'edilizia esistente: il caso delle residenze universitarie, relatore: Prof. A. Greco, ottobre 2015.
19. Babak Jafarzad Eslami (XXVIII Ciclo, XIV Ciclo Nuova Serie), Impiego di smorzatori sismici nella protezione dei beni architettonici, relatore: Prof. E.A. Del Grosso, aprile 2016.
20. Michele Vece (XXIX Ciclo, XV Ciclo Nuova Serie) Shifting from a standard protocol of communication to an emergency protocol in the monitoring of large infrastructural systems, relatore: Prof. F. Casciati, dicembre 2016.
21. Giammaria Gabbianelli (XXIX Ciclo, XV Ciclo Nuova Serie) Numerical model for framed structures with thin-walled cross-section members, relatore: Prof. A. Gobetti, dicembre 2016.
22. Matteo Locatelli (XXIX Ciclo, XV Ciclo Nuova Serie) Strumento per la valutazione e definizione di strategie per il miglioramento dell'edilizia scolastica esistente. Il tema della scuola primaria e secondaria, relatore: Prof. A. Greco, dicembre 2016.

23. Rosamaria Olivadese (XXIX Ciclo, XV Ciclo Nuova Serie) Il riuso degli edifici esistenti a scopo residenziale in Italia: nuovi standard per l'innovazione dei modelli abitativi, relatore: Prof. C. Berizzi, dicembre 2016.
24. Elisabetta Maria Venco (XXIX Ciclo, XV Ciclo Nuova Serie) La pianificazione preventiva per la riduzione del rischio: definizione di scenari preventivi nel contesto della città flessibile e resiliente, relatore: Prof. R. De Lotto, dicembre 2016.
25. Francesca Maria Torchia (XXIX Ciclo, XV Ciclo Nuova Serie) Materiali da riciclo e da scarto innovativi per l'edilizia: caratterizzazione acustica, termica ed analisi del ciclo di vita, relatore: Prof. P. Ricciardi, dicembre 2016.
26. Laura Menoni (XXIX Ciclo, XV Ciclo Nuova Serie) Sviluppo di "smart control strategies" per l'automazione di processo negli impianti a fanghi attivi, relatore: Prof. G. Bertanza, dicembre 2016.



## Abstract

The aim of this thesis is to develop an adequate tool for the analysis of beam elements with thin-walled open cross-sections. Although the topic has been exhaustively investigated through the years by different authors, for the moment there are not suitable commercial software able to predict the behavior of such elements. In the last decades, the use of thin-walled steel members is significantly increased, in particular in the field of logistic, where goods and products are stored in pallet racks. These structures are generally composed by uprights which have mono-symmetric lipped channel cross-sections. Hence, a suitable finite element software should be characterized by seven degree of freedom per node. Indeed, only the presence of the seventh degree of freedom makes possible to correctly estimate both displacements and internal stresses, including warping displacements and bimoment stresses. Furthermore, this formulation is able to correctly predict the flexural-torsional and lateral-torsional buckling, derived by the coupling between flexure and torsion.

The previously mentioned effects are neglected in the routine rack design, mainly because no useful indications can be found in literature on this topic. Because of that, a research project in conjunction between the Politecnico di Milano and the University of Pavia has been established with the aim of improving the design rules for those types of structures.

After an introduction to the racks in the first chapter, the second shows the matrices developed. Similar formulations have been presented in the past. One of these introduces the seventh degree of freedom, but neglects the eccentricity of the shear center from the centroid and, as a consequence, does not consider all the Wagner coefficients, limiting the formulation to bi-symmetric cross-sections. The second one is more general and it is usable for non-symmetric cross-sections, but it does not take into account the reduction of the axial stiffness, as effect of the second-order.

Considering all the previous features, an academic open-source software has been modified. The new software has been called *Śiva* (System of Incremental and Vibration Analysis) and allows to perform several types of analyses.

An exhaustive validation, dealt in the Appendix A, permits to consider adequate the software.

As the first phase of research has been successfully completed, attention is herein focused on the study of the behavior of the steel storage pallet racks. Different scientific articles have been produced. At the beginning the static design and the member stability have been considered. Consequently, the use of simplified approaches for the structural analysis has been evaluated. Then the beam design of non-symmetric cross-section has been investigated and currently attention is paid on the procedures adopted for seismic design.



## Table of Contents

Chapter 1	Introduction to the steel storage pallet racks.....	1
1.1	Steel rack structures .....	1
1.1.1	Types of rack structures.....	1
1.1.2	Structural typology .....	6
1.2	Design approaches according to the codes.....	11
1.2.1	Design for monotonic loads: introduction to EN15512.....	12
1.2.2	Design for seismic loads: introduction to EN16681 .....	15
1.3	General aspects .....	18
Chapter 2	Buckling and geometric nonlinear analysis .....	23
2.1	Kinematics for thin-walled beam .....	24
2.2	Equilibrium and constitutive equations.....	27
2.3	Finite element beam formulation .....	30
2.3.1	Elastic stiffness matrices.....	33
2.3.2	Geometric stiffness matrix.....	36
Chapter 3	Warping influence in steel storage pallet racks .....	41
3.1	Design rules for rack uprights .....	43
3.2	The considered rack frames .....	45
3.3	Warping influence: internal forces and moments.....	50
3.4	Warping influence: global resistance checks .....	54
3.5	Warping influence: local resistance checks .....	56
Chapter 4	Beam design of non-symmetric cross-section .....	61
4.1	Introduction.....	61
4.2	Design rules for pallet beams in storage systems .....	64
4.3	Lipped channel members .....	66
4.3.1	Serviceability limit state .....	67
4.3.2	Ultimate limit state .....	70
4.3.3	Load carrying capacity .....	75

4.4	Zed profiles .....	76
4.4.1	Serviceability limit state .....	77
4.4.2	Ultimate limit state .....	77
4.4.3	Load carrying capacity .....	81
Chapter 5	Experimental pushover analysis on shelving racks.....	83
5.1	Introduction.....	83
5.2	Components tests .....	85
5.2.1	Upright tests.....	86
5.2.2	Tests on connections.....	91
5.3	Full scale tests .....	98
5.4	Pushover tests.....	100
5.5	Numerical simulations with Síva software.....	106
Chapter 6	Conclusion .....	113
Chapter 7	References .....	115
A.	Appendix – Tests and Validations .....	121
A.1	Static analysis.....	122
A.2	Buckling analysis .....	127

# **Chapter 1 Introduction to the steel storage pallet racks**

## **1.1 Steel rack structures**

The process of moving manufactured goods from the producer to the consumer involves the need for storage somewhere along the line. Within companies, a tremendous volume of material is being stored in this process and the cost of such storage is by no means a negligible part of the total cost for the consumer. There is therefore considerable need for improvement in storage techniques, in handling efficiency for increasing mechanization and increasing storage density.

These requirements can be met only by a highly engineered development of industrial storage rack facilities.

The requirements for a storage system vary widely with the nature of the storage situation. However, a general criterion is the ability to store as much material as possible in a given limited volume.

While providing sufficient and convenient access for efficient moving of the goods, warehouses are most commonly used for storing a multitude of different kinds of goods, and the storage system must be versatile and adjustable. In addition, once again because of changing needs over the years, it is often desirable to have installations able to be readily demountable and capable of reassembly.

Because of its versatility in providing solutions to these problems, the cold-formed steel construction, is by far the most common type of construction for storage systems. Because of the special nature of storage structures, their design presents many problems and the solutions often require advanced analysis methods. Such methods will be used extensively in this master thesis for the purposes of undertaking a high-profile comparative analysis that will be the core subject of this academic work.

### *1.1.1 Types of rack structures*

#### **1.1.1.1 Classical rack structures**

A review of different types of racks provides an idea of the large variety of possible structures and their specificities. In general, pallet racks are used for relatively low density storage or in situations where all the goods must be accessible at all times. The vertical

## Chapter 1

load carrying elements consist of "upright frames." An upright frame, in terms of the rack industry, is an assembly of two posts truss-braced against each other. The posts are in general cold-rolled lipped channel sections. The upright frames support the horizontal "shelf beams" which are perpendicular to the planes of the upright frames. The goods are usually stored on wooden or metal pallets which are placed by forklift trucks on the shelf beams.

Horizontal stability in the direction of the shelf beams is provided either by rigid or semi-rigid joint frame action of the shelf beams and posts, or by x-bracing in the rear plane. Quite often two rows of pallet racks are tied back-to-back, thus resulting in a structure that is more stable against overturning and also provides a higher density storage system. An example of a pallet rack can be seen on Figure 1-1.



**Figure 1-1. Steel storage pallet racks.**

### 1.1.1.2 Drive-in and drive-thru pallet racks

Drive-in racks:

When high density storage is required and access to all the goods at all times is not needed, the Drive-in rack system may be used as shown in Figure 1-2. Usually, the upright frames are connected at the top, thus forming a series of portal frames. At appropriate elevations, as the storage situation requires, arms are connected to the posts. These arms, in turn, support the horizontal rail beams which are parallel to the planes of the upright frames. Pallets are placed on the rail beams, again by fork-lift trucks. Thus, rows of uprights provide rows of storage spaces and several pallets can be stored in each row. In

these types of rack systems, the plane of the innermost posts has truss- or x-bracing perpendicular to the planes of the upright frames. The maximum height of the rack is determined by the vertical reach of the fork-lift truck.

Drive-thru racks:

This type is similar to drive-in racks with the exception that the bracing of the innermost posts is omitted as illustrated on Figure 1-2. This provides access to the stored goods from both ends of all storage rows. Drive-thru racks, when not connected to an external support, behave as portal frames. In contrast, drive-in racks rely for horizontal stability in part on the same portal frame action, but also on the previously described braced plane and the rail beam assemblies cantilevering out from that plane.

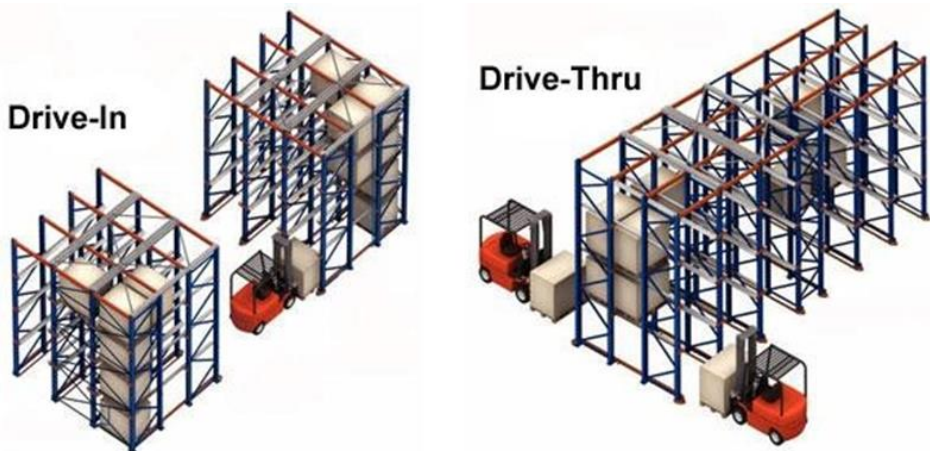
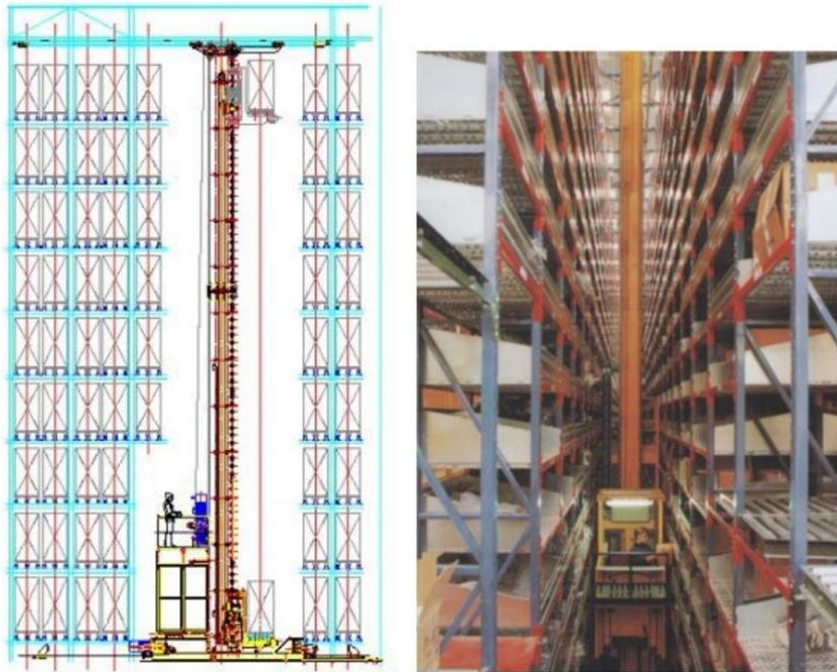


Figure 1-2. Drive-in and drive-thru racks.

#### 1.1.1.3 Stacker racks and high braced pallet racks

When storage requires a rack system higher than those discussed above, a stacker rack or a high braced pallet rack may be used. The stacker rack is basically a one-deep high rise drive-in rack. The pallets are placed on the rail beams by means of a stacker crane whose operation is often highly automated. High braced pallet racks are a high rise version of simple pallet racks with additional bracing for horizontal stability. An example of a high braced pallet racks is illustrated in Figure 1-3. These structures provide a very high storage capacity with the possibility of obtaining a high level of automatization for the loading and unloading of goods. With all the benefits that derive from having such types of pallet rack structures, there are also a lot of challenges concerning their design and maintenance. They require cutting edge specialized knowledge and considerable amount of time to understand the main issues that must be considered when it comes to designing them against seismic actions.



**Figure 1-3. High braced pallet racks.**

1.1.1.4 Cantilever racks

An example of a cantilever rack can be seen on Figure 1-4 and Figure 1-5. No discussion on such types of racks shall be provided.



**Figure 1-4. Cantilever racks.**



**Figure 1-5. Cantilever racks.**

#### 1.1.1.5 Cladding racks

An illustration of a cladding pallet rack structure is presented in Figure 1-6 and Figure 1-7. It is a type of rack that carries the weight of the pallets, the weight of the walls and the roof. This means that the actions due to wind and snow are directly carried by the pallet racks. Such structures can achieve heights of more than 30 meters and longitudinal lengths of more than 160 meters. These structures require a complex set of tools for their design and analysis.



**Figure 1-6. Cladding pallet rack structure.**

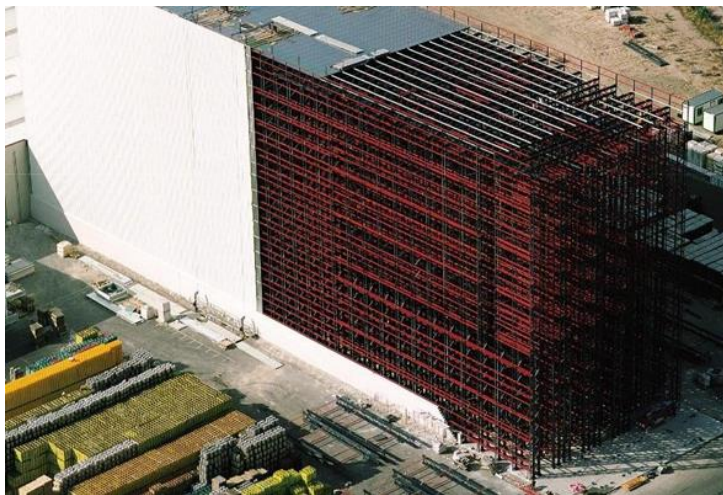


**Figure 1-7. Autoware pallet rack structure.**

### *1.1.2 Structural typology*

The design process of rack structures involves well-established criteria, but it is affected by much more complex problems with respect to those associated with traditional steel structures, due to peculiar geometry of some elements composing the structure (for example stiffened C sections of the uprights). The uprights of the rack structures are made by cold-forming process and as a consequence, are subject to all the issues regarding these types of elements. Furthermore, knowing that the pallets are positioned on the shelf beams

connected to the uprights, one can assume that the gravitational force deriving from the pallets will be transmitted to the gravity center of the uprights. As these have a thin-walled profile subject to compression, local and distortional instability phenomena could easily arise, putting into crisis the whole structure.

Regarding the stability of the whole structure in down-aisle direction, the basic factors depend on the beam-to-column joints and column base connections. The stability in the cross-aisle direction depends on the lateral bracing system. The joint modelling and of the holes is another crucial phase of rack structure design. The restraints, the functional and executive demands of the different load applications, the shape of the mechanical components (the presence of discontinuities in the profile) influence the stresses so that they differ noticeably from the ones assumed in the theoretical analysis. This fact brings to some modifications in the stress distribution and causes high local stresses, usually limited to the small zone around the discontinuity. The presence of the holes in the uprights causes a discontinuity in the domain and alters the uniform state of stress that would persist without having the holes. Therefore, in these zones it would be more correct to abandon the nominal distribution of the stresses and to identify the point of maximum stress.

The steel frames can be classified as *braced* (Figure 1-8) if the presence of the bracing system guarantees such stiffness that the transversal forces can be considered applied directly to the bracing system. According to *EC3*, a steel frame can be considered braced if the bracing system reduces the horizontal displacement by 80%. Equivalently, the structural system can be considered braced if the braced structure has 5 times greater stiffness than the unbraced one.

The presence of the bracing system simplifies the structural analysis as the behavior due to vertical loads, which are supported by the frame, can be decoupled from the bracings' behavior, which will have to support horizontal actions and the part of vertical loads acting on them.

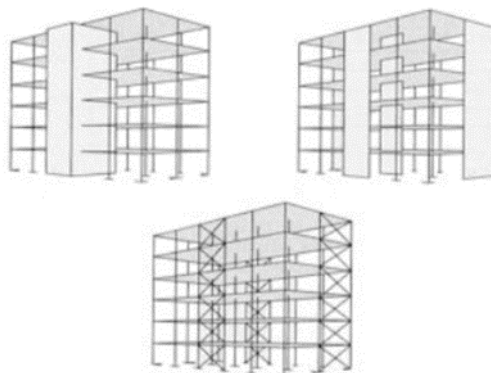


Figure 1-8. Examples of braced frames.

## 1.1.2.1 Transversal stability

Frame structures are classified as non-sway frames if the response to transverse actions is so that the internal actions resulting from horizontal displacement of the nodes are negligible. Theoretically, a frame without any bracing system should be considered a sway frame. It's important to clarify that 'braced frame' and 'non-sway frame' aren't equivalent, as the first term refers to the resistance of the structure with respect to a certain type of actions and mechanisms of force transfer, while the second term concerns the transversal deformability of the structure. *EC3* states that a frame can be considered a non-sway frame if for certain loading conditions, the ratio with respect to the critical load for that condition doesn't exceed the value of 0.1:

$$\frac{V_{sd}}{V_{cr}} \leq 0.1 \quad 1.1$$

where  $V_{sd}$  indicates the total vertical design load;

$V_{cr}$  represents the elastic critical load owed to the transversal displacement.

The flexural stiffness of the beam-column joint, i.e. its capacity of transmitting the internal forces for bending, has relevant importance when determining the structural behavior. For correctly evaluating the joint response it is useful to recur to the moment-curvature diagrams as the one shown in the Figure 1-9:

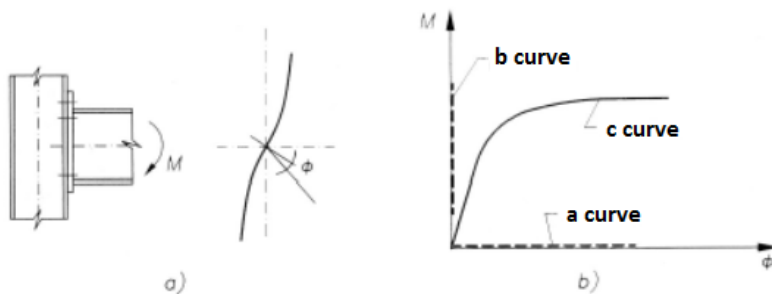


Figure 1-9. Moment-curvature diagram of the joints.

Based on illustrations shown in the figure, the next classification is determined:

- *Sway frame*: the joints are schematized as hinges, curve a, so they don't transmit bending moments between beam and column. Rotations between the elements

are allowed. In this case, during the design phase it's very important to provide an adequate bracing system.

- *Semi-continuous frame*: the joint is semi-rigid; it allows simultaneously the relative rotation and the bending moment transmission between beam and column, curve c;
- *Non-sway frame*: no rotation is allowed between two elements, curve b, there is continuity in the bending moment diagram.

Joints classified as hinges underestimate the bending actions inside the column and simultaneously provoke the over-dimensioning of the beams. With the modelling corresponding to fixed joints, the transversal stiffness of the frame is underestimated, with consequent transversal displacements smaller than the effective ones; in addition, with this schematization there is a risk of under-dimensioning the beam.

#### 1.1.2.2 Flexural continuity of joints

These joints, indeed, have a halfway behavior between the one of the hinge and the fix one:

- joints classified as hinges are also endowed with a flexural stiffness, and this decreases the contribution of the beams and increases the flexural contribution of the column.
- joints classified as fixed can have significant deformations for shear and bending, making the structure more sensitive to second-order effects.

The best way for representing the joints is to use a rotational spring with nonlinear behavior. In Figure 1-10, the first (elastic) phase is characterized by the stiffness,  $C_i$ , and the elastic limit moment value,  $M_e$ ; the second (post-elastic) segment, owed to a nonlinear phenomenon and to some local plasticization, has  $C_{red}$  stiffness and plastic moment  $M_p$ . Finally, the graph shows a hardening part where the ultimate moment value,  $M_u$ , is reached having  $C_p$  stiffness; the curve ends with a plastic segment. In the unloading phase, the curve is characterized by a straight line of stiffness  $C_{uni}$  similar to the initial elastic one.

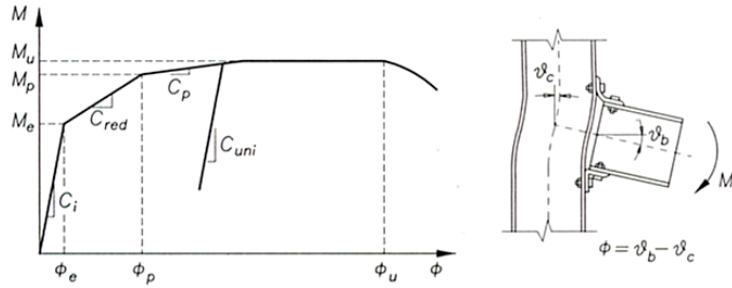


Figure 1-10. Moment-rotation behavior of the joints.

The joint classification can be made following the indications of EC3, showed in Figure 1-11:

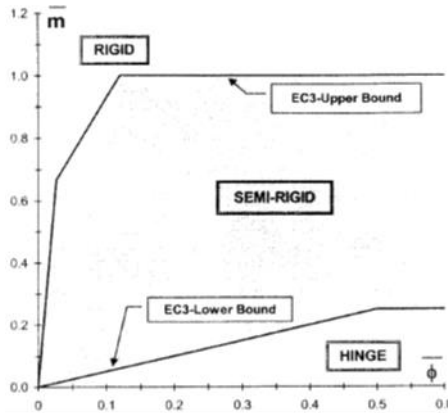


Figure 1-11. Joint classification according to EC3 for unbraced frames.

where the abscissa and ordinate indicate the following quantities:

$$\bar{m} = \frac{M}{M_{pl,Rd}} \tag{1.2}$$

$$\bar{\phi} = \phi \frac{EI_b}{LM_{pl,Rd}}$$

where  $M_{pl,Rd}$  represents the plastic moment of the beam;  
 $I_b$  is the moment of inertia of the beam;  
 $L_b$  is the length of the beam;  
 $E$  is Young's modulus.

It is important to say that beam-to-column joints are provided with modest degree of flexural continuity so that the most suitable structural scheme for their modelling is the one similar to hinges. However, many analyses reveal that the influence of joint modelling in steel rack structures is relevant for the structural response; as a consequence, the modelling of joints as semi-rigid elements is always suggested, even though the joint's response falls into the domain representing the hinge behavior.

In conclusion, the response of steel storage pallet racks depends on several parameters, which reflects directly on the complexity of rack design. Individual members are prone to different forms of buckling, while the regular perforation systems of uprights increase the difficulties in the prediction of the component local behavior. Moreover, the presence of nonlinear partial strength semi-rigid connections, the non-negligible influence of second-order effects, and the geometrical and mechanical imperfections do not allow to base design on pure theoretical approaches. Tests aimed at the characterization of the structural key components are required. Because of the great variability of member and joint geometries, pallet rack design is traditionally carried out by using hybrid procedures [1], which combine experiments with the state of knowledge developed for traditional steel structures. Design provisions have been very recently updated in Europe ([2], [3]), in the United States [4] and in Australia and New Zealand [5]. As clearly stated by [6], this last, and most recent, code acknowledges that refined analyses should be based on shell element modelling, in order to express appropriately the effects of local and distortional buckling: it includes also other important provisions for analysis, suggesting advanced analysis approaches, which should incorporate the dominant nonlinear effects. At present, common structural 2D or 3D rack models employing beam elements may not consider correctly torsion, and in particular warping torsion. Furthermore, practical indications on the minimum technical requirements for the finite element (FE) analysis software programs, which appear necessary to guarantee an adequate safety level in design, are omitted in all these codes. It should be noted that in the past, on the basis of the Author's knowledge, only [7] focused their attention on the influence of warping on the structural analysis of racks. In particular, they investigated the implications of using 'simple' 3D beam elements available in commercial frame analysis programs to determine the buckling load factor of a double-sided high-rise steel pallet rack frame. Only the research project in which the Author is involved considers deeply the influence of warping on steel storage pallet racks ([8], [9], [10], [11]).

## **1.2 Design approaches according to the codes**

Steel storage pallet racks are structures very flexible to lateral loads, owing to the great slenderness of the uprights, to the modest degree of rotational stiffness of beam-to-column joints and base-plate connections and to the absence of longitudinal bracings the down-aisle direction. As a consequence, a second-order analysis is often

## Chapter 1

required in routine design, which in some extent, can be developed also via approximated approaches. Moreover, owing to the extensive use of thin-walled cold-formed members, the traditional design methods of analysis proposed for the mostly used frames made by hot-rolled members can't be directly adopted.

### 1.2.1 Design for monotonic loads: introduction to EN15512

The evaluation of the static rack performance can be carried out by the General Method design approach, proposed by Eurocode 3.

Eurocode 3 in its part 1-1 proposes an innovative design approach, the so-called *General Method* (GEM), which takes into account the sole lack-of-verticality imperfections. This approach, which appears as very promising owing to its simplicity and efficiency when applied to racks, allows for accounting warping effects both for resistance and buckling checks. The overall buckling resistance of the whole skeleton frame is verified when:

$$\frac{\chi_{op}\alpha_{ult,k}}{\gamma_m} \geq 1 \quad 1.3$$

where  $\chi_{op}$  is the reduction factor for the non-dimensional slenderness  $\bar{\lambda}_{op}$ , to take account of lateral and lateral torsional buckling;

$\alpha_{ult,k}$  is the minimum load amplifier of the design loads to reach the characteristic resistance of the most critical cross section of the structural component, considering its in-plane behavior without taking lateral or lateral torsional buckling into account however accounting for all effects due to in-plane geometrical deformation and imperfections, global and local, where relevant;

$\gamma_m$  is the material safety factor.

The reduction factor  $\chi_{op}$  may be determined as the minimum value of

- the reduction factor for lateral buckling  $\chi = \frac{1}{\phi + \sqrt{\phi^2 - \bar{\lambda}^2}} \leq 1$
- the reduction factor for lateral torsional buckling  $\chi_{LT} = \frac{1}{\phi_{LT} + \sqrt{\phi_{LT}^2 - \bar{\lambda}_{op}^2}} \leq 1$

where

$$\begin{aligned} \phi &= 0.5[1 + \alpha(\bar{\lambda}_{op} - 0.2) - \bar{\lambda}_{op}^2] \\ \phi_{LT} &= 0.5[1 + \alpha_{LT}(\bar{\lambda}_{op} - 0.2) - \bar{\lambda}_{op}^2] \end{aligned} \quad 1.4$$

$\alpha$  and  $\alpha_{LT}$  are imperfection factors  $\alpha = 0.34$ ,  $\alpha_{LT} = 0.34$ .

The global non dimensional slenderness  $\bar{\lambda}_{op}$  should be determined from:

$$\bar{\lambda}_{op} = \sqrt{\frac{\alpha_{ult,k}}{\alpha_{cr,op}}} \quad 1.5$$

where  $\alpha_{cr,op}$  is the minimum amplifier for the in plane design loads to reach the elastic critical resistance of the structural component with regards to lateral or lateral torsional buckling without accounting for in-plane flexural buckling. In determining  $\alpha_{cr,op}$  and  $\alpha_{ult,k}$  Finite Element Analysis may be used.

The minimum load multiplier  $\alpha_{ult,k}$  is determined by the cross-section check:

$$\frac{1}{\alpha_{ult,k}} = \frac{N_{Ed}}{N_{Rk}} + \frac{M_{y,Ed}}{M_{y,Rk}} + \frac{M_{z,Ed}}{M_{z,Rk}} = \frac{N_{Ed}}{A_{eff}f_y} + \frac{M_{y,Ed}}{W_{eff,y}f_y} + \frac{M_{z,Ed}}{W_{eff,z}f_y} \quad 1.6$$

Where:

$N_{Ed}$  is the design normal force;

$M_{y,Ed}$  and  $M_{z,Ed}$  are the design bending moments;

$N_{Rk}$  is the design resistance to normal force;

$M_{y,Rk}$  and  $M_{z,Rk}$  are the design bending moment resistances;

$A_{eff}$  is the effective area of the cross-section;

$f_y$  is the yield strength;

$W_{eff,y}$  and  $W_{eff,z}$  are the effective section modulus.

With reference to the symbols already presented, the verification criterion can be more conveniently expressed in terms of the evaluation of the Resistance Safety Index,  $SI_G$ :

$$SI_G = \frac{\gamma_m}{\chi_{op}\alpha_{ult,k}} \leq 1 \quad 1.7$$

Another possibility is to adopt the method proposed directly by the EN15512: the method takes into account the lack-of- verticality imperfections neglecting out-of-straightness of members and it is the most preferred approach by rack designers because of the very generous values of the load carrying capacity. The EN15512 code declares in fact that structure shall be considered a no-sway frame and buckling lengths shall be put equal to system (geometrical) lengths. Effective length for member stability checks results hence independent on the degree of rotational stiffness of beam-to-column joints and base- plate connections, without any distinction between braced and unbraced racks.

## Chapter 1

The following verification formula is used by this method and is based on stability criteria:

$$\frac{N_{Ed}}{\chi_{min}A_{eff}f_y/\gamma_m} + \frac{k_y M_{y,Ed}}{W_{y,eff}f_y/\gamma_m} + \frac{k_z M_{z,Ed}}{W_{z,eff}f_y/\gamma_m} \leq 1 \quad 1.8$$

Where:

$$\begin{aligned} k_y &= 1 - \frac{\mu_y N_{Ed}}{\chi_y A_{eff} f_y} \quad \text{but} \quad k_y \leq 1.5 \\ \mu_y &= \bar{\lambda}_y (2\beta_{M,y} - 4) \quad \text{but} \quad \mu_y \leq 0.9 \\ k_z &= 1 - \frac{\mu_z N_{Ed}}{\chi_z A_{eff} f_y} \quad \text{but} \quad k_z \leq 1.5 \\ \mu_z &= \bar{\lambda}_z (2\beta_{M,z} - 4) \quad \text{but} \quad \mu_z \leq 0.9 \end{aligned} \quad 1.9$$

And  $\chi_{min}$  is the lesser of  $\chi_{db}$ ,  $\chi_y$  and  $\chi_z$ , meanwhile  $\beta_{M,y}$  and  $\beta_{M,z}$  are equivalent uniform moment factors for flexural buckling. This expression is valid for bi-symmetric sections not exposed to lateral-torsional buckling and the unknown terms can be easily calculated from EN15512.

For the case of mono-symmetric cross-sections, the following expression has to be used:

$$\frac{N_{Ed}}{\chi_{min}A_{eff}f_y/\gamma_m} + \frac{k_{LT} M_{y,Ed}}{\chi_{LT} W_{y,eff}f_y/\gamma_m} + \frac{k_z M_{z,Ed}}{W_{z,eff}f_y/\gamma_m} \leq 1 \quad 1.10$$

Where:

$$\begin{aligned} k_{LT} &= 1 - \frac{\mu_{LT} N_{Ed}}{\chi_z A_{eff} f_y} \quad \text{but} \quad k_{LT} \leq 1.0 \\ \mu_{LT} &= 0.15 \bar{\lambda}_z \beta_{M,LT} - 0.15 \quad \text{but} \quad \mu_{LT} \leq 0.9 \end{aligned} \quad 1.11$$

And  $\beta_{M,LT}$  is an equivalent uniform moment factor for lateral-torsional buckling.

### 1.2.2 Design for seismic loads: introduction to EN16681

Different methods of analysis can be adopted for seismic design [12], that are the same adopted for conventional buildings, and in particular:

- the lateral force method of analysis (LFMA);
- the modal response spectrum analysis (MRSA);
- the pushover analysis (POA);
- the time history analysis (THA).

The choice of the method of analysis is governed by the value of the inter-story drift sensitivity coefficient ( $\theta$ ), that approximates the buckling critical load multiplier ( $\alpha_{cr}$ ), being defined in the seismic code as:

$$\theta = \max \left( \frac{P_{E,i} d_{r,i}}{V_{E,i} h_i} \right) \cong \alpha_{cr} \quad 1.12$$

where  $P_{E,i}$  and  $V_{E,i}$  are the total vertical load and the total shear at the base of the  $i$ -th inter-story, respectively,  $h_i$  is its height and  $d_{r,i}$  is the lateral drift.

With reference to the contents of the Table 1-1, it is worth mentioning that the possibility to design racks having  $\theta > 0.3$  is instead prohibited by EC8 [13], which limits  $\theta \leq 0.3$  for structures with dissipative components in class 1 according to the EC3 classification criteria [14]. Moreover, by considering that  $\theta \cong 1/\alpha_{cr}$ , the indications provided in the table for  $\theta > 0.5$  are misleading and out of interest from an engineering point of view.

**Table 1-1. Summary of methods of analysis.**

$\theta$	$q \leq 2$ low dissipative structural behavior		$q > 2$ high dissipative structural behavior	
	Method of analysis	Second order effects	Method of analysis	Second order effects
$\theta \leq 0.1$	LFMA or MRSA	Negligible	LFMA or MRSA	Negligible
$\theta \leq 0.3$		Considered either directly or indirectly *		Considered either directly or indirectly*
$\theta \leq 0.5$			POA according to EC8 or LDMA	
$\theta > 0.5$			THA including geometrical and material nonlinearity	

## Chapter 1

The LFMA method is the one preferred by designers, due to its simplicity. The effect of earthquake ground motion, typically defined by a seismic design response spectrum are simulated by means of a suitable set of lateral forces acting on the rack and assuming that it mainly responds in the fundamental mode. For this to be true, the racks must be low-rise and must not twist significantly when the ground moves. From the practical point of view, its application is possible when the response is not significantly affected by contribution of higher modes of vibration in each principal direction. For its applicability, it is in fact required that both the following conditions have to be met:

- in case of stiffness and mass regular in elevation, the fundamental (greatest) period of vibration,  $T_1$ , along the two principal directions has to satisfy:

$$\begin{aligned} T_1 &\leq 4T_c \\ T_1 &\leq 2s \end{aligned} \tag{1.13}$$

where  $T_c$  is the upper limit of the period of the constant spectral acceleration branch in the elastic design spectrum;

- the modal mass associated to the fundamental period is greater than 90% of the total mass.

The seismic base shear force  $V_E$  for each main direction is determined as follows:

$$V_E = S_{d,mod}(T_1)W_{E,tot}\lambda \tag{1.14}$$

where  $S_{d,mod}(T_1)$  is the ordinate of the modified design spectrum defined for translational motion in the direction under consideration,  $W_{E,tot}$  is the total weight of the seismic mass of the rack and  $\lambda$  is a numerical coefficient not greater than unity.

The seismic action  $V_i$  for each load level is derived from the equation:

$$V_i = V_E \frac{W_i z_i}{\sum W_i z_i} \tag{1.15}$$

where  $W_i$  and  $z_i$  are the weight of the total pallet units and the height for each load level, respectively.

The MRSA approach is the most used, owing to the fact that generally the high value of  $T_l$  characterizing and/or the percentage of the participating mass hampers in practice the use of LFMA approach. A linear-dynamic static analysis is required by MRSA, measuring the contribution of each natural mode of vibration, by obtaining its peak value acceleration  $a_g$  from the design spectrum.

According to this procedure, the number of the modes to consider are related to the percentage of the mass involved; in general, the design is based on a number of modes involving at last 90% of the participant masses. Different rules can be adopted to combine their effects in order to assess the total response: the most frequently used are as the absolute sum (ABSSUM), the square root of sum of squares (SRSS), and the complete quadratic combination (CQC). In the present study, the CQC rule has been adopted according to the requirements of Eurocode 8, and hence reference is hence made to the following equation:

$$r_o \cong \left( \sum_{i=1}^N \sum_{n=1}^N \rho_{in} r_{io} r_{no} \right)^{1/2} \quad 1.16$$

where  $r_o$  is the product of the peak responses in the  $i^{th}$  and  $n^{th}$  modes and  $\rho_{in}$  is the correlation coefficient for these two modes, which varies between 0 and 1 ( $\rho_{in}=1$  when  $i=n$ ) and is expressed as:

$$\rho_{in} = \frac{8\zeta^2(1 + \beta_{in})\beta_{in}^{3/2}}{(1 - \beta_{in}^2)^2 + 4\zeta^2\beta_{in}(1 + \beta_{in})^2} \quad 1.17$$

where  $\beta_{in}$  is the ratio of the natural circular frequency of vibration of the two considered modes  $\omega_i$  on  $\omega_n$  and  $\zeta$  is the damping value.

Once all the sets of displacements and generalized forces are obtained from MRSA, they have to be added to the results of a static analysis, which considers mainly the effects of the vertical load (weight) of the pallets. The combination of the two load cases consists in an envelope of both the associated contributions, where the one deriving from MRSA is considered with its absolute value (subscripts MRSA), meanwhile the one deriving from the static analysis (subscripts STAT) conserve its sign, according to:

$$r_{seism} = r_{stat} + |r_{mrsa}| \quad 1.18$$

## Chapter 1

where  $r_k$  indicates the parameter of interest belonging to the set of the generalized forces.

The POA method is a well-known technique to assess the structural performance of traditional buildings in seismic zones by means of a static non-linear analysis [15], which has been developed and proposed since few years by major seismic provisions. A pattern of forces (generally inverse triangular or uniform) is applied to a structural FE refined model that includes mechanical non-linear behavior of members and/or joints, and second-order effects. On the basis of the FE pushover capacity curve for the multi-degree-of-freedom (MDOF) system, the push-over capacity curve of the equivalent single-degree-of-freedom (SDOF) system is obtained by means of the assessment of a suitable transformation factor  $\Gamma$ , depending on the mass on each story and on the assumed displacement deformed shape. POA method seems nowadays very promising also when applied to other types of structures, such as industrial steel storage racks, characterized by a linear response of members that are in classes 3 or 4 and a non-linear mechanical behavior of joints.

The THA method, also called non-linear dynamic analysis, utilizes the combination of ground motion records with a detailed structural nonlinear FE analysis model. On the contrary of the three previously discussed methods, this approach is the sole able to account for the joint response under cyclic loads, which is characterized by noticeable pinching and very limited energy adsorption capabilities. This approach is the most rigorous, which is required by some building codes for buildings of unusual configuration or of special importance. However, the assessed structural response can be very sensitive to the characteristics of the individual ground motion used as seismic input. Therefore, several analyses are required using different ground motion records to achieve a reliable estimation of the probabilistic distribution of key parameters governing the structural response. Also in this case, it is essential to carry out advanced nonlinear structural analyses by using appropriate FE formulations, not only to account for the presence of a sole symmetry axis but also the cyclic joint behavior with deterioration of stiffness and strength.

In order to calculate the rack performance and the verification checks for the members, reference can be made to the methods proposed for the static analysis.

### 1.3 General aspects

Rack uprights usually present open single symmetric thin-walled cross sections, which are generally perforated along their length at regular intervals to allow the connections with both beams and bracing members. This induces a significant local weakening of the resistant section causing a substantial reduction of the structural performance. Moreover, the upright behavior is significantly affected by different forms of buckling: local,

distortional, global buckling and their interaction should be necessarily considered in the design. The beams are generally characterized by boxed cross-sections, which are welded at their ends to an angle end-plate (beam-end-connector) in order to allow a mechanical connection to the uprights. The bracing members in the cross-aisle direction are channel profiles or hollow rectangular profiles, which are eccentrically connected to the uprights via bolts or, more rarely, welds. The connection to the pavement is realized by base plates, which can be either bolted or welded to the upright end, and anchored to the floor. The peculiar mechanical behavior of the connected members and of the connection itself results in a remarkable non linearity of both the beam-to-column and pavement connections. In addition, in case of pavement connection, the response is quite complex to predict, owing to the strong influence of the level of the axial load applied to the upright.

The great variety of rack components and the non-linear response of both members and joints make the use of pure theoretical design approaches unsuitable. The more recent standards for the design of racks suggest specific tests to quantify the main parameters characterizing the response of key rack components: tests on uprights, beam-to-column joints and base-plate connections have to be necessarily carried out in laboratories having adequate testing facilities. The re-analysis of tests data, allows the definition of key parameters for the design of racks, which is based on a suitable extension of the state-of-knowledge developed and codified in the last decades for traditional cold-formed structural systems. The slenderness and the shape of the members, the particular geometry of the connections, and the global and local imperfections of these structures make them quite sensitive to second order effects. As a consequence, rack design is strongly governed by the stability check results.

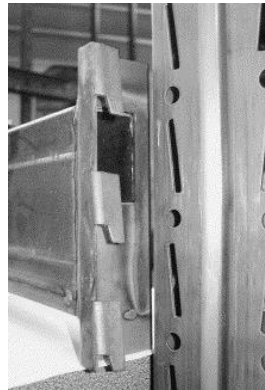
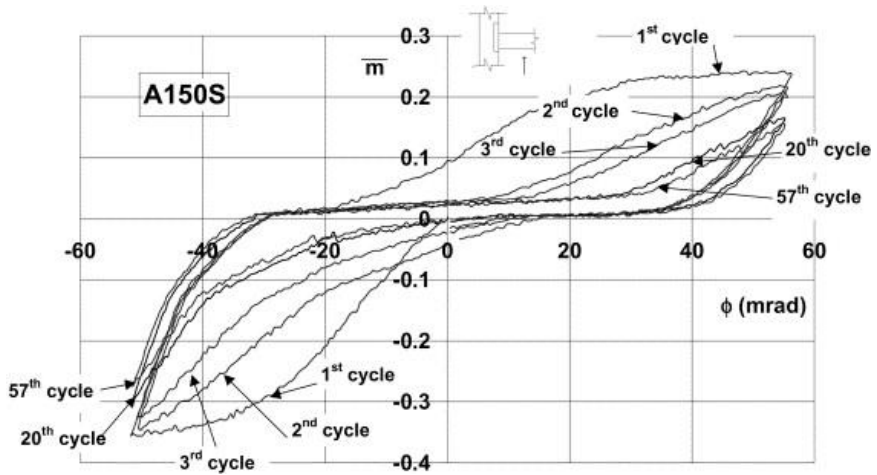
In European pallet rack practice, design is based on *EN15512* [2], while in North America, *RMI specifications* [4] are the reference for designers. Both Codes are very recent, as their current editions were published in 2008. Furthermore, in 2012, updated version of the *Australian standards* [5] for steel storage racking was also published.

Regarding the seismic design, the currently available standard provisions [3] are based on a direct extension to racks of the approaches typically used for the more traditional steel carpentry framed buildings. In particular, attention in the codes has been paid to the key aspects mainly associated with the definition of the seismic load effects, as well as to the rule for its combination with other type of loads, giving to the rack manufacturing designers the guidelines dealing only with the general aspects.

The same influence of the methods of analysis observed for static loads is of course expected also with reference to the seismic structural analysis. A key difference with respect to the more traditional steel framed systems is due to the response of the rack components under cyclic loads (Figure 1-12). Generally, rack components belong to classes 3 or 4 in accordance with the *Eurocode3* classification criteria [14], due to the

## Chapter 1

remarkable influence of local and distortional buckling phenomena preventing the achievement of plasticity in members [16]. As a consequence, design assisted by testing is required and the effective cross-section properties to be used by engineers are based on quite expensive experimental program that each rack manufacture has to execute on key components, sub-assemblages and joints. In absence of more accurate evaluation of the energy absorption capabilities associated with this type of structures, an elastic approach has to be used, by assuming a behavior  $q$ -factor equal to unity, despite the fact that, very generous factors are usually adopted in routine rack design, as recommended by codes.



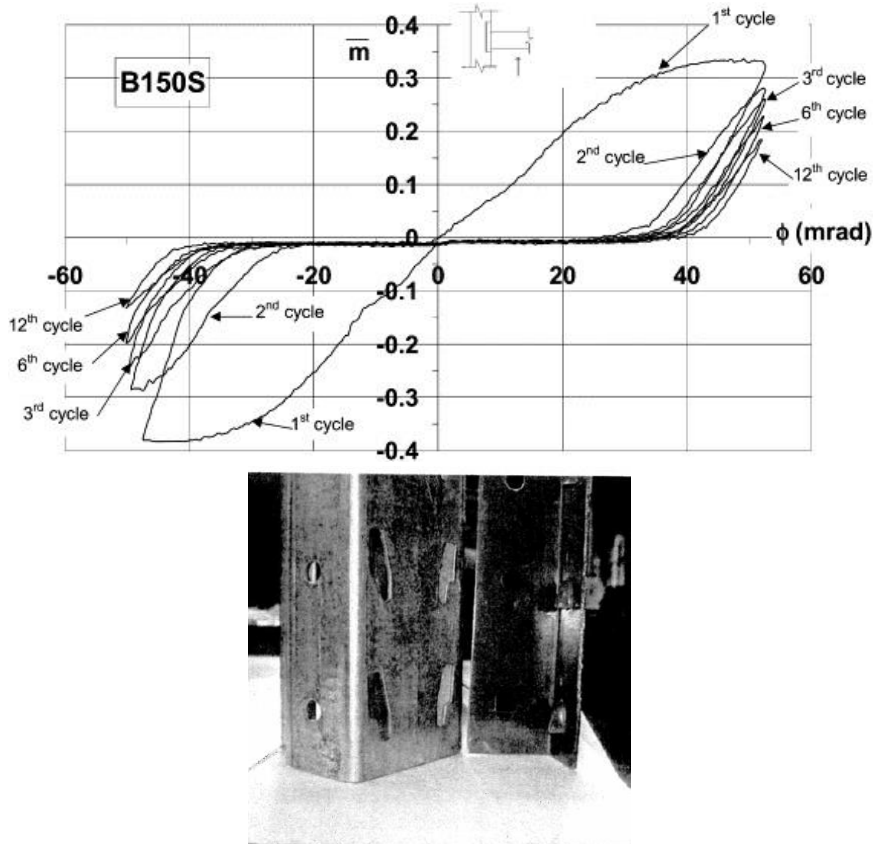


Figure 1-12. Typical cyclic moment-rotation relationships for beam-to-column joint of adjustable pallet racks [17].

Essential issues which need further improvements of the codes are related to the following topics:

- **Application Field:** just from the start, one must decide the application field, i.e. it should be clarified whether or not the current norms apply also to the considered rack structures. The norms say that the all the rules should also be valid for the industrial storage racks, for whom it is however mandatory to deposit the project at the corresponding authorities. Actually, if one considers that the regulations of the current norms do not apply to the storage rack systems, he must clearly state this aspect in the introduction of the project and, consequently, any reference to the norms have to disappear from the corresponding study. If the proposed rules also apply to the racks, it should also be declared. Therefore, the design process of industrial storage racks should be mainly done in accordance with the laws of the state.

## Chapter 1

- Seismic load: the distribution of the masses generates irregular behavior and therefore the fully-loaded condition is not always the more conservative. As the racks are complex systems with many stories, the sporadic lack of a pallet may generate behavior asymmetries.
- Floor-structure interaction: the industrial racks' field is definitely a very broad and varied world, so the relative norms should contain at least general indications with respect to the important and recurrent aspects. For example, a rack may be supported by a plate, so in this case its answer would be heavily affected also by the behavior of the plate.
- Behavior factor: the current norms propose some values for the behavior factor, function of the rack type. One may refer also to the existing indications in literature (for example [18]) which impose the usage of a unitary behavior factor. Since the steel used for this type of structures is a hardened steel and the cross-sections are obtained using a cold-formed manufactory process, one may try to understand what are the basis of these proposed values.
- Design method: the choice of the design method depends, according to the current norms, on the definition of the sensibility coefficient  $\theta$  already mentioned, evaluated using a linear analysis. This parameter should be able to identify the behavior of the structure.

According to *Eurocode 8*, if  $0.1 < \theta < 0.2$  the second order effects may be obtained by simply multiplying the seismic action results with  $1/(1 - \theta)$ , while the maximum value of the sensibility coefficient should be  $0.3$ . However, the specific rack norms do not suggest any limitation as to establish the importance of the second order effects, so one could require the evidence of scientific studies related to this issue.

- State-of-the-art of the research: a very limited number of studies has been conducted on the evaluation of behavior factors of storage industrial systems, which focused on medium-rise adjustable pallet racks. *Adamakos and Vayas* [19] simulated numerically the pushover response of six unbraced and three braced racks in the framework of the research activities associated with the European research project *Seisrack 2* [20], evaluating q-factors values ranging from 2 to 5.47. Full-scale tests on the same racks were carried out by applying pushover triangular inverted load in the rack longitudinal direction by *Kanyilmaz et al.* [21] while *Braham and Degèe* [22] characterized experimentally the rack response in the cross-aisle direction by testing uprights without gravity (pallet) loads.

## Chapter 2 Buckling and geometric nonlinear analysis

A stiffness method approach to the buckling and geometrical nonlinear analysis is herein developed. Both analyses employ the same form of the elastic and geometric stiffness matrices. Assuming a matrix system, a linear elastic analysis can be designated as:

$$K_E d = P \quad 2.1$$

In which  $K_E$  is the linear elastic stiffness matrix,  $d$  is the displacement vector and  $P$  is the load vector. However, when large deflections are present, the equations of force equilibrium must be formulated for the deformed configuration of the structure. In this case, the 2.1 can no longer be used. In order to account for the effects of changes in geometry as the applied loading is increased we may obtain solutions for the displacements  $d$  by treating this nonlinear problem in a sequence of linear steps, each step representing a load increment. Because of the presence of large deflections, strain-displacement equations contain nonlinear terms, which must be included in calculating the stiffness matrix  $K_E$ . Then the behavior can be traced adopting the following equation:

$$K_t \Delta d = \Delta P \quad 2.2$$

Where  $K_t$  is the tangent stiffness matrix,  $\Delta d$  is a vector of incremental displacements, and  $\Delta P$  is a vector of incremental loads. Typically,  $K_t$  has a linear elastic component and one or more additional components that are functions of the loads and/or displacements.

In second order elastic analysis the effects of finite deformations and displacements are accounted for in formulating the equations of equilibrium, which leads to reinterpreted the tangent stiffness matrix ( [23], [24], [25]) as:

$$K_t = K_E + K_G \quad 2.3$$

## Chapter 2

In which  $K_G$ , the geometric stiffness matrix, represents the change in stiffness that results from these effects.

In case of inelastic analysis, another matrix can be added to take account for the nonlinearities of the materials:

$$K_t = K_E + K_G + K_m \quad 2.4$$

Where  $K_m$  can be identified as the plastic reduction matrix, which represents the change in stiffness that results from inelastic behavior of the system.

For the calculation of elastic critical loads, the global stiffness equation is cast in the form of a generalized eigenvalue problem in which the equation of equilibrium at the critical state is:

$$[K_E + \lambda K_G]d = 0 \quad 2.5$$

Where in this case  $K_G$  is computed for a reference load  $P_{ref}$ ,  $\lambda$  is a load factor with respect to  $P_{ref}$ , and  $d$  is the buckled shape. The lowest value of  $\lambda$  yields the elastic critical load vector  $\lambda \cdot P_{ref}$ .

The aim of this chapter is to expose the matrices adopted in the academic software *Śiva*. Following the earlier studies about the thin-walled structures and the flexural-torsional buckling ([26], [27], [28]), similar matrices have been discussed in [23] and [29], meanwhile for taking account for large rotation effects with an Updated Lagrangian formulation reference can be made to [30]. Instead in [31] and [32] is described a co-rotational beam elements formulation which taking account the warping effects. Concerning the mass matrix for a beam with 7DOFs, it can be found in [33].

### 2.1 Kinematics for thin-walled beam

Let us consider a straight beam member with an asymmetric thin-walled cross-section, with a thickness  $t$ , as it is shown in Figure 2-1. A right-handed Cartesian co-ordinate system  $(x, y, z)$  is selected in such a way that axis  $x$  coincides with the beam axis passing through the centroid  $C$  of each cross-section.

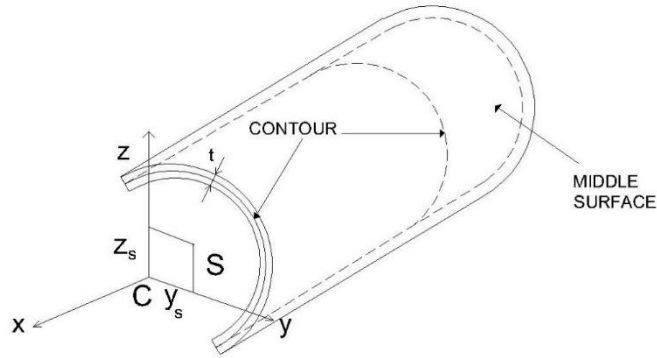


Figure 2-1. General thin-walled beam member.

The co-ordinate axes  $y$  and  $z$  are the principal inertial axes of the cross-section  $y_s$ ; and  $z_s$  are the co-ordinates of the shear center  $S$ . The plane in  $(y, z)$ , i.e. normal to the  $x$ -axis, cuts the middle surface in a line called contour of the cross-section. Displacement measures of a thin-walled cross-section are shown in Figure 2-2. The measures:  $w_C$ ,  $u_S$ ,  $v_S$  are rigid-body translations of the cross-section in the  $x$  direction at the centroid and in the  $y$  and  $z$  direction at the shear center, respectively;  $\varphi_x$ ,  $\varphi_y$  and  $\varphi_z$  are rigid-body rotations about the shear center axes  $x$ ,  $y$  and  $z$ , respectively;  $\theta$  is a parameter defining warping of the cross-section. In this, the following is valid:

$$\begin{aligned}
 w_C &= w_C(x), & u_S &= u_S(x), & v_S &= v_S(x), & \varphi_x &= \varphi_x(x), \\
 \varphi_y &= -\frac{dv_S}{dx} = \varphi_y(x), & \varphi_z &= \frac{du_S}{dx} = \varphi_z(x), \\
 \theta &= -\frac{d\varphi_x}{dx} = \theta(x)
 \end{aligned} \tag{2.6}$$

Under the assumption of small space rotations, the displacement components of an arbitrary point on the cross-section, defined by the position co-ordinates  $y$  and  $z$  and the warping function  $\omega(y, z)$  with respect to the shear center  $S$ , can be expressed as:

$$\begin{aligned}
 w(x, y, z) &= w_C(x) - y \frac{du_S}{dx}(x) - z \frac{dv_S}{dx}(x) - \omega(y, z) \frac{d\varphi_x}{dx}(x) \\
 u(x, y, z) &= u_S(x) - (z - z_S)\varphi_x(x)
 \end{aligned} \tag{2.7}$$

$$v(x, y, z) = v_s(x) + (y - y_s)\phi_x(x)$$

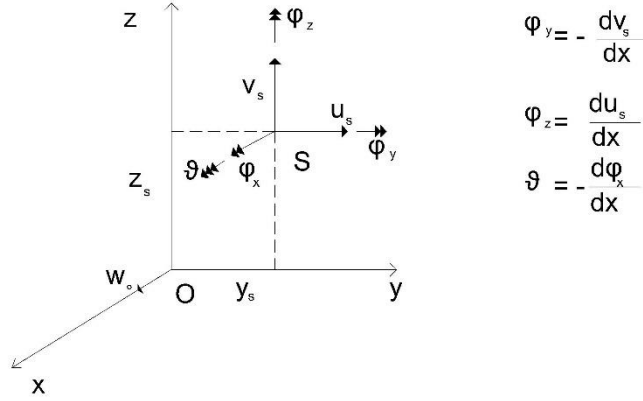


Figure 2-2. Displacement measures of a thin-walled cross-section.

The Green-Lagrange tensor can be written in the following form:

$$\varepsilon_{ij} = 0.5(u_{i,j} + u_{j,i} + u_{k,i} \cdot u_{k,j}) \quad 2.8$$

Substituting 2.7 in 2.8, and adopting the geometrical hypothesis of the cross-sectional in-plane rigidity ( $\varepsilon_{yy} = \varepsilon_{zz} = \varepsilon_{yz} = 0$ ), the non-zero strain components can be written as:

$$\begin{aligned} \varepsilon_{xx} &= \dot{w}_c - y\ddot{u}_s - z\ddot{v}_s - \omega(y, z)\ddot{\phi}_x + 0.5[\ddot{u}_s^2 - 2\dot{u}_s(z - z_s)\dot{\phi}_x + \dot{\phi}_x^2(z - z_s)^2] \\ &\quad + 0.5[\ddot{v}_s^2 + 2\dot{v}_s(y - y_s)\dot{\phi}_x + \dot{\phi}_x^2(y - y_s)^2] \\ &\quad + 0.5 \left[ \dot{w}_c - \underbrace{y\ddot{u}_s - z\ddot{v}_s - \omega(y, z)\ddot{\phi}_x}_{\text{neglected}} \right]^2 \\ \varepsilon_{xy} &= 0.5 \left[ -(z - z_s)\dot{\phi}_x - \frac{\partial \omega}{\partial y} \dot{\phi}_x + \phi_x [\dot{v}_s + (y - y_s)\dot{\phi}_x] \right. \\ &\quad \left. - \underbrace{\left( \dot{u}_s + \frac{\partial \omega}{\partial y} \dot{\phi}_x \right) (\dot{w}_c - y\ddot{u}_s - z\ddot{v}_s - \omega(y, z)\ddot{\phi}_x)}_{\text{neglected}} \right] \end{aligned} \quad 2.9$$

$$\varepsilon_{xz} = 0.5 \left[ (y - y_S) \dot{\varphi}_x - \frac{\partial \omega}{\partial z} \dot{\varphi}_x - \varphi_x [\dot{u}_S - (z - z_S) \dot{\varphi}_x] - \underbrace{\left( \dot{v}_S + \frac{\partial \omega}{\partial z} \dot{\varphi}_x \right) (\dot{w}_C - y \ddot{u}_S - z \ddot{v}_S - \omega(y, z) \ddot{\varphi}_x)}_{\text{neglected}} \right]$$

It should be noted that in the 2.9 the underlined terms are neglected because of the effect of the higher-order derivatives in  $\dot{w}_C$  is assumed to be negligible.

## 2.2 Equilibrium and constitutive equations

Equilibrium equations are obtained from stationary conditions of the total potential energy which is:

$$\delta(U - W) = 0 \quad 2.10$$

In this relationship,  $\delta$  denotes the virtual variation, meanwhile  $U$  and  $W$  are the strain energy and the external load work. The variation of the strain energy is:

$$\delta U = \int_V (\sigma_{xx} \delta \varepsilon_{xx} + 2\sigma_{xy} \delta \varepsilon_{xy} + 2\sigma_{xz} \delta \varepsilon_{xz}) dV \quad 2.11$$

Where  $\sigma_{ij}$  is the Piola-Kirchhoff stress tensor. Using 2.9, the variation of the strain tensor components is given by:

$$\begin{aligned} \delta \varepsilon_{xx} = & \delta \dot{w}_C - y \delta \ddot{u}_S - z \delta \ddot{v}_S - \omega(y, z) \delta \ddot{\varphi}_x + \delta \dot{w}_C \cdot \dot{w}_C \\ & + \delta \dot{u}_S [\dot{u}_S - (z - z_S) \dot{\varphi}_x] + \delta \dot{v}_S [\dot{v}_S + (y - y_S) \dot{\varphi}_x] \\ & + \delta \dot{\varphi}_x [-\dot{u}_S (z - z_S) + \dot{\varphi}_x (z - z_S)^2 + \dot{v}_S (y - y_S) \\ & + \dot{\varphi}_x (y - y_S)^2] \end{aligned} \quad 2.12$$

$$\begin{aligned}
2\delta\varepsilon_{xy} &= \delta\dot{\varphi}_x \left[ -(z - z_S) - \frac{\partial\omega}{\partial y} + \varphi_x(y - y_S) \right] + \delta\dot{v}_S\varphi_x + \delta\varphi_x\dot{v}_S \\
&\quad + \delta\varphi_x\dot{\varphi}_x(y - y_S) \\
2\delta\varepsilon_{xz} &= \delta\dot{\varphi}_x \left[ (y - y_S) - \frac{\partial\omega}{\partial z} + \varphi_x(z - z_S) \right] - \delta\dot{u}_S\varphi_x - \delta\varphi_x\dot{u}_S \\
&\quad + \delta\varphi_x\dot{\varphi}_x(z - z_S)
\end{aligned}$$

The strain energy variation can be expressed as a function of the stress resultants acting on cross-section of the thin-walled element in the deformed state. Choosing the coordinates  $y$  and  $z$  as the principal coordinates of the cross-section and selecting  $C$  and  $S$  as centroid and shear center, they can be defined as follows:

$$\begin{aligned}
N &= \int_A \sigma_{xx} dA; \quad F_y = \int_A \sigma_{xy} dA; \quad F_z = \int_A \sigma_{xz} dA; \\
M_y &= \int_A \sigma_{xx} z dA; \quad M_z = - \int_A \sigma_{xx} y dA; \quad B = \int_A \sigma_{xx} \omega dA; \\
M_x &= \int_A [\sigma_{xz}(y - y_S) - \sigma_{xy}(z - z_S)] dA; \\
T_\omega &= \frac{dB}{dx} = \int_A \dot{\sigma}_{xx} \omega dA = - \int_A \left( \frac{\partial\sigma_{xy}}{\partial y} + \frac{\partial\sigma_{xz}}{\partial z} \right) \omega dA \quad 2.13 \\
&= \int_A \left( \sigma_{xy} \frac{\partial\omega}{\partial y} + \sigma_{xz} \frac{\partial\omega}{\partial z} \right) dA; \\
T_{sv} &= M_x - T_\omega = \int_A \left[ \sigma_{xz} \left( y - y_S - \frac{\partial\omega}{\partial z} \right) - \sigma_{xy} \left( z - z_S + \frac{\partial\omega}{\partial y} \right) \right] dA; \\
\bar{K} &= \int_A \sigma_{xx} \rho^2 dA = \int_A \sigma_{xx} [(y - y_S)^2 + (z - z_S)^2] dA;
\end{aligned}$$

In the 2.13,  $N$  represents the axial force acting at the centroid,  $F_y$  and  $F_z$  are the shear forces acting at the shear center,  $M_y$  and  $M_z$  are the bending moments with respect to  $y$  and  $z$  axes,  $M_x$  is the total torsional moment with respect to the shear center,  $B$  is the bimoment, is the St. Venant or uniform torsional moment, is the warping or non-uniform torsional moment and is the Wagner coefficient [25].

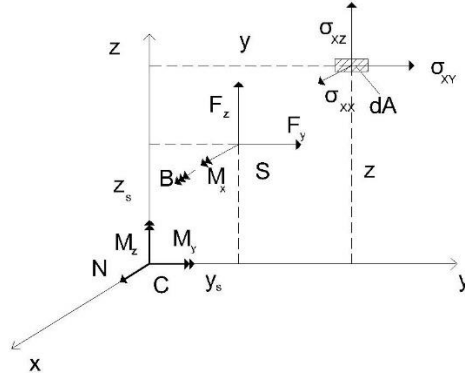


Figure 2-3. Stress state and stress resultants of a thin-walled cross-section.

Assuming Hooke's law is valid and substituting 2.9 into 2.13, the linearized incremental force-displacement relations can be written as:

$$\begin{aligned}
 N &= EA\dot{w}_C; \\
 M_y &= -EI_y\ddot{v}_S; \quad M_z = EI_z\ddot{u}_S; \quad B = -EI_w\ddot{\phi}_x; \\
 T_{sv} &= GI_x\dot{\phi}_x; \quad \bar{K} = N\alpha_x + M_y\alpha_y + M_z\alpha_z + B\alpha_\omega
 \end{aligned}
 \tag{2.14}$$

Where  $E$  and  $G$  are the elastic and shear moduli, respectively, while the cross-sectional properties are defined in the following way:

$$\begin{aligned}
 A &= \int_A dA; \\
 I_y &= \int_A z^2 dA; \quad I_z = \int_A y^2 dA; \quad I_w = \int_A \omega^2 dA; \\
 I_x &= \int_A \left[ \left( y - y_S - \frac{\partial \omega}{\partial z} \right)^2 + \left( z - z_S + \frac{\partial \omega}{\partial y} \right)^2 \right] dA; \\
 \alpha_x &= \frac{I_y + I_z}{A} + y_S^2 + z_S^2; \quad \alpha_y = \frac{1}{I_y} \int_A (y^2 z + z^3) dA - 2z_S;
 \end{aligned}
 \tag{2.15}$$

## Chapter 2

$$\alpha_z = -\frac{1}{I_z} \int_A (z^2 y + y^3) dA + 2y_S; \quad \alpha_\omega = \frac{1}{I_w} \int_A (y^2 + z^2) \omega dA$$

Adopting the 2.11, 2.12, 2.13, 2.14 and 2.15, the strain energy can be written as:

$$\begin{aligned} \delta U = & \int_0^l [\delta \dot{w}_c EA \dot{w}_c + \delta \dot{v}_s EI_y \dot{v}_s + \delta \dot{u}_s EI_z \dot{u}_s + \delta \dot{\varphi}_x GI_x \dot{\varphi}_x + \delta \dot{\varphi}_x EI_w \dot{\varphi}_x] dx \\ & + \\ & \int_0^l \left[ \delta \dot{w}_c N \dot{w}_c + \delta \dot{u}_s N \dot{u}_s - \delta \dot{u}_s M_y \dot{\varphi}_x + \delta \dot{u}_s (N \cdot z_S) \dot{\varphi}_x + \delta \dot{v}_s N \dot{v}_s \right. \\ & \quad - \delta \dot{v}_s M_z \dot{\varphi}_x - \delta \dot{v}_s (N \cdot y_S) \dot{\varphi}_x - \delta \dot{\varphi}_x M_y \dot{u}_s + \delta \dot{\varphi}_x (N \cdot z_S) \dot{u}_s \\ & \quad - \delta \dot{\varphi}_x M_z \dot{v}_s - \delta \dot{\varphi}_x (N \cdot y_S) \dot{v}_s \\ & \quad \left. + \delta \dot{\varphi}_x \underbrace{\sigma_{xx} [(y - y_S)^2 + (z - z_S)^2]}_{\bar{k}} \dot{\varphi}_x - \delta \dot{u}_s F_z \dot{\varphi}_x - \delta \dot{\varphi}_x F_z \dot{u}_s \right. \\ & \quad \left. + \delta \dot{v}_s F_y \dot{\varphi}_x + \delta \dot{\varphi}_x F_y \dot{v}_s \right] dx \\ & + \int_V \underbrace{[\delta \dot{\varphi}_x [\varphi_x (z - z_S) \sigma_{xz} + \varphi_x (y - y_S) \sigma_{xy}]]}_{neglected} dV \\ & + \int_V \underbrace{[\delta \dot{\varphi}_x [\dot{\varphi}_x (z - z_S) \sigma_{xz} + \dot{\varphi}_x (y - y_S) \sigma_{xy}]]}_{neglected} dV \end{aligned} \quad 2.16$$

The last part of the strain energy is not included by [29]; it is presumed small and then omitted from the final equations.

### 2.3 Finite element beam formulation

In order to satisfy 2.10, it is necessary to establish the force-displacement relationship for the beam-column element. Therefore, the continuous displacements are to be written in terms of nodal displacements at the ends and the integration is carried out throughout the length of the element. Figure 2-4 shows a thin-walled space beam element with nodes A and B at the element ends.

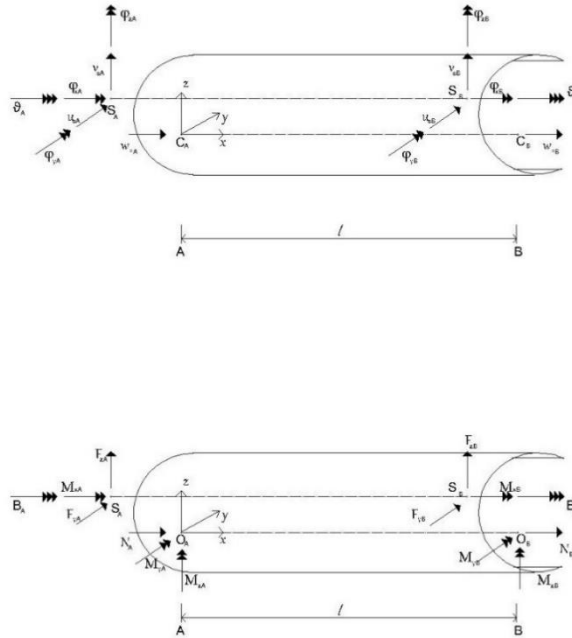


Figure 2-4. Thin-walled beam element: (a) nodal displacements and (b) nodal forces.

For any acceptable numerical formulation, the numerical solution must converge or tend to the exact solution of the problem, if the subdivision of the beam-column is made finer. It has been shown for the finite element formulation that under certain circumstances the displacement formulation provides an upper bound to the true stiffness of the beam-column and hence such a finite element formulation will converge to the exact displacement solution from below.

For the beam-column element the strain displacement relationship contains second derivatives in lateral displacements and twist and the first derivative in the axial displacement. Hence is necessary to choose the displacement function such that  $w_C$ ,  $u_S$ ,  $v_S$ ,  $\varphi_y = -\dot{v}_S$ ,  $\varphi_z = \dot{u}_S$  and  $\varphi_x$ ,  $\theta = -\dot{\varphi}_x$  must be continuous at the nodes. This can be achieved by adopting a linear displacement field for  $w_C$  and cubic displacement field for other degrees of freedom. Using the notation  $\langle \ \rangle$  for a row vector and  $[ \ ]$  for a column vector,  $u_S$  is written as:

$$u_S = \langle 1, x, x^2, x^3 \rangle \begin{bmatrix} \alpha_1 \\ \alpha_2 \\ \alpha_3 \\ \alpha_4 \end{bmatrix} \quad 2.17$$

$$\varphi_z = \dot{u}_S = \langle 0, 1, 2x, 3x^2 \rangle \begin{bmatrix} \alpha_1 \\ \alpha_2 \\ \alpha_3 \\ \alpha_4 \end{bmatrix}$$

Substituting the corresponding values of  $x$  at the ends A and B of the beam element shown in Figure 2-4, we get:

$$\begin{bmatrix} u_S^A \\ \varphi_z^A \\ u_S^B \\ \varphi_z^B \end{bmatrix} = \begin{pmatrix} 1 & 0 & 0 & 0 \\ 0 & 1 & 0 & 0 \\ 1 & l & l^2 & l^3 \\ 0 & 1 & 2l & 3l^2 \end{pmatrix} \begin{bmatrix} \alpha_1 \\ \alpha_2 \\ \alpha_3 \\ \alpha_4 \end{bmatrix} = (A_\alpha) \{ \alpha \} \quad 2.18$$

$$u_S = \langle 1, x, x^2, x^3 \rangle (A_\alpha)^{-1} \begin{bmatrix} u_S^A \\ \varphi_z^A \\ u_S^B \\ \varphi_z^B \end{bmatrix} = \langle n_u \rangle \{ \bar{u}_S \}$$

Where  $n_u$  is the cubic interpolation function given by:

$$\langle n_u \rangle = \left\langle \left( 1 - \frac{3x^2}{l^2} + \frac{2x^3}{l^3} \right), \left( x - \frac{2x^2}{l} + \frac{x^3}{l^2} \right), \left( \frac{3x^2}{l^2} - \frac{2x^3}{l^3} \right), \left( -\frac{x^2}{l} + \frac{x^3}{l^2} \right) \right\rangle \quad 2.19$$

And  $\{ \bar{u}_S \}$  the nodal displacement as:

$$\langle \bar{u}_S \rangle = \langle u_S^A, \varphi_z^A, u_S^B, \varphi_z^B \rangle \quad 2.20$$

Derivations for other quantities can be made in a similar manner.

$$\begin{aligned}
 \langle n_v \rangle &= \left\langle \left(1 - \frac{3x^2}{l^2} + \frac{2x^3}{l^3}\right), \left(-x + \frac{2x^2}{l} - \frac{x^3}{l^2}\right), \left(\frac{3x^2}{l^2} - \frac{2x^3}{l^3}\right), \left(\frac{x^2}{l} - \frac{x^3}{l^2}\right) \right\rangle \\
 \langle n_\varphi \rangle &= \left\langle \left(1 - \frac{3x^2}{l^2} + \frac{2x^3}{l^3}\right), \left(-x + \frac{2x^2}{l} - \frac{x^3}{l^2}\right), \left(\frac{3x^2}{l^2} - \frac{2x^3}{l^3}\right), \left(\frac{x^2}{l} - \frac{x^3}{l^2}\right) \right\rangle \\
 \langle n_w \rangle &= \left\langle \left(1 - \frac{x}{l}\right), \left(\frac{x}{l}\right) \right\rangle
 \end{aligned} \tag{2.21}$$

Finally, the displacement in an element is represented by the nodal displacements at the ends as:

$$\begin{aligned}
 u_S &= \langle n_u \rangle \{ \bar{u}_S \} \\
 v_S &= \langle n_v \rangle \{ \bar{v}_S \} \\
 \varphi_x &= \langle n_\varphi \rangle \{ \bar{\varphi}_x \} \\
 w_C &= \langle n_w \rangle \{ \bar{w}_C \}
 \end{aligned} \tag{2.22}$$

### 2.3.1 Elastic stiffness matrices

Total equilibrium equation for an elastic thin-walled beam-column element can now be obtained in terms of nodal displacements at the ends by substituting 2.22 in 2.16. The terms of 2.16 which form the elastic stiffness matrix are the following:

$$\int_0^l [\delta \dot{w}_C EA \dot{w}_C + \delta \dot{v}_S EI_y \dot{v}_S + \delta \dot{u}_S EI_z \dot{u}_S + \delta \dot{\varphi}_x GI_x \dot{\varphi}_x + \delta \dot{\varphi}_x EI_w \dot{\varphi}_x] dx \tag{2.23}$$

For example, the first term of the 2.23 can be written in matrix form as:

$$\begin{aligned}
 \int_0^l [\delta \dot{w}_C EA \dot{w}_C] dx &= EA \int_0^l [(\delta \dot{w}_C)^T (\dot{w}_C)] dx \\
 &= (\delta w_C)^T EA \int_0^l [(\dot{n}_w)^T (\dot{n}_w)] dx \cdot w_C \\
 &= (\delta w_C)^T EA \int_0^l \left[ \begin{bmatrix} -1 \\ 1 \end{bmatrix} \langle -1, 1 \rangle \right] dx \cdot w_C = (\delta w_C)^T \cdot k_E^w \cdot w_C
 \end{aligned} \tag{2.24}$$

Chapter 2

Where  $k_E^w$  is defined as:

$$k_E^w = \frac{EA}{l} \begin{pmatrix} 1 & -1 \\ -1 & 1 \end{pmatrix} \quad 2.25$$

In a similar manner we can proceed with the other contributions of the stiffness matrix:

$$\begin{aligned} \int_0^l [\delta \ddot{u}_S EI_z \ddot{u}_S] dx &= EI_z \int_0^l [(\delta \ddot{u}_S)^T (\ddot{u}_S)] dx \\ &= (\delta u_S)^T EI_z \int_0^l [(\ddot{n}_u)^T (\ddot{n}_u)] dx \cdot u_S = (\delta u_S)^T \cdot k_E^u \cdot u_S \end{aligned} \quad 2.26$$

$$k_E^u = EI_z \begin{pmatrix} \frac{12}{l^3} & \frac{6}{l^2} & -\frac{12}{l^3} & \frac{6}{l^2} \\ \frac{6}{l^2} & \frac{4}{l} & -\frac{6}{l^2} & \frac{2}{l} \\ -\frac{12}{l^3} & -\frac{6}{l^2} & \frac{12}{l^3} & -\frac{6}{l^2} \\ \frac{6}{l^2} & \frac{2}{l} & -\frac{6}{l^2} & \frac{4}{l} \end{pmatrix} \quad 2.27$$

$$\begin{aligned} \int_0^l [\delta \ddot{v}_S EI_y \ddot{v}_S] dx &= EI_y \int_0^l [(\delta \ddot{v}_S)^T (\ddot{v}_S)] dx \\ &= (\delta v_S)^T EI_y \int_0^l [(\ddot{n}_v)^T (\ddot{n}_v)] dx \cdot v_S = (\delta v_S)^T \cdot k_E^v \cdot v_S \end{aligned} \quad 2.28$$

$$k_E^v = EI_y \begin{pmatrix} \frac{12}{l^3} & -\frac{6}{l^2} & -\frac{12}{l^3} & -\frac{6}{l^2} \\ -\frac{6}{l^2} & \frac{4}{l} & \frac{6}{l^2} & \frac{2}{l} \\ -\frac{12}{l^3} & \frac{6}{l^2} & \frac{12}{l^3} & \frac{6}{l^2} \\ -\frac{6}{l^2} & \frac{2}{l} & \frac{6}{l^2} & \frac{4}{l} \end{pmatrix} \quad 2.29$$

$$\begin{aligned}
 & \int_0^l [\delta\dot{\varphi}_x GI_x \dot{\varphi}_x + \delta\dot{\varphi}_x EI_w \ddot{\varphi}_x] dx \\
 &= (\delta\varphi_x)^T \left\{ GI_x \int_0^l [(\dot{n}_\varphi)^T (\dot{n}_\varphi)] dx \right. \\
 & \quad \left. + EI_w \int_0^l [(\ddot{n}_\varphi)^T (\ddot{n}_\varphi)] dx \right\} \varphi_x = (\delta\varphi_x)^T \cdot k_E^\varphi \cdot \varphi_x
 \end{aligned} \tag{2.30}$$

$$k_E^\varphi = \begin{pmatrix} \frac{12EI_w}{l^3} + \frac{6GI_x}{5l} & -\frac{6EI_w}{l^2} - \frac{GI_x}{10} & -\frac{12EI_w}{l^3} - \frac{6GI_x}{5l} & -\frac{6EI_w}{l^2} - \frac{GI_x}{10} \\ -\frac{6EI_w}{l^2} - \frac{GI_x}{10} & \frac{4EI_w}{l} + \frac{2GI_x l}{15} & \frac{6EI_w}{l^2} + \frac{GI_x}{10} & \frac{2EI_w}{l} - \frac{GI_x l}{30} \\ -\frac{12EI_w}{l^3} - \frac{6GI_x}{5l} & \frac{6EI_w}{l^2} + \frac{GI_x}{10} & \frac{12EI_w}{l^3} + \frac{6GI_x}{5l} & \frac{6EI_w}{l^2} + \frac{GI_x}{10} \\ -\frac{6EI_w}{l^2} - \frac{GI_x}{10} & \frac{2EI_w}{l} - \frac{GI_x l}{30} & \frac{6EI_w}{l^2} + \frac{GI_x}{10} & \frac{4EI_w}{l} + \frac{2GI_x l}{15} \end{pmatrix} \tag{2.31}$$

Assembling 2.25, 2.27, 2.29 and 2.31 together, we obtain the elastic stiffness matrix  $K_E$ :

$$K_E = \begin{pmatrix} w_C^A & a & \cdot & \cdot & \cdot & \cdot & \cdot & \cdot & -a & \cdot & \cdot & \cdot & \cdot & \cdot & \cdot \\ u_S^A & \cdot & b1 & \cdot & \cdot & \cdot & c1 & \cdot & \cdot & -b1 & \cdot & \cdot & \cdot & c1 & \cdot \\ v_S^A & \cdot & \cdot & b2 & \cdot & -c2 & \cdot & \cdot & \cdot & -b2 & \cdot & \cdot & -c2 & \cdot & \cdot \\ \varphi_x^A & \cdot & \cdot & \cdot & d & \cdot & \cdot & -e & \cdot & \cdot & \cdot & -d & \cdot & \cdot & -e \\ \varphi_y^A & \cdot & \cdot & -c2 & \cdot & f2 & \cdot & \cdot & \cdot & \cdot & c2 & \cdot & g2 & \cdot & \cdot \\ \varphi_z^A & \cdot & c1 & \cdot & \cdot & \cdot & f1 & \cdot & -c1 & \cdot & \cdot & \cdot & \cdot & g1 & \cdot \\ \theta^A & \cdot & \cdot & \cdot & -e & \cdot & \cdot & h & \cdot & \cdot & \cdot & \cdot & \cdot & \cdot & i \\ w_C^B & -a & \cdot & \cdot & \cdot & \cdot & \cdot & \cdot & a & \cdot & \cdot & \cdot & \cdot & \cdot & \cdot \\ u_S^B & \cdot & -b1 & \cdot & \cdot & \cdot & -c1 & \cdot & \cdot & b1 & \cdot & \cdot & \cdot & -c1 & \cdot \\ v_S^B & \cdot & \cdot & -b2 & \cdot & c2 & \cdot & \cdot & \cdot & \cdot & b2 & \cdot & c2 & \cdot & \cdot \\ \varphi_x^B & \cdot & \cdot & \cdot & -d & \cdot & \cdot & \cdot & \cdot & \cdot & \cdot & d & \cdot & \cdot & e \\ \varphi_y^B & \cdot & \cdot & \cdot & \cdot & -c2 & \cdot & g2 & \cdot & \cdot & \cdot & \cdot & c2 & \cdot & f2 \\ \varphi_z^B & \cdot & c1 & \cdot & \cdot & \cdot & g1 & \cdot & \cdot & -c1 & \cdot & \cdot & \cdot & f1 & \cdot \\ \theta^B & \cdot & \cdot & \cdot & -e & \cdot & \cdot & i & \cdot & \cdot & \cdot & e & \cdot & \cdot & h \end{pmatrix} \tag{2.32}$$

Where

$$\begin{aligned}
a &= \frac{EA}{l}; & b1 &= \frac{12EI_z}{l^3}; & b2 &= \frac{12EI_y}{l^3}; & c1 &= \frac{6EI_z}{l^2}; & c2 &= \frac{6EI_y}{l^2}; \\
d &= \frac{12EI_w}{l^3} + \frac{6GI_x}{5l}; & e &= \frac{6EI_w}{l^2} + \frac{GI_x}{10}; & f1 &= \frac{4EI_z}{l}; & f2 &= \frac{4EI_y}{l}; \\
g1 &= \frac{2EI_z}{l}; & g2 &= \frac{2EI_y}{l}; & h &= \frac{4EI_w}{l} + \frac{2GI_x l}{15}; & i &= \frac{2EI_w}{l} - \frac{GI_x l}{30};
\end{aligned} \tag{2.33}$$

### 2.3.2 Geometric stiffness matrix

First we need to define the internal forces for the nodes of the beam element as follow (see Figure 2-4):

$$\begin{aligned}
N &= -N_A = N_B; & F_y &= -F_{yA} = F_{yB} = -\frac{1}{l}(M_{zA} + M_{zB}); \\
F_z &= -F_{zA} = F_{zB} = \frac{1}{l}(M_{yA} + M_{yB}); & M_y &= -M_{yA} - F_{zA}x \\
&= -M_{yA}\left(1 - \frac{x}{l}\right) + M_{yB}\frac{x}{l} \\
M_z &= -M_{zA} + F_{yA}x = -M_{zA}\left(1 - \frac{x}{l}\right) + M_{zB}\frac{x}{l}; & M_x &= -M_{xA} = M_{xB}; \\
B &= -B_A = B_B; & \bar{K} &= (N\alpha_x + M_y\alpha_y + M_z\alpha_z + B\alpha_\omega) = \\
&= N\alpha_x + \left[-M_{yA}\left(1 - \frac{x}{l}\right) + M_{yB}\frac{x}{l}\right]\alpha_y + \left[-M_{zA}\left(1 - \frac{x}{l}\right) + M_{zB}\frac{x}{l}\right]\alpha_z \\
&\quad + B_B\alpha_\omega
\end{aligned} \tag{2.34}$$

Then, applying the same method of the elastic stiffness matrix, we can deduce the geometric stiffness matrix from the other components of the strain energy. The terms are the following:

$$\begin{aligned}
\int_0^l \{ & N[\delta\dot{w}_C\dot{w}_C + \delta\dot{u}_S\dot{u}_S + \delta\dot{u}_S z_S \dot{\phi}_x + \delta\dot{v}_S\dot{v}_S - \delta\dot{v}_S y_S \dot{\phi}_x + \delta\dot{\phi}_x z_S \dot{u}_S \\
& - \delta\dot{\phi}_x y_S \dot{v}_S] + F_y[\delta\dot{v}_S\dot{\phi}_x + \delta\dot{\phi}_x \dot{v}_S] - F_z[\delta\dot{u}_S\dot{\phi}_x + \delta\dot{\phi}_x \dot{u}_S] \\
& - M_y[\delta\dot{u}_S\dot{\phi}_x + \delta\dot{\phi}_x \dot{u}_S] - M_z[\delta\dot{v}_S\dot{\phi}_x + \delta\dot{\phi}_x \dot{v}_S] \\
& + \bar{K}[\delta\dot{\phi}_x \dot{\phi}_x] \} dx
\end{aligned} \tag{2.35}$$

Splitting the strain energy for each stress, we have:

$$\begin{aligned}
 & \int_0^l N[\delta \dot{w}_C \dot{w}_C + \delta \dot{u}_S \dot{u}_S + \delta \dot{u}_S z_S \dot{\phi}_x + \delta \dot{v}_S \dot{v}_S - \delta \dot{v}_S y_S \dot{\phi}_x + \delta \dot{\phi}_x z_S \dot{u}_S \\
 & \quad - \delta \dot{\phi}_x y_S \dot{v}_S] dx = \\
 N_B & \left[ \delta w_C \int_0^l [(\dot{n}_w)^T (\dot{n}_w)] dx \cdot w_C + \delta u_S \int_0^l [(\dot{n}_u)^T (\dot{n}_u)] dx \cdot u_S \right. \\
 & \quad + \delta u_S z_S \int_0^l [(\dot{n}_u)^T (\dot{n}_\phi)] dx \cdot \phi_x + \delta v_S \int_0^l [(\dot{n}_v)^T (\dot{n}_v)] dx \quad 2.36 \\
 & \quad \cdot v_S - \delta v_S y_S \int_0^l [(\dot{n}_v)^T (\dot{n}_\phi)] dx \cdot \phi_x \\
 & \quad + \delta \phi_x z_S \int_0^l [(\dot{n}_\phi)^T (\dot{n}_u)] dx \cdot u_S \\
 & \quad \left. - \delta \phi_x y_S \int_0^l [(\dot{n}_\phi)^T (\dot{n}_v)] dx \cdot v_S \right]
 \end{aligned}$$

$$\begin{aligned}
 & \int_0^l F_y [\delta \dot{v}_S \phi_x + \delta \phi_x \dot{v}_S] dx \\
 & \quad = -\frac{1}{l} (M_{zA} + M_{zB}) \left[ \delta v_S \int_0^l [(\dot{n}_v)^T (n_\phi)] dx \cdot \phi_x \quad 2.37 \right. \\
 & \quad \left. + \delta \phi_x \int_0^l [(n_\phi)^T (\dot{n}_v)] dx \cdot v_S \right]
 \end{aligned}$$

$$\begin{aligned}
 & \int_0^l -F_z [\delta \dot{u}_S \phi_x + \delta \phi_x \dot{u}_S] dx \\
 & \quad = -\frac{1}{l} (M_{yA} + M_{yB}) \left[ \delta u_S \int_0^l [(\dot{n}_u)^T (n_\phi)] dx \cdot \phi_x \quad 2.38 \right. \\
 & \quad \left. + \delta \phi_x \int_0^l [(n_\phi)^T (\dot{n}_u)] dx \cdot u_S \right]
 \end{aligned}$$

$$\begin{aligned}
 & \int_0^l -M_y [\delta \dot{u}_S \dot{\phi}_x + \delta \dot{\phi}_x \dot{u}_S] dx = \\
 & \quad = \left[ -M_{yA} \left(1 - \frac{x}{l}\right) + M_{yB} \frac{x}{l} \right]_0^l \left[ \delta u_S \int_0^l [(\dot{n}_u)^T (\dot{n}_\phi)] dx \cdot \phi_x \quad 2.39 \right. \\
 & \quad \left. + \delta \phi_x \int_0^l [(\dot{n}_\phi)^T (\dot{n}_u)] dx \cdot u_S \right]
 \end{aligned}$$

$$\begin{aligned}
 & \int_0^l -M_z[\delta v_S \dot{\varphi}_x + \delta \dot{\varphi}_x v_S] dx = \\
 & = \left[ -M_{zA} \left(1 - \frac{x}{l}\right) + M_{zB} \frac{x}{l} \right]_0^l \left[ \delta v_S \int_0^l [(\dot{n}_v)^T (\dot{n}_\varphi)] dx \cdot \varphi_x \right. \\
 & \quad \left. + \delta \varphi_x \int_0^l [(\dot{n}_\varphi)^T (\dot{n}_v)] dx \cdot v_S \right]
 \end{aligned} \tag{2.40}$$

$$\begin{aligned}
 & \int_0^l \bar{K} [\delta \dot{\varphi}_x \dot{\varphi}_x] dx = \left[ N \alpha_x + \left[ -M_{yA} \left(1 - \frac{x}{l}\right) + M_{yB} \frac{x}{l} \right] \alpha_y \right. \\
 & \quad \left. + \left[ -M_{zA} \left(1 - \frac{x}{l}\right) + M_{zB} \frac{x}{l} \right] \alpha_z \right. \\
 & \quad \left. + B_B \alpha_\omega \right] \left[ \delta \varphi_x \int_0^l [(\dot{n}_\varphi)^T (\dot{n}_\varphi)] dx \cdot \varphi_x \right]
 \end{aligned} \tag{2.41}$$

Assembling from 2.36 to 2.41, we obtain the geometric stiffness matrix  $K_G$ :

$$K_G = \begin{pmatrix} w_C^A & a & \cdot & \cdot & \cdot & \cdot & \cdot & -a & \cdot & \cdot & \cdot & \cdot & \cdot & \cdot \\ u_S^A & \cdot & b & \cdot & c & \cdot & e & f & \cdot & -b & \cdot & c1 & \cdot & e & f1 \\ v_S^A & \cdot & \cdot & b & d & -e & \cdot & g & \cdot & \cdot & -b & d1 & -e & \cdot & g1 \\ \varphi_x^A & \cdot & c & d & h & i & j & k & \cdot & -c & -d & -h & i1 & j1 & k1 \\ \varphi_y^A & \cdot & \cdot & -e & i & b1 & \cdot & m & \cdot & \cdot & e & -i & b2 & \cdot & n \\ \varphi_z^A & \cdot & e & \cdot & j & \cdot & b1 & m1 & \cdot & -e & \cdot & -j & \cdot & b2 & n1 \\ \theta^A & \cdot & f & g & k & m & m1 & h1 & \cdot & -f & -g & -k & n2 & n3 & h3 \\ w_C^B & -a & \cdot & \cdot & \cdot & \cdot & \cdot & \cdot & a & \cdot & \cdot & \cdot & \cdot & \cdot & \cdot \\ u_S^B & \cdot & -b & \cdot & -c & \cdot & -e & -f & \cdot & b & \cdot & -c1 & \cdot & -e & -f1 \\ v_S^B & \cdot & \cdot & -b & -d & e & \cdot & -g & \cdot & \cdot & b & -d1 & e & \cdot & -g1 \\ \varphi_x^B & \cdot & c1 & d1 & -h & -i & -j & -k & \cdot & -c1 & -d1 & h & -i1 & -j1 & -k1 \\ \varphi_y^B & \cdot & \cdot & -e & i1 & b2 & \cdot & n2 & \cdot & \cdot & e & -i1 & b1 & \cdot & m2 \\ \varphi_z^B & \cdot & e & \cdot & j1 & \cdot & b2 & n3 & \cdot & -e & \cdot & -j1 & \cdot & b1 & m3 \\ \theta^B & \cdot & f1 & g1 & k1 & n & n1 & h3 & \cdot & -f1 & -g1 & -k1 & m2 & m3 & h4 \end{pmatrix} \tag{2.42}$$

Where

$$a = \frac{N_B}{l}; \quad b = \frac{6 N_B}{5 l}; \quad b1 = \frac{2}{15} N_B l; \quad b2 = -\frac{N_B l}{30}; \tag{2.43}$$

$$\begin{aligned}
 c &= \frac{6 N_B}{5 l} z_S + \frac{11 M_{yA} - M_{yB}}{10 l}; & c1 &= -\frac{6 N_B}{5 l} z_S - \frac{M_{yA} - 11 M_{yB}}{10 l}; \\
 d &= -\frac{6 N_B}{5 l} y_S + \frac{11 M_{zA} - M_{zB}}{10 l}; & d1 &= \frac{6 N_B}{5 l} y_S - \frac{M_{zA} - 11 M_{zB}}{10 l}; \\
 e &= \frac{N_B}{10}; & f &= -\frac{N_B}{10} z_S - \frac{M_{yA}}{10}; & f1 &= -\frac{N_B}{10} z_S + \frac{M_{yB}}{10}; & g &= \frac{N_B}{10} y_S - \frac{M_{zA}}{10} \\
 & & g1 &= \frac{N_B}{10} y_S + \frac{M_{zB}}{10}; \\
 h &= \frac{6 N_B}{5 l} \alpha_x + \frac{3 (M_{yB} - M_{yA})}{5 l} \alpha_y + \frac{3 (M_{zB} - M_{zA})}{5 l} \alpha_z + \frac{6 B_B}{5 l} \alpha_\omega \\
 h1 &= \frac{2}{15} N_B \alpha_x l - \frac{(3 M_{yA} - M_{yB}) l}{30} \alpha_y - \frac{(3 M_{zA} - M_{zB}) l}{30} \alpha_z + \frac{2}{15} B_B \alpha_\omega l \\
 h2 &= \frac{1}{30} N_B \alpha_x l - \frac{(3 M_{yA} - M_{yB}) l}{60} \alpha_y - \frac{(3 M_{zA} - M_{zB}) l}{60} \alpha_z + \frac{2}{15} B_B \alpha_\omega l \\
 h3 &= -\frac{1}{30} N_B \alpha_x l + \frac{(M_{yA} - M_{yB}) l}{60} \alpha_y + \frac{(M_{zA} - M_{zB}) l}{60} \alpha_z - \frac{1}{30} B_B \alpha_\omega l \\
 h4 &= \frac{2}{15} N_B \alpha_x l - \frac{(M_{yA} - 3 M_{yB}) l}{30} \alpha_y - \frac{(M_{zA} - 3 M_{zB}) l}{30} \alpha_z + \frac{2}{15} B_B \alpha_\omega l \\
 i &= \frac{N_B}{10} y_S + \frac{M_{zA}}{10} + \frac{M_{zB}}{5}; & i1 &= \frac{N_B}{10} y_S - \frac{M_{zA}}{5} - \frac{M_{zB}}{10}; & j & \\
 & & &= \frac{N_B}{10} z_S - \frac{M_{yA}}{10} - \frac{M_{yB}}{5}; \\
 j1 &= \frac{N_B}{10} z_S + \frac{M_{yA}}{5} + \frac{M_{yB}}{10}; & k &= -\frac{N_B}{10} \alpha_x - \frac{M_{yB}}{10} \alpha_y - \frac{M_{zB}}{10} \alpha_z - \frac{B_B}{10} \alpha_\omega; \\
 k1 &= -\frac{N_B}{10} \alpha_x + \frac{M_{yA}}{10} \alpha_y + \frac{M_{zA}}{10} \alpha_z - \frac{B_B}{10} \alpha_\omega; & m & \\
 & & &= -\frac{2}{15} N_B y_S l + \frac{(3 M_{zA} - M_{zB}) l}{30}; \\
 m1 &= -\frac{2}{15} N_B z_S l - \frac{(3 M_{yA} - M_{yB}) l}{30}; & m2 &= -\frac{2}{15} N_B y_S l + \frac{(M_{zA} - 3 M_{zB}) l}{30}; \\
 m3 &= -\frac{2}{15} N_B z_S l - \frac{(M_{yA} - 3 M_{yB}) l}{30}; & n &= \frac{1}{30} N_B y_S l - \frac{M_{zA} l}{30}; \\
 n1 &= \frac{1}{30} N_B z_S l + \frac{M_{yA} l}{30}; & n2 &= \frac{1}{30} N_B y_S l + \frac{M_{zB} l}{30}; & n3 &= \frac{1}{30} N_B z_S l - \frac{M_{yB} l}{30}
 \end{aligned}$$

## Chapter 2

.

## Chapter 3 Warping influence in steel storage pallet racks

As already mentioned in Chapter 1, in logistic field goods and products are stored in pallet racks (mainly, adjustable and drive-in pallet racks), i.e. in structural framed systems made of components manufactured from cold forming steel coils ([34], [35], [36]). As it can be noted from Figure 3-1, adjustable pallets racks (in the following simply indicated as racks) are composed by a regular sequence of upright frames, i.e. built-up laced members. They are connected to each other in the down-aisle (longitudinal) direction by pairs of horizontal beams sustaining pallet units, which generally have boxed cross-section. The structural system is braced by the upright frames in the cross-aisle direction (transversal) but the need to optimize the rack performances in terms of stored pallet units should hamper to locate bracing systems in the down-aisle direction. In these cases, stability to lateral loads is hence provided by the sole degree of flexural continuity associated with the beam-to-column joints and the base-plate connections.

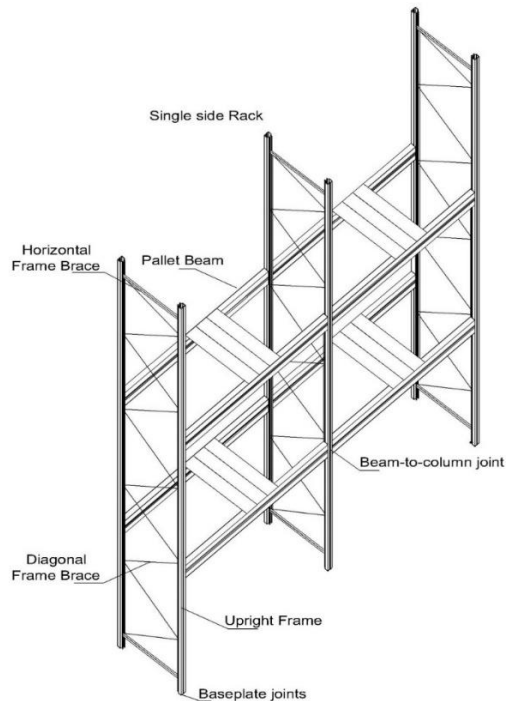
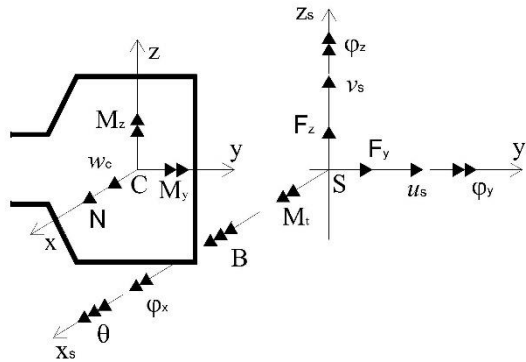


Figure 3-1. Typical-adjustable pallet rack configuration and key rack components.

Otherwise, if it is possible to locate longitudinal vertical bracings, the semi-continuous braced frame model has to be considered for design. Other key elements of the structural system are the columns (uprights), which have in many cases mono-symmetric lipped channel cross-sections (Figure 3-3), generally completed by additional lips located at the end of the rear flanges used to bolt, or to weld, lacings to uprights. Uprights are oriented to have their symmetry axis parallel to the cross-aisle direction and the shear center of the cross-section (point *S* in Figure 3-2) is never coincident with its centroid (point *C*).



**Figure 3-2. Nodal displacements and internal forces and moments for a 7DOFs beam element.**

Routine rack design, also in case of complex warehouses, is currently developed neglecting all the aspects associated with non-uniform torsion, mainly because no practical indications arise from researchers on this topic. No significant studies have been up-to-now developed to investigate the influence of warping effects on pallet rack response, despite the fundamental need to guarantee a safe design. Design provisions have been very recently updated for Europe ([2], [3]), for United States [4] and for Australia and New Zealand [5], but practical indications on the key rules to adopt for the numerical analysis, as well as on the minimum requirements of the FE analysis software, are completely omitted in these Codes. As a consequence, the verification checks actually adopted for serviceability and ultimate limit states are incorrect, being based on values of internal action and moments and displacements deriving from traditional FE analysis programs with 6DOFs beam element. This should lead to a very unsafe design but no indications are available to quantify the effective degree of reliability of a design carried out assuming these incorrect assumptions for mono-symmetric cross-section members.

This research, which regards other racks configurations, is focused on the resistance checks and presents main outcomes of a numerical analysis on medium-rise racks. Two different beam formulations have been considered in order to appraise the differences in the internal forces and moments due to the presence of the 7<sup>th</sup> degree of freedom. The complete research can be found in [37].

### 3.1 Design rules for rack uprights

Attention is focused on the resistance verification checks. Reference is made to the contents of the European design rules for steel structures (EC3), which have been prevalently developed with reference to the cases of members having cross-section with two axes of symmetry. In part 1-1 of EC3 [14], which regards the general rules and the rules for building, the non-coincidence between the shear center and the centroid of the cross-section is ignored and the verification checks of beam-columns are mainly referred to bisymmetric I-shaped and hollow cross-sections. As to resistance check, a very general yield criterion is proposed in European as well as in the other steel codes for the elastic verification. With reference to the critical point of the cross-section, the following condition has to fulfil:

$$\left(\frac{\sigma_{x,Ed}}{f_{y,EU1}}\right)^2 + \left(\frac{\sigma_{z,Ed}}{f_{y,EU1}}\right)^2 - \left(\frac{\sigma_{x,Ed}}{f_{y,EU1}}\right) \cdot \left(\frac{\sigma_{z,Ed}}{f_{y,EU1}}\right) + 3 \cdot \left(\frac{\tau_{Ed}}{f_{y,EU1}}\right)^2 \leq 1 \quad 3.1$$

where  $\sigma_{x,Ed}$  and  $\sigma_{z,Ed}$  are the design value of the local longitudinal and transverse stress respectively,  $\tau_{Ed}$  is the design value of the local shear stress and  $f_{y,EU1}$  represents the design yielding stress (i.e. the value of the yielding stress divided by the material safety factor associated with the considered code).

It should be noted that it is clearly recommended in [14] to take into account the stresses due to torsion in 3.1 and, in particular:

- the shear stress  $\tau_{Ed}$  has to include the contribution  $\tau_{t,Ed}$  due to the St. Venant torsion  $T_{t,Ed}$  and  $\tau_{w,Ed}$  due to the warping torsion  $T_{w,Ed}$ ;
- the normal stress  $\sigma_{x,Ed}$  has to include  $\sigma_{w,Ed}$  due to the bimoment  $B_{Ed}$ .

No practical indications are provided to engineers for the correct evaluation of stresses  $\tau_{t,Ed}$  and  $\sigma_{w,Ed}$ , which usually can require very complex computations due to the complex rack upright geometry (Figure 3-3). Furthermore, a conservative approximation for all the cross-section classes is proposed in this code: in cases of cross-sections subjected to axial load ( $N_{Ed}$ ) and bending moments along principal axes ( $M_{y,Ed}$  and  $M_{z,Ed}$ ) it is required that:

$$\frac{N_{Ed}}{N_{Rd,EU1}} + \frac{M_{y,Ed}}{M_{y,Rd,EU1}} + \frac{M_{z,Ed}}{M_{z,Rd,EU1}} \leq 1 \quad 3.2$$

where  $N_{Rd}$ ,  $M_{y,Rd}$  and  $M_{z,Rd}$  are the design values of the resistance depending on the cross section classification and subscript EU1 indicates the accordance with design procedure of ref. [14].

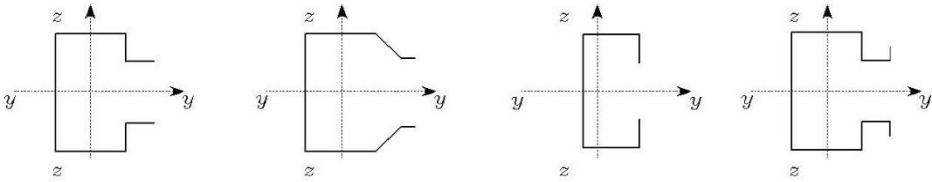


**Figure 3-3 - Examples of cross-section for uprights in adjustable pallet racks.**

As to cold formed members, which are considered in part 1-3 of EC3 [16], it should be noted that very general statements are provided with regard to the possible influence of torsional moments. The direct stresses ( $\sigma_{N,Ed}$ ) due to the axial force  $N_{Ed}$ , and the ones ( $\sigma_{M_y,Ed}$  and  $\sigma_{M_z,Ed}$ ), associated with bending moments  $M_{y,Ed}$  and  $M_{z,Ed}$ , respectively, should be based on the relative effective cross-sections. Properties of the gross cross-section have to be considered to evaluate the shear stresses  $\tau$  due to transverse shear forces,  $\tau_{F_y,Ed}$  and  $\tau_{F_z,Ed}$ , the shear stresses due to uniform torsion,  $\tau_{t,Ed}$ , and both the normal,  $\sigma_{w,Ed}$ , and shear stresses,  $\tau_{w,Ed}$ , due to warping. Owing to the need to reduce the parameters influencing the outcomes of this study, only class 3 profiles are herein considered, for which the effective and the gross cross-sections are coincident.

The total direct stress  $\sigma_{tot,Ed}$  and the total shear stress  $\tau_{tot,Ed}$  must be respectively obtained as:

$$\sigma_{tot,Ed} = \sigma_{N,Ed} + \sigma_{M_y,Ed} + \sigma_{M_z,Ed} + \sigma_{w,Ed} \quad 3.3$$

$$\tau_{tot,Ed} = \tau_{F_y,Ed} + \tau_{F_z,Ed} + \tau_{t,Ed} + \tau_{w,Ed} \quad 3.4$$

In cross-sections subject to torsion, it is required that the following conditions have to be satisfied:

$$\begin{aligned} \sigma_{tot,Ed} &\leq f_{ya,EU3} \\ \tau_{tot,Ed} &\leq \frac{f_{ya,EU3}}{\sqrt{3}} \\ \sqrt{\sigma_{tot,Ed}^2 + 3\tau_{tot,Ed}^2} &\leq 1.1 \cdot f_{ya,EU3} \end{aligned} \quad 3.5$$

where  $f_{ya,EU3}$  is the increased average yield strength due to the forming process and subscript EU3 indicates that reference has to be done to the design safety factor of ref. [16].

European engineers base the rack design on EN15512 [2], which declares clearly that pallet racks are standard products for which design by calculation alone may not be appropriate. Only the expression to evaluate torsional and flexural-torsional buckling load of isolated members are directly presented [2]. Current design practice neglects hence warping for both analysis as well as verification checks and this could lead to a very non-conservative design. Only the very recent Australian standards [5] includes a more adequate resistance check criteria for mono-symmetric profiles. In particular, in case of uprights, the section capacity requirement must include also the contribution due to bi-moment ( $B_{Ed}$ ) acting on the cross-section. It is required that:

$$\frac{N_{Ed}}{N_{Rd,AS}} + \frac{M_{y,Ed}}{M_{y,Rd,AS}} + \frac{M_{z,Ed}}{M_{z,Rd,AS}} + \frac{B_{Ed}}{B_{Rd,AS}} \leq 1 \quad 3.6$$

where subscript AS indicates that the cross-section resistance is evaluated in accordance with the design philosophy of ref [5] and  $B_{Rd,AS}$  is the bimoment section capacity defined as:

$$B_{Rd,AS} = \frac{I_w}{\omega_{max}} f_{y,AS} \quad 3.7$$

where  $I_w$  is the warping constant and  $\omega_{max}$  is the maximum value of the static moment of the sectorial area.

### 3.2 The considered rack frames

In order to appraise the warping influence on the resistance check, attention has been focused on typical medium-rise rack configurations. This study, which comprised of structural analyses and design verifications, has been carried out by considering the following key parameters:

1. the frame geometry (Figure 3-4): two racks differing for their inter-story height (h) and overall height (H) were considered:
  - a. rack M\_5 is characterized by 5 stories with h = 1.20 m and H = 6.13 m;

b. rack M\_4 is characterized by 4 stories with  $h = 1.80$  m and  $H = 7.33$  m.

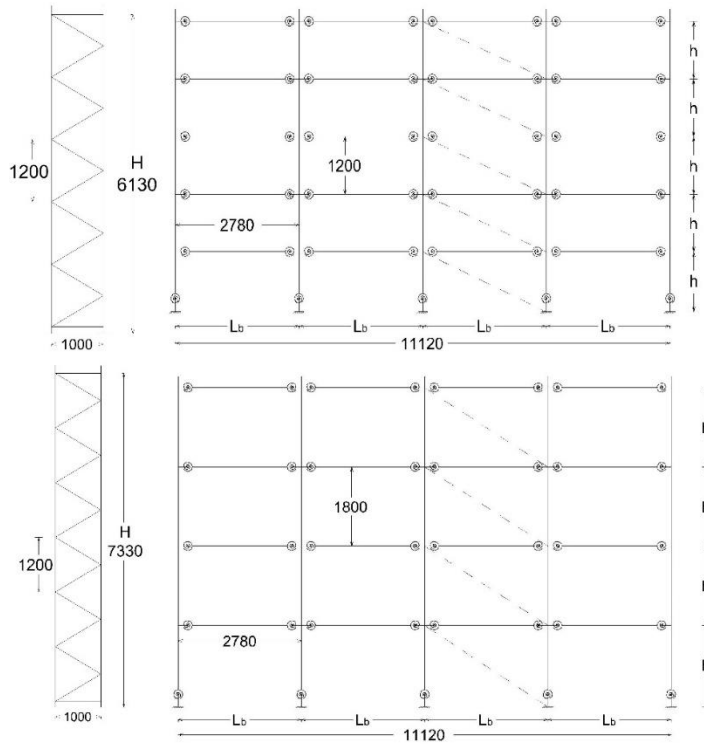


**Figure 3-4 - Geometry of M\_5 and M\_4 racks (all dimension are in millimeters): D-brace upright frame (cross-aisle direction) and semi-continuous frames models (down-aisle direction).**

For both frames, a 5 equal bay rack configuration (bay span of 2.78 m) was considered. Only the case of *D*-brace upright frame (Figure 3-4), with alternate tension or compression diagonals, was included in this study with a panel height of 1.20 m, owing to the very limited influence of the type as well as of the height of the upright frame panel, as demonstrated in a previous research of one of the authors [20]. As to the rack components, they have been selected with reference to the most common adopted solutions. Upright cross-section is presented in Figure 3-5, while rectangular hollow sections have been considered for the upright lacings (30x30x3mm) and for the beams (100x50x3mm).

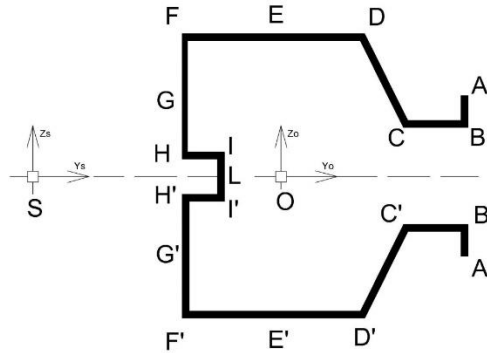


**Figure 3-5 - The upright cross-section of the considered racks.**

An overall frame imperfection equal to 3 mrad in terms of out-of-plumb of the uprights in both the cross-aisle and the down-aisle directions has been considered contemporaneously, which has been simulated via horizontal forces concentrated on each load level;

2. the frame typology: for each frame both the cases of unbraced (UNBR) and braced (BR) frames in the down-aisle direction were considered. In case of braced frames, in addition to the bracing in the vertical plane parallel to the main aisle of the rack (spine bracing), also a horizontal bracing has been located on each floor;
3. the degree of flexural stiffness of beam-to-column joints: attention was focused on semi-rigid beam-to-column joints of interest for practical application in rack routine. Considering the elastic rotational stiffness  $S_j$  of beam-to-column joints, reference was made to the classification criteria of EC3 1-8 [38]. In particular, the selected values of stiffness  $S_j$  have been defined as multiple (by means of term  $\rho$ ) of a reference stiffness,  $S_j^{EC3-LB}$ , as:

$$S_j = \rho \cdot S_j^{EC3-LB} \quad 3.8$$

where  $S_j^{EC3-LB}$  is the stiffness corresponding to the transition between flexible and semi-rigid joint domains, defined by the code as:

$$S_j^{EC3-LB} = 0.5 \frac{EI_b}{L_b} \quad 3.9$$

where  $E$  is the Young modulus,  $I_b$  the second moment of area of beam section,  $L_b$  the beam length and  $\rho$  is the stiffness parameter which has been considered, in the present study, ranging from 0.67 to 13.10, as it appears from Figure 3-6 where they are plotted in the moment ( $M$ ) - rotation ( $\phi$ ) reference system, together with the upper limit of the semi-rigid domain associated with both unbraced ( $\rho = 50$ ) and braced frames ( $\rho = 16$ ). All the considered values of joint stiffness, which are typical of the possible configurations of beam-to-column joints associated with the considered upright (Figure 3-5), have been deduced by test reports related to beam-to-column joint tests executed in accordance with ref. [2].

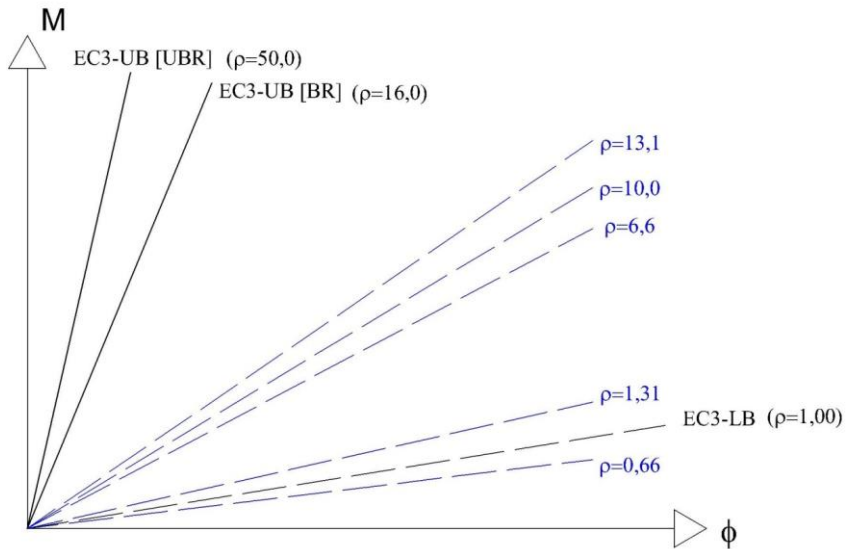


**Figure 3-6 - Rotational stiffness of the beam-to-column joints considered in the analysis (dashed lines).**

4. the load condition (Figure 3-7): rack bays have been considered directly loaded by pallets and a uniform distributed load acting on each beam was assumed. Four different load conditions have been identified as representative for rack design:
  - a. fully loaded condition, i.e. each bay is loaded (in the following indicated as S1);
  - b. alternate loaded condition giving rise to single curvature on uprights when the rack is braced (S2);
  - c. external bays only loaded on each load levels (S3);

- d. full load on the rack with the exception of few lowest beam level, near the middle of the racks (S4), as indicated in Figure 3-7. It should be noted that S1 and S4 load conditions are recommended also by rack standard codes, while the other ones have been identified on the basis of the expertise of the authors in rack design.

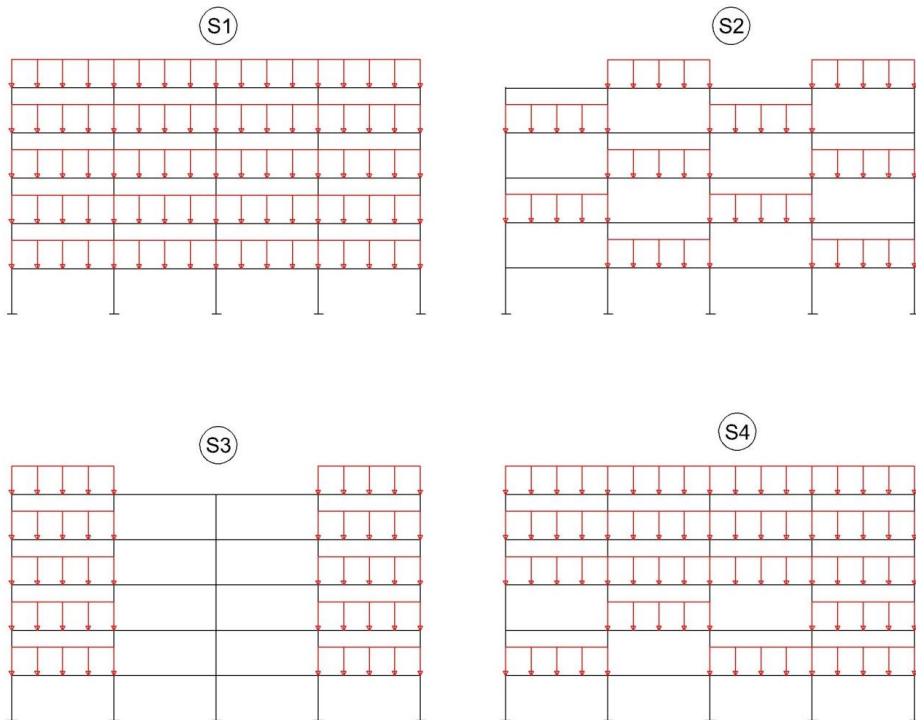


Figure 3-7 - The considered load conditions for the parametric analysis.

The sole case of semi-rigid joints has been considered, owing to the need of limiting the number of variables influencing warping effects. The value of the base-plate joint stiffness corresponds to 0.11 and to 0.17 times the flexural upright stiffness ( $E \cdot I_u / L$ ) for M\_5 and M\_4 frames, respectively.

Finite element analysis has been executed by Śiva software: in addition to the beam element formulation including warping, i.e. the beam formulation with 7DOFs, Śiva's library offers also the more traditional beam element based on the classical 6DOFs beam formulation [39]. Both type of analysis, i.e. with 6DOFs and 7DOFs beam element formulations have been executed for all the considered rack frames. Warping restraint has been considered free for the upright top as well as for the bracing upright members, also

in correspondence of the intersection with upright. As to the end of beams, due to the available forms of end connectors, warping has been considered blocked. Owing to the different possibilities to connect the upright end to the industrial floor, i.e. due to the different types of available connections, both the cases of column base with warping totally prevented (-a) or free (-b) have been considered. Figure 3-8 presents the analyses layout explaining symbols used to present main research outcomes.

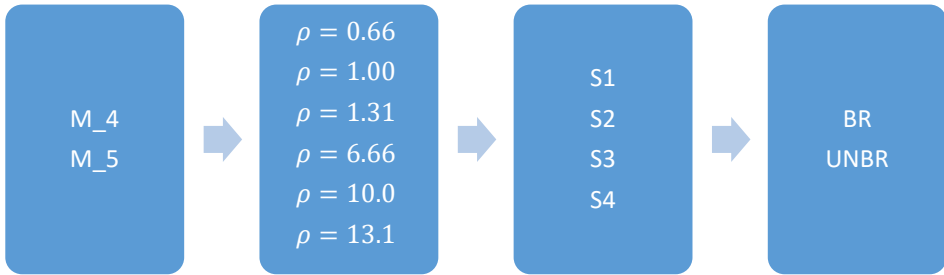


Figure 3-8. Summary of the parameters of the numerical analysis.

### 3.3 Warping influence: internal forces and moments

At first attention has been focused on the influence of the warping restraint at the column bases related to the 7DOFs beam analyses. Table 3-1 and Table 3-2 present the ratio of  $\frac{M_y^{7-a}}{M_y^{7-b}}$  and  $\frac{M_z^{7-a}}{M_z^{7-b}}$  between the bending moment ( $M_y^7$  or  $M_z^7$ ) obtained by considering prevented (\_a) or free (\_b) the column base warping. Mean value and standard deviation for all the racks under the same load conditions are reported in the tables together with the maximum (max) and the minimum (min) values of the ratio. These values are practically independent from the beam-to-column joint stiffness as well as from the location of the considered upright, i.e., internal (C.U.) or external (E.U.).

Table 3-1. Influence of the warping base restraint on  $M_y$  and  $M_z$  for  $M_5$  racks (\_a prevented; \_b free warping).

Rack $M_5$		UNBR				BR			
		C.U.		E.U.		C.U.		E.U.	
L.C.		$\frac{M_y^{7-a}}{M_y^{7-b}}$	$\frac{M_z^{7-a}}{M_z^{7-b}}$	$\frac{M_y^{7-a}}{M_y^{7-b}}$	$\frac{M_z^{7-a}}{M_z^{7-b}}$	$\frac{M_y^{7-a}}{M_y^{7-b}}$	$\frac{M_z^{7-a}}{M_z^{7-b}}$	$\frac{M_y^{7-a}}{M_y^{7-b}}$	$\frac{M_z^{7-a}}{M_z^{7-b}}$
		S1	mean	1.08	0.77	1.05	1.00	1.13	0.87
dev	0.14		0.07	0.07	0.07	0.07	0.11	0.04	0.13
min	0.77		0.55	0.91	0.71	0.92	0.50	0.94	1.00

Warping influence in steel storage pallet racks

	max	1.60	0.98	1.36	1.19	1.33	1.10	1.15	1.67
S2	mean	0.95	1.13	0.97	1.14	0.99	1.00	0.93	1.15
	dev	0.12	0.21	0.03	0.29	0.04	0.13	0.03	0.21
	min	0.61	0.67	0.89	0.50	0.88	0.67	0.83	0.80
	max	1.31	2.00	1.04	2.40	1.12	1.50	1.00	2.10
S3	mean	0.97	1.15	0.93	1.11	0.97	1.16	1.14	0.88
	dev	0.02	0.08	0.16	0.24	0.06	0.23	0.08	0.09
	min	0.89	1.00	0.62	0.50	0.73	0.50	0.96	0.50
	max	1.02	1.43	1.56	2.10	1.13	2.00	1.34	1.00
S4	mean	0.98	1.13	0.98	0.97	0.92	1.08	1.00	1.09
	dev	0.01	0.10	0.03	0.04	0.01	0.06	0.05	0.08
	min	0.96	0.90	0.86	0.80	0.90	1.00	0.92	0.90
	max	1.02	1.50	1.04	1.00	0.93	1.25	1.20	1.30

**Table 3-2. Influence of the warping base restraint on  $M_y$  and  $M_z$  for M\_4 racks ( \_a prevented; \_b free warping).**

Rack M_4		UNBR				BR			
		C.U.		E.U.		C.U.		E.U.	
L.C.		$\frac{M_y^{7,a}}{M_y^{7,b}}$	$\frac{M_z^{7,a}}{M_z^{7,b}}$	$\frac{M_y^{7,a}}{M_y^{7,b}}$	$\frac{M_z^{7,a}}{M_z^{7,b}}$	$\frac{M_y^{7,a}}{M_y^{7,b}}$	$\frac{M_z^{7,a}}{M_z^{7,b}}$	$\frac{M_y^{7,a}}{M_y^{7,b}}$	$\frac{M_z^{7,a}}{M_z^{7,b}}$
S1	mean	0.95	1.13	1.00	1.15	0.98	0.88	0.94	1.13
	dev	0.04	0.19	0.01	0.12	0.04	0.14	0.06	0.09
	min	0.77	0.80	0.96	0.91	0.87	0.50	0.72	1.00
	max	1.00	2.00	1.04	1.50	1.10	1.25	1.12	1.50
S2	mean	1.04	0.83	0.89	0.95	1.04	1.00	1.01	0.87
	dev	0.02	0.18	0.06	0.13	0.03	0.00	0.02	0.07
	min	1.00	0.50	0.65	0.72	0.95	1.00	0.95	0.67
	max	1.13	1.50	1.03	1.50	1.17	1.00	1.09	1.00
S3	mean	1.07	1.08	1.03	0.95	1.11	0.97	1.02	1.01
	dev	0.05	0.22	0.04	0.12	0.06	0.08	0.02	0.06
	min	1.00	0.50	1.00	0.67	1.00	0.67	0.97	0.83
	max	1.25	2.00	1.21	1.36	1.39	1.25	1.08	1.25
S4	mean	1.00	0.94	0.95	1.00	0.97	0.85	1.00	1.21
	dev	0.01	0.03	0.08	0.00	0.04	0.12	0.03	0.15
	min	0.99	0.88	0.60	1.00	0.80	0.50	0.88	1.00
	max	1.00	1.00	1.10	1.00	1.02	1.11	1.11	1.74

As it can be noted from Figure 3-9 and Figure 3-10, related respectively to the distribution of  $M_y$  and  $M_z$  bending moment ratios, the greatest values of the relative frequency are in correspondence of unity. Furthermore, the great dispersion for bending moment ratios confirms the relevant influence of the warping base restraints. No general conclusions seem possible on the basis of re-analysis of these ratios but the importance of a correct

### Chapter 3

base restraint modeling should be underlined, owing to the non-negligible influence on the values of internal forces and moments and, as a consequence, on design verifications.

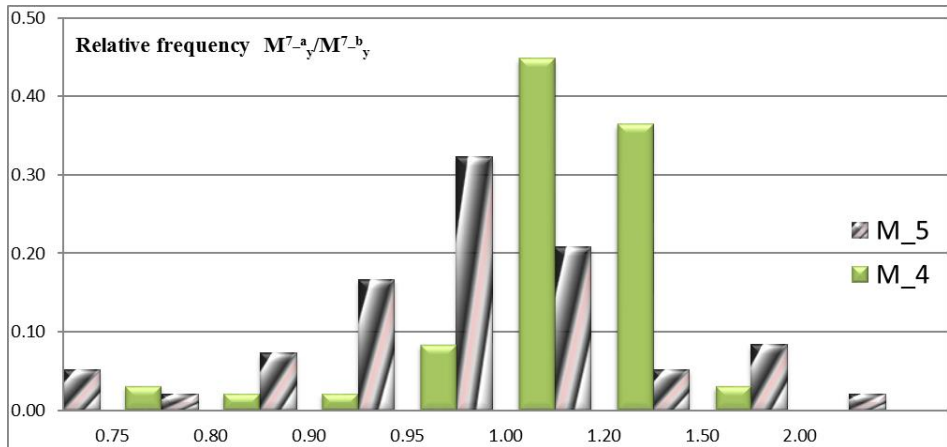


**Figure 3-9. Influence of the warping restraint at the base column on  $M_y$  (data related to both the more stressed C.U. and E.U.).**

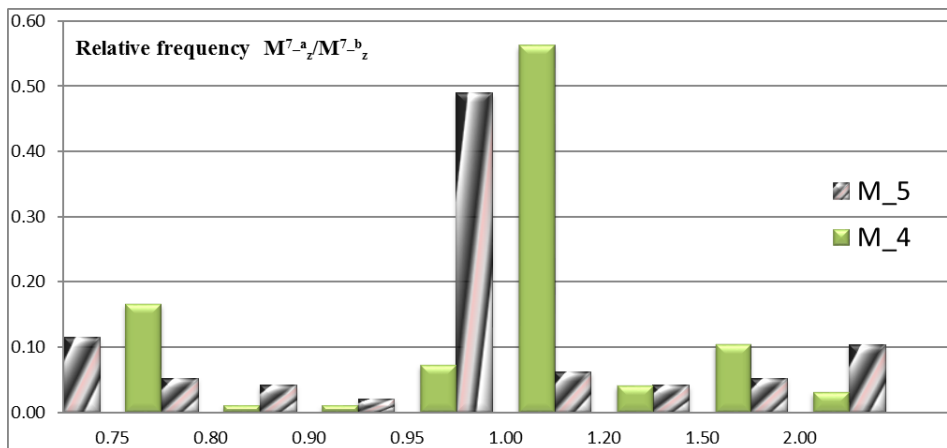


**Figure 3-10. Influence of the warping restraint at the base column on  $M_z$  (data related to both the more stressed C.U. and E.U.).**

Due to the differences in the stiffness matrices of 6DOFs and 7DOFs beam formulations, upright warping is expected to influence significantly the values of internal forces and moments and racks displacements. As to axial load ( $N$ ) no significant differences have been observed while influence of warping is non negligible for shear forces ( $F_y$  and  $F_z$ ), despite the fact that generally shear doesn't represent a parameter governing rack design, as shown in the following. As to bending moments  $M_y$  and  $M_z$ , a summary of the differences can be directly appraised via Table 3-3 and Table 3-4 related to  $\frac{M_y^7}{M_y^6}$  and  $\frac{M_z^7}{M_z^6}$

Warping influence in steel storage pallet racks

ratio, where data are grouped for each load condition. The mean value and the standard deviation of the ratio are reported, together with the maximum and minimum values of these ratios.

**Table 3-3. Influence of the warping on  $M_y$  and  $M_z$  for M\_5 racks.**

Rack M_5		UNBR				BR			
		C.U.		E.U.		C.U.		E.U.	
L.C.		$\frac{M_y^7}{M_y^6}$	$\frac{M_z^7}{M_z^6}$	$\frac{M_y^7}{M_y^6}$	$\frac{M_z^7}{M_z^6}$	$\frac{M_y^7}{M_y^6}$	$\frac{M_z^7}{M_z^6}$	$\frac{M_y^7}{M_y^6}$	$\frac{M_z^7}{M_z^6}$
		S1	mean	0.83	2.41	1.24	0.84	1.30	1.77
dev	0.06		0.58	0.07	0.11	0.15	0.69	0.12	0.07
min	0.56		0.70	0.94	0.29	0.34	0.15	1.04	0.34
max	1.22		7.05	1.53	1.48	1.86	6.75	2.08	1.10
S2	mean	1.28	3.32	1.71	0.94	1.12	1.53	1.04	1.44
	dev	0.12	0.71	0.11	0.33	0.04	0.28	0.04	0.31
	min	0.67	0.62	1.29	0.30	0.87	0.64	0.89	0.52
	max	2.07	6.53	2.18	4.16	1.37	3.15	1.32	3.62
S3	mean	1.80	1.10	1.51	0.66	0.96	3.13	1.14	1.57
	dev	0.27	0.12	0.12	0.07	0.05	0.80	0.07	0.15
	min	0.82	0.41	0.94	0.29	0.70	0.43	0.89	0.52
	max	2.82	1.67	2.23	1.10	1.22	6.99	1.73	2.27
S4	mean	1.00	1.44	1.00	3.79	1.09	0.49	0.98	2.54
	dev	0.02	0.06	0.02	0.61	0.04	0.04	0.03	0.27
	min	0.92	1.14	0.92	1.77	0.87	0.34	0.80	1.64
	max	1.08	1.72	1.17	8.36	1.25	0.59	1.13	3.42

**Table 3-4. Influence of the warping on  $M_y$  and  $M_z$  for M\_4 racks.**

Rack M_4		UNBR				BR			
		C.U.		E.U.		C.U.		E.U.	
L.C.		$\frac{M_y^7}{M_y^6}$	$\frac{M_z^7}{M_z^6}$	$\frac{M_y^7}{M_y^6}$	$\frac{M_z^7}{M_z^6}$	$\frac{M_y^7}{M_y^6}$	$\frac{M_z^7}{M_z^6}$	$\frac{M_y^7}{M_y^6}$	$\frac{M_z^7}{M_z^6}$
		S1	mean	2.03	2.93	0.98	7.15	1.36	0.80
dev	0.31		0.77	0.01	0.47	0.12	0.17	0.04	0.07
min	0.46		0.64	0.91	5.29	0.86	0.28	0.91	1.28
max	2.94		8.34	1.04	9.83	1.96	1.78	1.35	1.95
S2	mean	1.10	3.53	2.90	7.01	1.00	1.75	3.39	5.17
	dev	0.04	0.38	0.15	0.45	0.02	0.22	0.07	0.61
	min	0.93	2.69	2.08	4.20	0.84	0.67	3.00	2.18
	max	1.26	5.58	3.51	9.02	1.08	2.86	3.74	8.76
S3	mean	0.99	3.23	1.03	6.41	1.07	1.64	1.25	1.63
	dev	0.06	0.37	0.03	0.38	0.06	0.25	0.02	0.26
	min	0.67	2.55	0.88	5.58	0.78	0.63	1.10	0.52
	max	1.23	6.30	1.15	8.57	1.51	2.86	1.34	2.59

S4	mean	1.01	3.11	1.02	7.58	1.24	0.64	1.01	1.27
	dev	0.02	0.15	0.05	0.45	0.03	0.06	0.02	0.10
	min	0.91	2.42	0.93	6.13	0.95	0.44	0.95	1.08
	max	1.08	3.59	1.54	9.37	1.36	0.95	1.20	2.19

Data related to free and prevented base warping have been treated together in  $M_y^7$  and  $M_z^7$  and these ratios are presented for the more stressed both internal (C.U.) and external (E.U.) upright. In a very limited number of cases the mean value of  $\frac{M_y^7}{M_y^6}$  is lower than unity.

If ratio  $\frac{M_z^7}{M_z^6}$  is considered, the number of cases with mean value lower than unity increases slightly. Owing to the great dispersion of these ratios, which is independent from the load conditions, as it can be directly appraised by the values of the standard deviation, it can be concluded that no prediction can be a priori made associated with the considered parameters on the influence of warping and hence the sole 7DOFs beam formulation appears adequate to evaluate correctly design internal actions.

### 3.4 Warping influence: global resistance checks

Modern design codes base verification checks on the evaluation of a safety index ( $SI$ ), which are fulfilled if  $SI \leq 1$ , and for routine rack design are associated with the use of beam formulations with 6DOFs per node. Owing to the fact that the considered upright belongs to class 3, the corresponding safety index ( $SI_G^6$ ) is referred to the global properties of the cross-section in terms of axial ( $N_{Rd}$ ) and bending resistance ( $M_{y,Rd}$  and  $M_{z,Rd}$ ), and it is defined from the 3.2 as:

$$SI_G^6 = \frac{N_{Ed}}{N_{Rd}} + \frac{M_{y,Ed}}{M_{y,Rd}} + \frac{M_{z,Ed}}{M_{z,Rd}} = \frac{N_{Ed}}{A f_y} + \frac{M_{y,Ed}}{I_y f_y} z_{max} + \frac{M_{z,Ed}}{I_z f_y} y_{max} \quad 3.10$$

In case of beam formulations including the influence of warping, the global safety index ( $SI_G^7$ ) has to be taken into account necessarily also for the bimoment contribution, as very recently recommended by Australian standards [5]. In accordance with the criteria associated with the 3.6,  $SI_G^7$  can be defined as:

$$SI_G^7 = SI_G^6 + \frac{B_{Ed}}{I_w f_y} \omega_{max} \quad 3.11$$



### 3.5 Warping influence: local resistance checks

Normal  $\sigma_{w,Ed}(y, z)$  and shear  $\tau_{w,Ed}(y, z)$  stresses due to the bimoment  $B_{Ed}$  in a general point P of co-ordinate  $(y, z)$  defined with reference to the cross-section centroid can be expressed as:

$$\begin{aligned}\sigma_{w,Ed}(y, z) &= \frac{B_{Ed}}{I_w} \omega(y, z) \\ \tau_{w,Ed}(y, z) &= \frac{T_w S_\omega(y, z)}{I_w t}\end{aligned}\tag{3.12}$$

where  $T_w$  represent the non-uniform torsional moment,  $t$  is the thickness of the cross-section and all the other symbols have been previously defined.

As already mentioned, the use of 3.11 in resistance checks could lead to a slightly conservative design, owing to the fact that the maximum of the sectorial area ( $\omega_{max}$ ), as well as of its first moment of area ( $S_{\omega,max}$ ), is not at the same location where stresses due to bending moments reach the maximum values. As a consequence, it should appear more appropriate, in order to guarantee an optimal use of the material, to evaluate the local distribution of the normal stresses summing the values of the stresses occurring at the same point of the cross-section. The distributions of the sectorial area  $\omega(y, z)$  and of its first moment  $S_\omega(y, z)$  are presented in the Figure 3-13 for the cross-section geometry of the considered upright. With reference to the sole normal stresses, owing to the influence of warping, the non-coincidence between the points where normal stress is maximum if a 6DOFs or a 7DOFs beam formulation is used can be noted in Figure 3-14. Maximum normal stress is in point  $D'$  if the sole axial load and positive bending moments are considered. Otherwise, if bimoment  $B_{Ed}$  acts on cross-section, maximum stress is in correspondence of point  $F'$  ( $B_{Ed} > 0$ ) or point  $B'$  if ( $B_{Ed} < 0$ ).

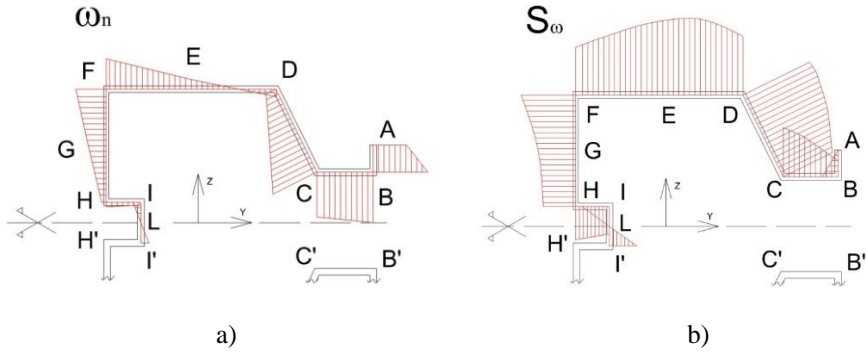


Figure 3-13. Distribution of the sectorial area,  $\omega_n$  (a) and the static moment,  $S_{\omega}$  (b) for the considered upright cross-section.

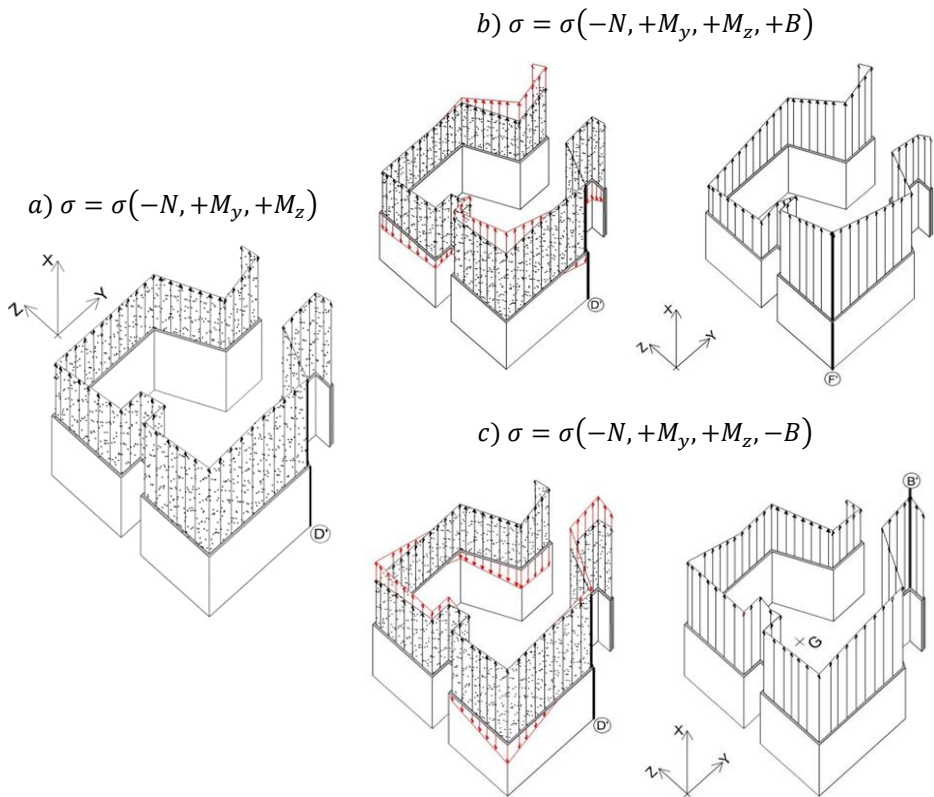


Figure 3-14. Examples of influence of the bimoment  $B$  on the location of the maximum normal stress in the cross-section upright.

Neglecting the presence of material safety factors  $\gamma_m$ , which depends on the considered code, resistance safety index based on the local stress value  $SI_\sigma$  can be defined, in accordance with 3.5, as:

$$SI_\sigma = \frac{\sqrt{[\sigma_{tot}(y, z)]^2 + 3[\tau_{tot}(y, z)]^2}}{f_y} \quad 3.13$$

In the following, for the generic point  $P$  of co-ordinates  $(y, z)$ , the verification checks associated with the use of both 6DOFs and 7DOFs beam elements can be expressed in terms of safety index, as:

$$\begin{aligned} SI_\sigma^6 &= \frac{\sqrt{[\sigma_{tot}^6(y, z)]^2 + 3[\tau_{tot}^6(y, z)]^2}}{f_y} \\ &= \frac{\sqrt{[\sigma_{tot}^6(y, z)]^2 + 3[\tau_{F_y}(y, z) + \tau_{F_z}(y, z)]^2}}{f_y} \\ SI_\sigma^7 &= \frac{\sqrt{[\sigma_{tot}^7(y, z)]^2 + 3[\tau_{tot}^7(y, z)]^2}}{f_y} \\ &= \frac{\sqrt{[\sigma_{tot}^6(y, z) + \sigma_{w,Ed}(y, z)]^2 + 3[\tau_{tot}^6(y, z) + \tau_{w,Ed}(y, z)]^2}}{f_y} \end{aligned} \quad 3.14$$

where terms  $\tau_{F_y}(y, z)$  and  $\tau_{F_z}(y, z)$  represent the tangential stresses due to the shear forces  $F_y$  and  $F_z$ , respectively.

As previously mentioned, the contribution of  $F_y$  and  $F_z$  to the resistance verification check is very modest and the influence of the term  $\tau_{tot}^6(y, z)$  on the evaluation of  $SI_\sigma^6$  is very limited, not greater than 0.1% of the maximum normal stress. If the bimoment contribution is considered to evaluate  $\tau_{tot}^7(y, z)$ , shear stress influence on  $SI_\sigma^7$  is greater than in the previous case, but, however, remains negligible, not greater than 0.5%. For each of the points of the upright cross-section indicated in Figure 3-5 the local state of stress has been evaluated.

The maximum values of the relative frequency plotted in Figure 3-15 (M\_5 racks) and Figure 3-16 (M\_4 racks) are in the range  $1.08 \div 1.12$  despite the fact that a great dispersion

can however be observed. In a very limited number of cases, the ratio  $\frac{SI_{\sigma}^7}{SI_{\sigma}^6}$  is slightly lower than unity. This is due to the greater flexibility of the rack modeled via a 7DOFs beam formulation to which correspond slightly lower values of the bending moments acting on the cross-section; only in these very few cases a moderate conservative design could hence be obtained via a 6DOFs beam formulation. In all the other cases it appears fundamental to take adequately into account warping, owing to great influence also on the local verification safety index  $SI_{\sigma}^7$ , which is in some cases up to 2.5 times  $SI_{\sigma}^6$ .

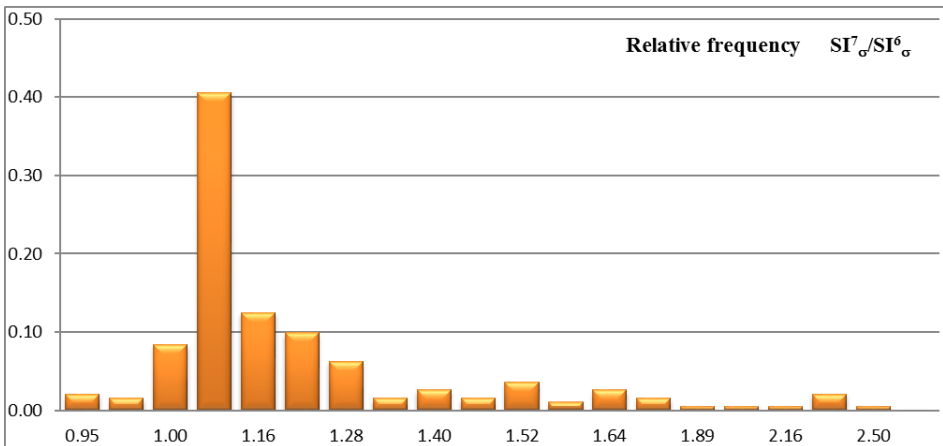


Figure 3-15. Influence of warping on the local resistance check for M\_5 racks (more stressed C.U. and E.U.)

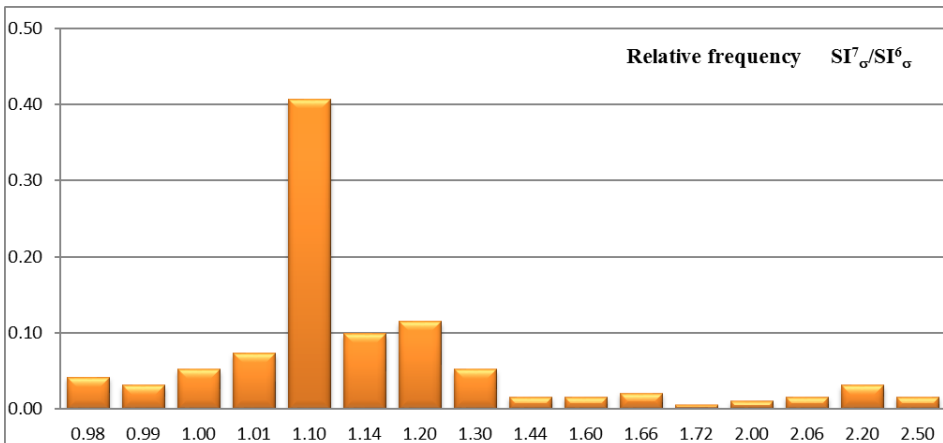


Figure 3-16. Influence of warping on the local resistance check for M\_4 racks (more stressed C.U. and E.U.)



## Chapter 4 Beam design of non-symmetric cross-section

### 4.1 Introduction

One of the most important uses of thin steel sheets is for producing cold-formed members [40], which are used worldwide in industrial pallet racking systems. Different types of racks are nowadays offered by manufactures to accommodate the existing space [41] but in the current work attention is focused on the horizontal components of selective, drive-in and drive-through pallet racks. The former has transverse beams that support the load units and contribute to the overall system stability in the down-aisle direction (Figure 4-1, a) by means of semi-rigid beam-to-column joints. Forklift access to the products in the down-aisle direction has to be unobstructed for improving handling of the stored goods and reduction of the picking time. The main disadvantage of these systems is the presence of the aisles, which reduce the space available for product storage.

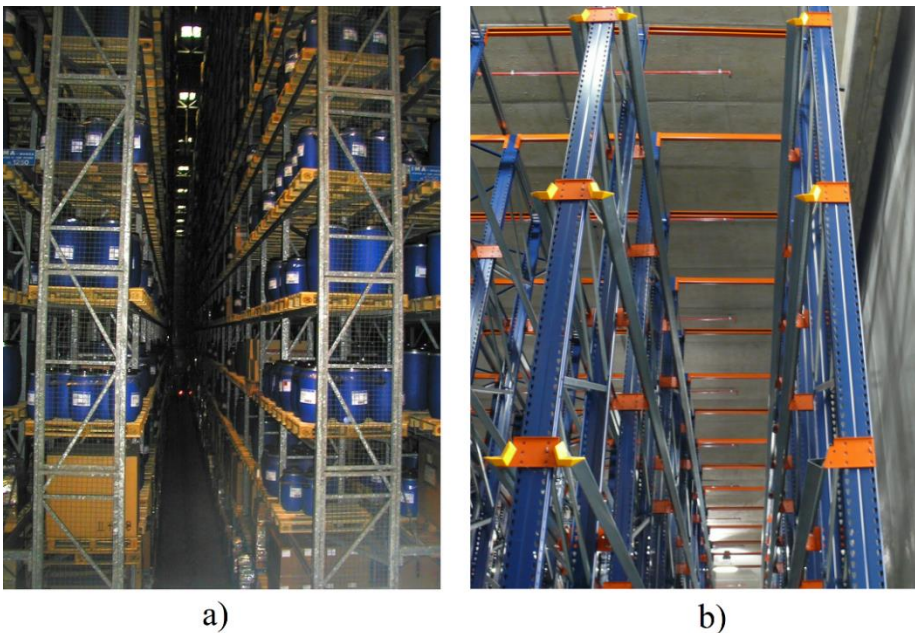


Figure 4-1. Typical storage systems: (a) selective and (b) non selective (drive-in) pallet racks.

## Chapter 4

Drive-in structures (Figure 4-1, b) are characterized by a multi-level product loading system in the cross-aisle direction. Differently from pallet racks, in drive-in systems the rail beams supporting pallet units run along the rack depth, allowing a very high storage space utilization at the cost of a reduced accessibility; the operating front face permits the forklift entry/exit while the opposite (rear) face provides vertical bracing to guarantee the stability of the system to lateral loads. Complete research can be found in [42].

Furthermore, the absence of transverse beams in the cross-aisle direction due to the need to allow for forklift movement makes these racks more susceptible to buckling in this direction. Lateral stability is obtained primarily from the flexural stiffness of the base-plate connections and from the semi-rigidity of beam-to-column joints at the ends of the beams connecting the uprights at the top of the structure. When the vertical post bracings are omitted, the system is named drive-through and the stability under lateral loading is significantly reduced. The core of this research assesses the adequacy of the routine design rules for the beams supporting the pallet units (pallet beams), and therefore in the following, the term *drive-rack* is used to identify both drive-in and drive-through pallet racks.

There are significant differences between selective pallet and drive-racks and, for this reason, the design codes give different requirements, especially for which analysis methods are to be used. In particular, with regard to the European practice, pallet rack design is governed by EN 15512 “*Steel static storage systems – Adjustable pallet racking systems – Principles for structural design*” [2] while for drive-type structures, FEM 10.02.07 “*The design of drive-in and drive-through racking’ drive-in design code*” is the reference code [43]. A common aspect of both types of structures regards the pallet beams that often have a non-symmetric cross-section. Independent on the reference code, design rules neglect this very important aspect and propose verification approaches that do not adequately account for the effects associated with warping torsion and with the non-coincidence of the shear center and the cross-section centroid. It is worth noting that several studies have been developed on selective pallet racks ([40], [41]), while more limited attention has been paid to drive-racks ([44], [45], [46], [47]). There is no research dealing with the response of beams in industrial storage systems, nor do key features of their response seem to be adequately accounted by the most recent rack design codes.

Rack manufactures frequently use the same types of vertical elements (uprights) for both storage system types but differences can be observed in the pallet beams. In the case of selective pallet racks, the most commonly used beam cross-sections are presented in Figure 4-2, where they can be distinguished as sensitive (a) or not sensitive (b) to lateral buckling.

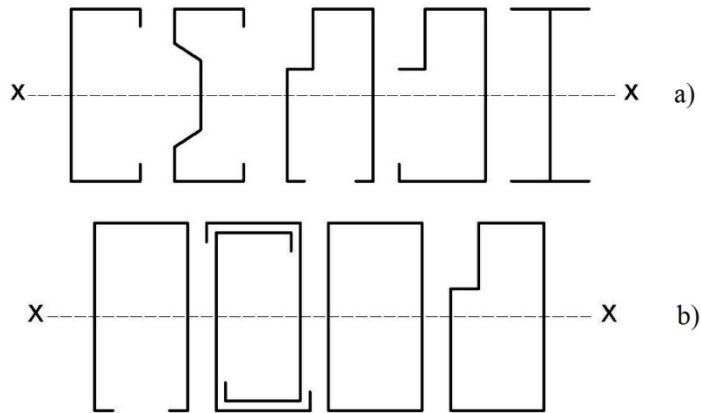


**Figure 4-2. Pallet beam cross-sections interested (a) or not interested (b) by lateral buckling.**

It is worth mentioning that lipped channels, or very similar cross-section types, are commonly used as pallet beams, whose top flange supports directly the pallets while the web allows for the connection with the uprights (Figure 4-3). A non-negligible advantage consists in the fact that a single member should be used to connect more than two subsequent uprights, hence behaving like a continuous beam instead of connecting only two adjacent uprights.



**Figure 4-3. Example of lipped channels used as pallet beams.**

In the case of drive-racks, the rail beams supporting pallet units generally have non-bi-symmetric cross-sections, which can be distinguished in mono- (a) and non-symmetric (b) cross-sections (Figure 4-4). It can be noted that when it is necessary to also guarantee efficient protection from the incorrect placing of pallet units, a lateral pallet guard is required, which is included directly in the rail beam cross-section.

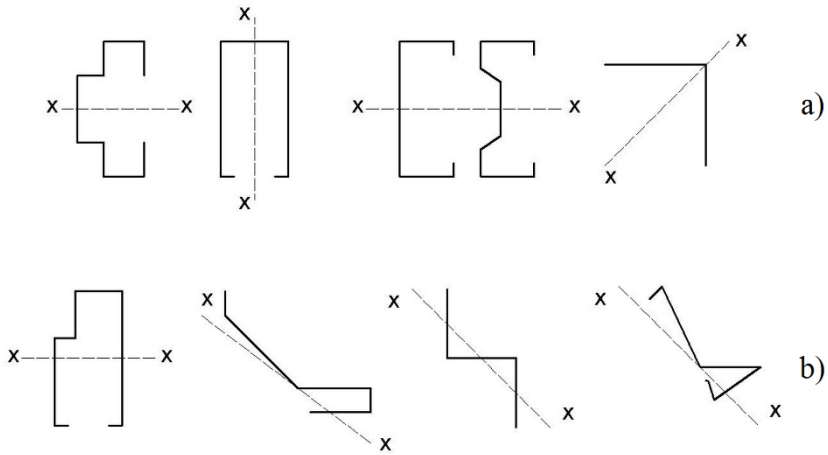


**Figure 4-4. Typical drive-in rail beam mono- (a) and non-symmetric (b) cross-sections.**

Very general criteria are available in the European rack provisions ([2], [43]) for the verification checks and up to now adequate attention does not appear to have been paid to the key features of the structural analysis phase nor to the associated design verification rules. In particular, as shown in the following, routine design is carried out by considering the traditional approaches usually adopted for bi-symmetric cross-sections: warping effects, Wagner’s coefficients and the coupling between flexure and torsion are usually neglected. This reflects directly on the accuracy of the evaluation of the effective performance guaranteed by the storage systems, i.e. on the effective degree of reliability of the design.

This research deals with pallet beam design: reference is made to lipped channel and zed members, focusing on the design criteria associated with serviceability and ultimate limit states. An open source finite element (FE) analysis software package for academic use [48], has been modified to accurately model the behavior of non bi-symmetric cross-section members. Furthermore, the traditional design results neglecting warping have been directly compared to the more refined results of Šiva, highlighting their differences and, as a consequence, identifying the effective accuracy of the design results.

## 4.2 Design rules for pallet beams in storage systems

In general, loads associated with the stored units induce on pallet beams, in addition to flexure and shear also torsion and the European reference code for the design of industrial beams is EN 15512 [2], as explicitly recommended also by the drive-racks standard [43]. Both codes are in accordance with the limit state design philosophy [49], and, for these members, as for girders in multistory steel buildings, serviceability conditions should

govern design and hence have to be suitably accounted for by manufacturing engineers. Owing to the need to reduce the number of parameters influencing the outcomes of this study, only class 3 profiles are herein considered [14], for which the effective and the gross cross-sections are assumed to be coincident.

As to the serviceability limit states, adequate checks are required guaranteeing that the vertical displacements do not exceed the limit values provided by specifications, which are associated with the class of use of the racks [50]: generally, the limit displacement is a fraction of the beam length  $L_b$ , between  $L_b/300$  and  $L_b/200$ . Furthermore, it should be noted that rack provisions also recommend that the twist angle of the beam cross-section does not exceed the limit value of 6 degrees (0.105 rad). If bi-symmetric cross-section profiles are used, pallet beam design is extremely simple and quick, otherwise very complex calculations are often required to designers. Despite the expected relevance of this aspect for design purposes, no detailed criteria, tables or equations are provided in the code like the one included to account for the influence of the semi-rigidity of the beam-to-column joints in the vertical displacement and bending moment distribution on pallet beams. For the ultimate limit state, in the case of non-symmetric cross-sections, it is recommended to account for bending about the principal axes also considering the presence of torsion. Due to the lack of more detailed requirements, EN 1993-1-3 [16] should be considered also for pallet design, which provides very general statements, and reference can be made to the sub-chapter 3.1 for the equations adopted.

As previously mentioned, rack design in many instances is carried out by means of FEA packages offering beam formulations characterized by six degrees-of-freedom per node, i.e. the member cross-section properties for structural analysis are defined by the area, second moments of area and uniform torsion constant. Usually, the eccentricity between the shear-center and the cross-section centroid, the Wagner coefficients and the warping constant are excluded from the input data, leading to a design based on generalized displacements and stresses, which are very different from the actual ones. To this purpose, in the following paragraphs, two cases of interest for beam design in storage structures have been investigated, namely:

- lipped channels, typically used as pallet beams in selective pallet racks;
- zed profiles, typically used as rail beams in drive-racks.

The considered structural schemes are presented in Figure 4-5, which are adequately representative for routine design cases, differing in the number of spans (from 1 to 3) and for the type of end beam restraints. Generally, semi-rigid behavior is guaranteed at the ends of the beam connected to the uprights [51], which depend on the connection details, and, as a consequence, the degree of flexural stiffness influences beam response. In the following, reference is made to idealized simple support or fixed end restraints, owing to the need to limit the number of the variables affecting research outcomes. As for the beam length ( $L_b$ ), a value of 2500 mm was considered for each span, but the findings are expected to cover the whole range of values of  $L_b$  typically used for storage applications.

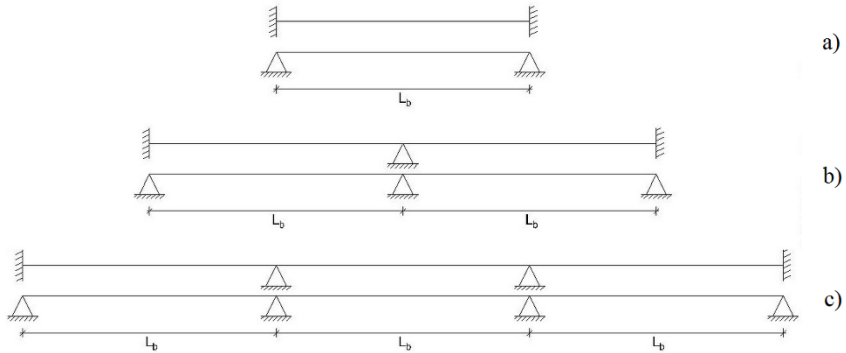


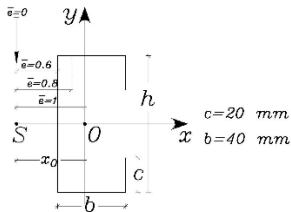
Figure 4-5. Static schemes of the parametric analysis: one (a), two (b) and three (c) spans.

### 4.3 Lipped channel members

Reference for pallet beams in selective racks is herein made to lipped channels differing in the ratio between the web height ( $h$ ) and the flange width ( $b$ ), as shown in Table 4-1. The main geometric properties of the cross-sections are reported in terms of area ( $A$ ), second moments of area ( $I_y$  and  $I_z$ ), torsion ( $I_t$ ) and warping ( $I_w$ ) constants and coordinate of the shear center with respect to the cross-section centroid ( $y_0$ ). It is worth mentioning that the different materials (steel, wood, plastic materials, etc.) typically used for pallets as well as for the stored units lead to different distributions of the contact stresses on the supporting pallet beam flange. As a consequence, owing to the impracticality of defining a sole standard load position, it has been decided in the numerical analysis to vary the load application line from the beam web to the cross-section centroid. In particular, reference is made to the non-dimensional eccentricity  $\bar{e}$  expressed as the distance between the load application line and the shear center over the distance between the shear center and the cross-section centroid; three values of  $\bar{e}$  have been considered:  $\bar{e} = 0.6$  (corresponding to load applied on the channel web),  $\bar{e} = 0.8$  and  $\bar{e} = 1$  (corresponding to load on the centroid).

Table 4-1. Geometric characteristic of lipped channels cross-sections.

	<b>h/b [-]</b>	<b>2</b>	<b>2.5</b>	<b>3</b>
	<b>h [mm]</b>	<b>80</b>	<b>100</b>	<b>120</b>
	<b>A [mm<sup>2</sup>]</b>	$4.00 \cdot 10^2$	$4.40 \cdot 10^2$	$4.80 \cdot 10^2$
	<b>I<sub>y</sub> [mm<sup>4</sup>]</b>	$41.6 \cdot 10^4$	$69.7 \cdot 10^4$	$107 \cdot 10^4$
	<b>I<sub>z</sub> [mm<sup>4</sup>]</b>	$11.1 \cdot 10^4$	$12.0 \cdot 10^4$	$12.8 \cdot 10^4$
	<b>I<sub>t</sub> [mm<sup>4</sup>]</b>	$0.053 \cdot 10^4$	$0.059 \cdot 10^4$	$0.064 \cdot 10^4$
	<b>I<sub>w</sub> [mm<sup>6</sup>]</b>	$229 \cdot 10^6$	$331 \cdot 10^6$	$459 \cdot 10^6$
	<b>y<sub>0</sub> [mm]</b>	-39.6	-36.9	-34.5



4.3.1 Serviceability limit state

Pallet unit loads cannot be applied directly on the shear center of lipped channels ( Figure 4-6, a) and, as a consequence, attention for serviceability checks has to be paid not only to the vertical deflection but also to the twist rotation. Routine 6DOF design is carried out by assuming that pallet beams are always loaded directly above the centroid but designers have the possibility to account for the torsional moment due to the shear center load eccentricity (Figure 4-6, b).

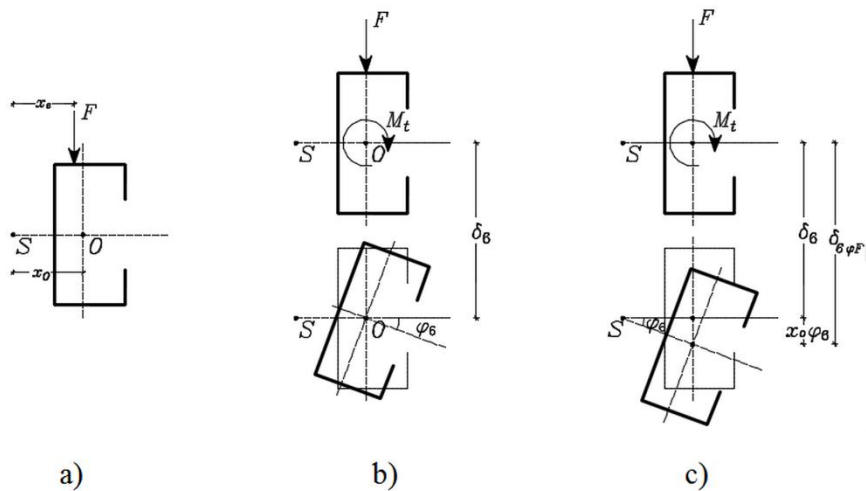


Figure 4-6. The loaded cross-section (a) and the approach to evaluate the vertical displacement.

Chapter 4

A more refined approach, very rarely used in rack design, consists in adding to the flexural deflection due to the load applied at the cross-section centroid ( $\delta_6$ ) the contribution due to the rigid translation associated with the rotation along the shear center (Figure 4-6, c). Consequently, the actual displacement ( $\delta_{6\varphi F}$ ) should be assessed via a traditional 6DOF beam formulation as:

$$\delta_{6\varphi F} = \delta_6 + \varphi_6 \cdot y_o \tag{4.1}$$

where  $\varphi_6$  is the rotation due to the torsional moment obtained by multiplying the applied load for its eccentricity ( $y_e$ ) with respect to the shear center and  $y_o$  is the distance between the cross-section centroid and the shear center.

It is expected that a similar design procedure, based on the check of the twist rotation  $\varphi_6$  and of the vertical deflection  $\delta_{6\varphi F}$  should be acceptable for practical design purposes, also because no alternatives are associated with 6DOF FE beam formulations. A comparison with the Siva values of rotation and displacement ( $\varphi_7$  and  $\delta_7$ , respectively) shows surprisingly different results, as it can be observed in Table 4-2 and Table 4-3.

**Table 4-2. Values of the  $\varphi_6/\varphi_7$  ratio for lipped channels.**

	h/b = 2	h/b = 2.5	h/b = 3
1 bay	2.72	3.25	3.87
2 bays	5.23	6.51	7.99
3 bays	4.55	5.56	6.74

**Table 4-3. Valued of the  $\delta_6/\delta_7$  and  $\delta_{6\varphi F}/\delta_7$  ratios for lipped channels.**

Simply supported ends		$\delta_6/\delta_7$			$\delta_{6\varphi F}/\delta_7$		
		$\bar{e} = 0.6$	$\bar{e} = 0.8$	$\bar{e} = 1$	$\bar{e} = 0.6$	$\bar{e} = 0.8$	$\bar{e} = 1$
h/b = 2	1 Bay	0.48	0.41	0.36	1.89	2.01	2.10
	2 Bays	0.43	0.36	0.31	3.41	3.71	3.92
	3 Bays	0.46	0.38	0.33	2.93	3.18	3.37
h/b = 2.5	1 Bay	0.45	0.39	0.34	2.23	2.38	2.50
	2 Bays	0.41	0.35	0.30	4.24	4.61	4.87
	3 Bays	0.43	0.36	0.32	3.59	3.90	4.12
h/b = 3	1 Bay	0.44	0.38	0.33	2.60	2.79	2.93
	2 Bays	0.41	0.34	0.30	5.14	5.59	5.91

Beam design of non-symmetric cross-section

		3 Bays	0.42	0.36	0.31	4.29	4.67	4.94
Fixed ends		$\delta_6/\delta_7$			$\delta_{6\varphi F}/\delta_7$			
		$\bar{e} = 0.6$	$\bar{e} = 0.8$	$\bar{e} = 1$	$\bar{e} = 0.6$	$\bar{e} = 0.8$	$\bar{e} = 1$	
h/b = 2	1 Bay	0.13	0.12	0.10	2.01	2.51	2.54	
	2 Bays	0.26	0.21	0.17	4.12	4.35	4.49	
	3 Bays	0.24	0.19	0.16	3.71	3.88	4.00	
h/b = 2.5	1 Bay	0.14	0.11	0.09	2.93	3.00	3.05	
	2 Bays	0.27	0.22	0.18	5.57	5.89	6.10	
	3 Bays	0.22	0.18	0.15	4.57	4.77	4.90	
h/b = 3	1 Bay	0.14	0.11	0.09	3.48	3.56	3.62	
	2 Bays	0.25	0.20	0.17	6.28	6.61	6.83	

If the twist rotation is considered (Table 4-2), the ratio  $\varphi_6/\varphi_7$  is, as expected, independent of the eccentricity  $\bar{e}$  and from the boundary conditions at the beam ends, being an elastic first-order analysis as usually carried out in routine pallet beam design. It can be noted that increasing the slenderness of the cross-section also increases this ratio. It is always significantly greater than unity, ranging approximately from 2.7 up to 8.0, and the maximum values are associated with 2-span beams. It therefore results that an approach based on a 6DOF FE beam formulation is always too conservative, leading to overestimation of the cross-section rotation. As to the maximum vertical displacement, the reference data are provided in Table 4-3, which are distinguished on the basis of both structural scheme and non-dimensional load eccentricity  $\bar{e}$ . Neglecting the effects of torsion angle  $\varphi_6$  on the rigid translation of the cross-section (Figure 4-7), it can be noted that the  $\delta_6/\delta_7$  ratio is always significantly lower than unity, ranging from 0.48 to 0.09 and the lowest values are associated with beams having fixed ends. Increasing the value of  $\bar{e}$ ,  $\delta_6/\delta_7$  decreases and the use of six degrees-of-freedom leads to a significant underestimation of the vertical displacements. Otherwise, by adopting the more refined eq. 8), the  $\delta_{6\varphi F}/\delta_7$  ratio is always greater than unity, ranging from 1.89 up to 6.83, and this large overestimation of the vertical displacement is mainly due to the inaccurate and extremely conservative assessment of the twist 6DOFs angle ( $\varphi_6$ ), which was observed previously.

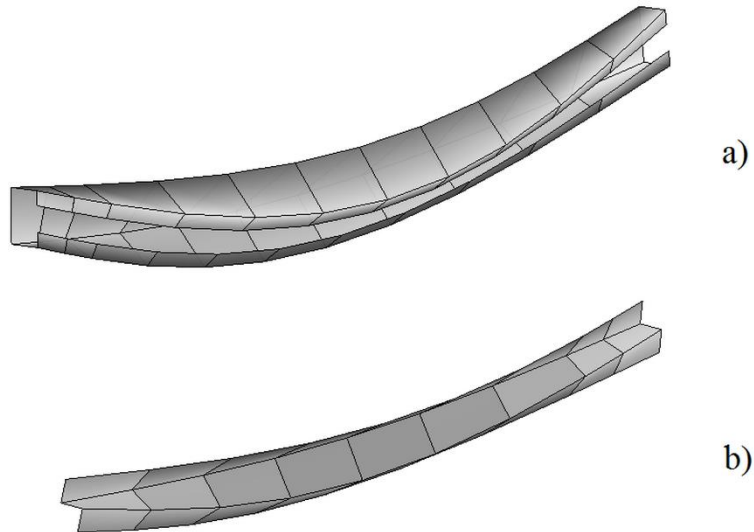


**Figure 4-7. Deformed configuration of a lipped channel (a) and zed (b) profile by using *Śiva*.**

As a preliminary conclusion, it can be noted that serviceability checks based on the use of a 6DOF FE beam formulation leads to the prediction of a member response that is always significantly different from the reality: neglecting or considering the influence of the load eccentricity leads to the vertical displacement being greatly under- or over-estimated, respectively, and the analysis results are in any case very far from having any kind of engineering interest.

#### 4.3.2 *Ultimate limit state*

Due to the presence of pallet beams restrained to lateral-torsional buckling by the sustained load units, attention is herein paid only to the resistance verification checks. Only the longitudinal stresses due to bending ( $\sigma_F$ ) and warping torsion ( $\sigma_w$ ) have been considered, with shear stresses being limited in these cross-section types and not relevant from the design point of view.

## Beam design of non-symmetric cross-section

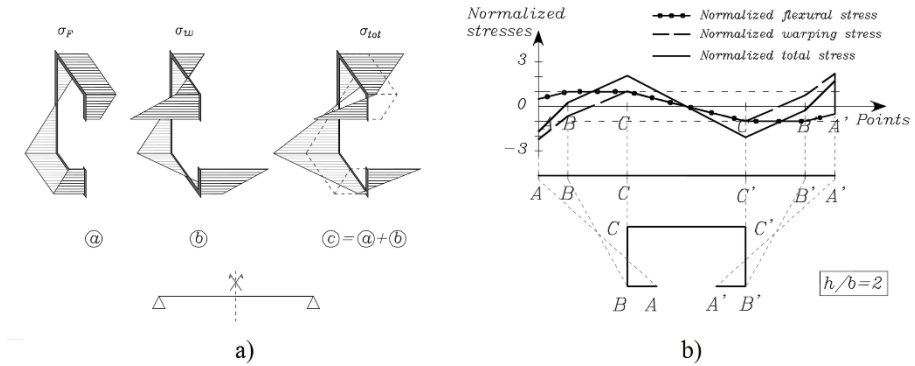


**Figure 4-8. Lipped channel mid-span stress distribution of a simply supported beam (a) and normalized stresses (b).**

The importance of  $\sigma_F$  and  $\sigma_w$  can be appraised via Figure 4-8 and Figure 4-9, which depict the stress distribution at the mid-span of a beam simply supported and fixed at its ends. In addition to flexural and warping stresses, the total stress ( $\sigma_{tot}$ ) is also presented: part a) of each figure presents a solid view of these distributions, which are shown in part b) by plotting these stresses divided by the yielding stress, which is assumed to be reached in the more highly stressed cross-sections of the members in bending, that is at the mid-span for simply supported beam and at the ends for fixed end beam.

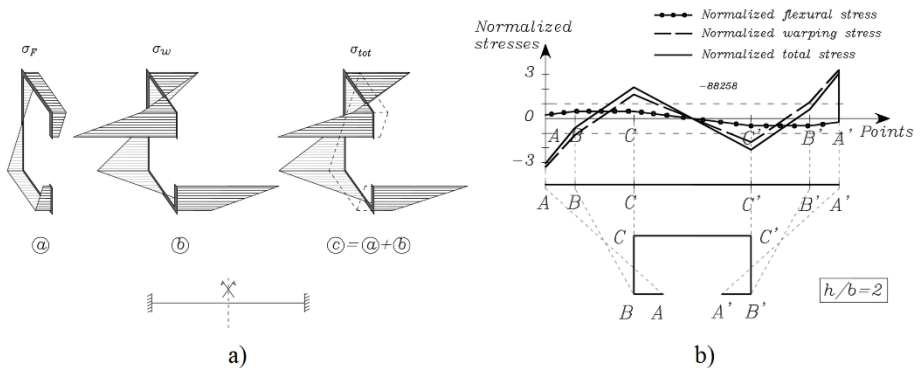


**Figure 4-9. Lipped channel mid-span stress distribution of a fixed ends beam (a) and normalized stresses (b).**

These figures, which are also representative of the other cases considered in the numerical analysis, shown clearly that warping stresses ( $\sigma_w$ ) can never be neglected in channel design as they are always greater than the flexural stresses ( $\sigma_F$ ). At the beam mid-span cross-section (Figure 4-8), maximum bending stress occurs at the flanges (elements BC and C'B'), but in points C and C' warping stresses have to be algebraically summed to the flexural stresses, thus leading to an increment of 108% (i.e.  $\sigma_{tot}/\sigma_y = 2.08$ ) of the

Chapter 4

resistance safety index. The same mid-span cross-section has to be considered also in case of fixed ends (Figure 4-9), despite the more severe state of flexural stresses at the member ends, because of the very large warping stresses.

Maximum stresses correspond to points A and A', where, despite the fact that flexural and warping stresses are opposite, the contribution due to warping is so great that  $\sigma_{tot}/\sigma_y$  is approximately equal to 3.06 (i.e.  $\sigma_w/\sigma_y = 3.31$ ), hence underlining that the mid-span cross-section, instead of the end cross-sections, must be considered in the design. Furthermore, the warping influence along the member can be appraised via Figure 4-10 and Figure 4-11, referring to the cases of beams having simply supported and fixed ends, respectively. In both cases, the data associated with  $\bar{e} = 0.6$  (solid lines) and  $\bar{e} = 1.0$  (dashed lines) have been plotted in terms of stress  $\sigma_{tot}/\sigma_F$  ratio in selected longitudinal cross-sections: data related to  $\bar{e} = 0.8$  have not be considered as they lie in between the values for  $\bar{e} = 0.6$  and  $\bar{e} = 1.0$ . With reference to the cross-section governing resistance design, identified by a circle, it can be noted that, neglecting warping, the maximum strength is significantly under-estimated, by approximately 64% to 146% for simply supported end conditions (Figure 4-10) and up to 12 times for fixed ends (Figure 4-11). In particular, in the case of fixed ends, the  $\sigma_{tot}/\sigma_F$  ratio is significantly greater than in cases of beams with simply supported ends because of the difference of the bending and torsion moment distributions.

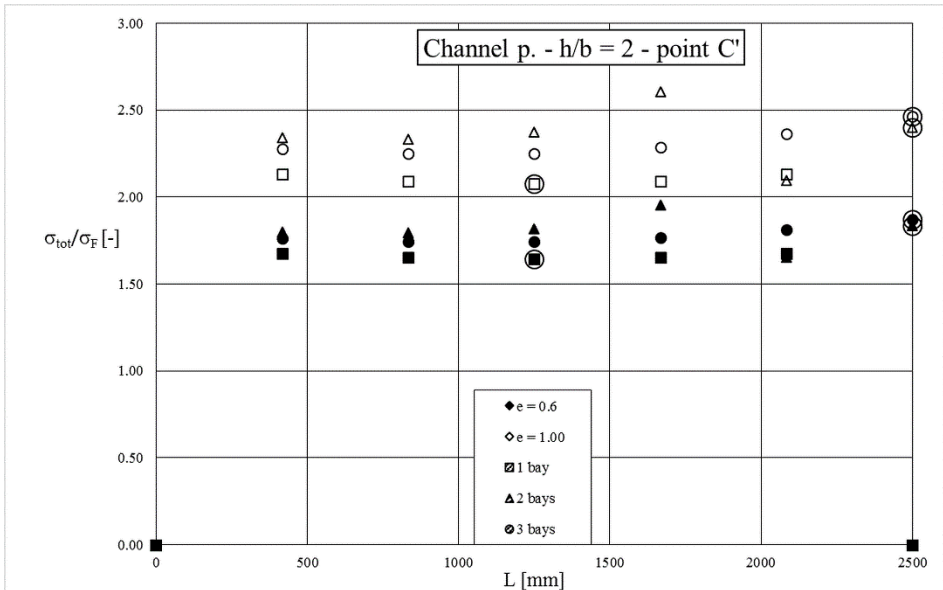


Figure 4-10. Lipped channel distribution of  $\sigma_{tot}/\sigma_F$  along the beams with simple end supports.

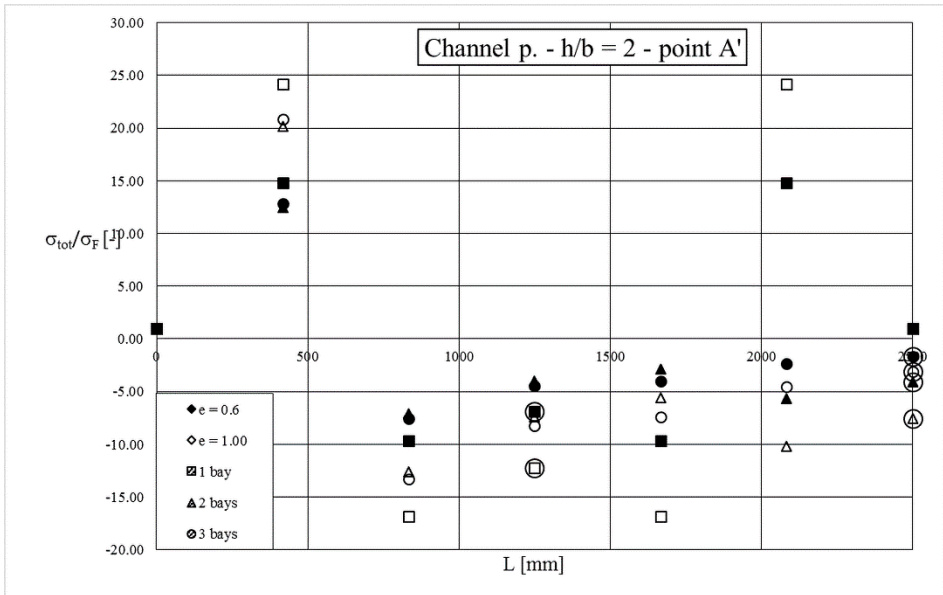


Figure 4-11. Lipped channel distribution of  $\sigma_{tot}/\sigma_F$  along the beam with fixed end.

Furthermore, it should be noted that the presence of warping stresses changes the location of the cross-section governing the design. In several cases, as already mentioned, despite the flexural strength being maximum in the zones under hogging moments, reference has to be however made to the mid-span zone, owing to the relevance of warping stresses.

Moreover, to better appraise once again the relevance of warping stresses, reference should be made to Figure 4-12 and Figure 4-13, which plot the maximum cross-section stress ( $\sigma_{tot}$ ) over the maximum flexural stress ( $\sigma_{F,max}$ ) along the whole length of the member. It can be noted that the trend of these curves reflects the distribution of the bending moment diagrams. In the case of simply supported ends (Figure 4-12), underestimation based on the flexural only design is between 64% and 108%, while the errors with reference to continuous beams increases remarkably, ranging in terms of  $\sigma_{tot}/\sigma_{F,max}$  from 1.83 to 2.46.

For beams with fixed ends (Figure 4-13), the largest errors are observed: the ratio  $\sigma_{tot}/\sigma_{F,max}$  is calculated to be up to 3.06 (of single span) and 3.79 (three-span beams).

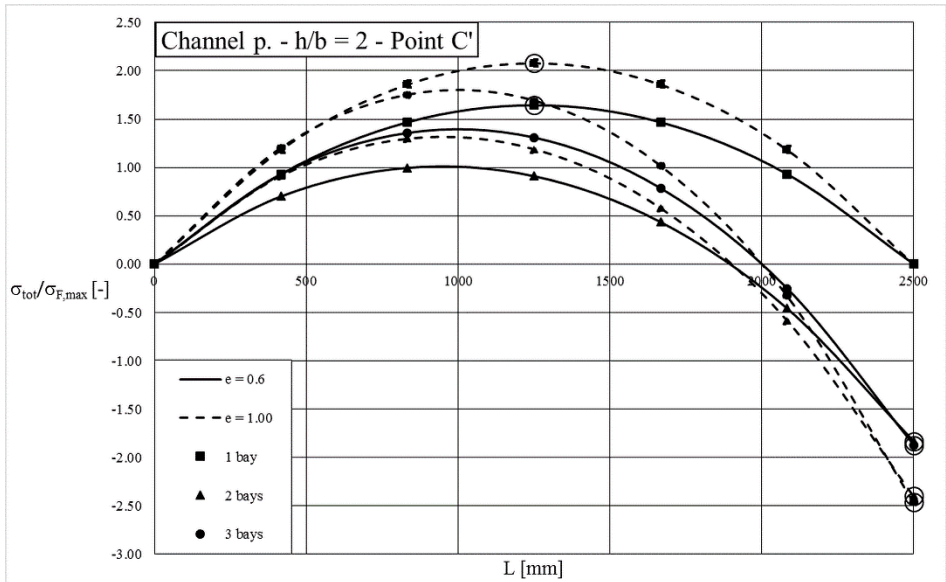


Figure 4-12. Lipped channel distribution along the beam span of  $\sigma_{tot}/\sigma_{F,max}$ , point C'.

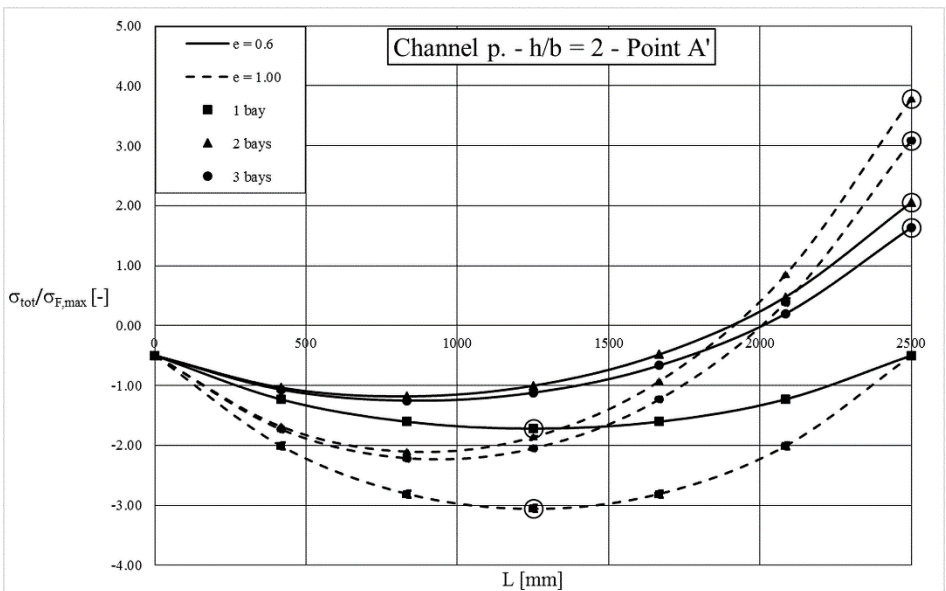


Figure 4-13. Lipped channel distribution along the beam span of  $\sigma_{tot}/\sigma_{F,max}$ , point A'.

4.3.3 Load carrying capacity

From the previous conclusions, separately proposed for serviceability and ultimate limit states, it appears that routine design procedures based on 6DOF FE beam formulations cannot lead to a reliable assessment of pallet beam performance: the significant over-estimation of the rotation should lead to a conservative design while neglecting warping stresses should lead to an over-estimation of resistance. In the following, by assuming for lipped channels a S355 steel grade, the load carrying capacity (LCC), has been evaluated for each structural scheme. The following design approaches have been considered:

- a) a traditional 6DOF design approach accounting for the influence of the load eccentricity on both rotation and displacement via 4.1. Warping stresses are neglected at the ultimate limit state verification because they cannot be evaluated directly by FE software. The associated load carrying capacity is identified as  $LCC^{6\phi F}$ ;
- b) a refined design approach based on the use of Síva or equivalent 7DOF FE analysis packages. The associated effective load carrying capacity is identified as  $LCC^7$ .

Table 4-4 presents the  $LCC^{6\phi F}/LCC^7$  ratio: the governing design condition is always based on the achievement of the limit rotation and, as a consequence,  $LCC^{6\phi F}/LCC^7$  ratio, which corresponds to the reciprocal of the data reported in Table 4-2, is independent on the value of the load eccentricity as well as the restraint at the ends of the beam.

**Table 4-4. Values of the ratio  $LCC^{6\phi F}/LCC^7$  for lipped channels.**

	h/b = 2	h/b = 2.5	h/b = 3
1 bay	0.36	0.30	0.25
2 bays	0.18	0.15	0.12
3 bays	0.21	0.17	0.14

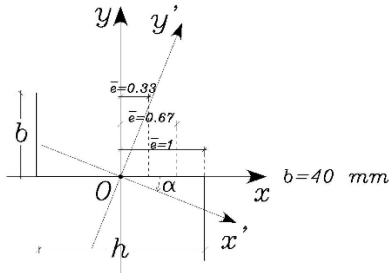
Owing to the already discussed over-estimation of the cross-section rotation, it appears that the use of the 6DOF approach leads to a very conservative design, significantly underestimating the effective beam performance. Increasing the bay numbers also results in an increase in the difference between the performance predictions. In the case of simply supported beams, the term  $LCC^7$  ranges between 3 and 4 times  $LCC^{6\phi F}$ , despite the presence of large warping stresses. Ratio  $LCC^{6\phi F}/LCC^7$  decreases significantly with reference to continuous beams, up to 0.12, i.e. the effective load carrying capacity is up to 8 times the one evaluated via the traditional routine design approaches.

### 4.4 Zed profiles

Focusing attention on rail beams for drive-racks, zed cross-section members have been considered, where the top flange serves also as protection for pallet units. The main geometric data are presented in Table 4-5, where the second moments of area with respect to the principal axes  $z'$  ( $I_{y'}$ ) and  $y'$  ( $I_{z'}$ ) are reported together with the ones associated with the horizontal and vertical axes ( $I_y$ ,  $I_z$  and  $I_{yz}$ ).

**Table 4-5. Geometric characteristic of zed cross-sections.**

	<b>h/b [-]</b>	<b>2</b>	<b>2.5</b>	<b>3</b>
	<b>h [mm]</b>	<b>80</b>	<b>100</b>	<b>120</b>
	<b>A [mm<sup>2</sup>]</b>	$3.80 \cdot 10^2$	$3.48 \cdot 10^2$	$3.88 \cdot 10^2$
	<b>I<sub>y'</sub> [mm<sup>4</sup>]</b>	$2.82 \cdot 10^4$	$3.23 \cdot 10^4$	$3.53 \cdot 10^4$
	<b>I<sub>z'</sub> [mm<sup>4</sup>]</b>	$35.5 \cdot 10^4$	$56.3 \cdot 10^4$	$84.1 \cdot 10^4$
	<b>I<sub>t</sub> [mm<sup>6</sup>]</b>	$0.041 \cdot 10^4$	$0.046 \cdot 10^4$	$0.052 \cdot 10^4$
	<b>I<sub>ω</sub> [mm<sup>6</sup>]</b>	$70.1 \cdot 10^6$	$118 \cdot 10^6$	$180 \cdot 10^6$
	<b>I<sub>y</sub> [mm<sup>4</sup>]</b>	$7.32 \cdot 10^4$	$7.32 \cdot 10^4$	$7.32 \cdot 10^4$
	<b>I<sub>z</sub> [mm<sup>4</sup>]</b>	$31.03 \cdot 10^4$	$52.18 \cdot 10^4$	$80.3 \cdot 10^4$
	<b>I<sub>yz</sub> [mm<sup>4</sup>]</b>	$11.26 \cdot 10^4$	$14.15 \cdot 10^4$	$17.04 \cdot 10^4$
	<b>α [degrees]</b>	21.8	16.1	12.5



Load position influence has been considered via the non-dimensional eccentricity  $\bar{e}$  defined as the ratio of the distance between the shear center and the load application line over half web width: the considered  $\bar{e}$  values are 0 (load on the shear center), 0.33, 0.66 and 1 (load directly on the web). As in the cases of lipped channels, main remarks have been separately proposed for serviceability and ultimate state followed by a discussion related to the effective load-carrying capacity based on both limit states.

4.4.1 *Serviceability limit state*

Due to the coincidence of the shear center and the cross-section centroid, no differences can be observed in the vertical displacements associated with the use of 6DOF and 7DOF FE beam formulations, referred to as  $\delta_6 = \delta_7$ . Otherwise, if reference is made to the twist rotation, with the exception of  $\bar{e} = 0$  cases being  $\varphi_6 = \varphi_7$ ,  $\varphi_6$  and  $\varphi_7$  values are expected to be significantly different, not only for the presence, of the 7<sup>th</sup> DOF but also for the torsional rigidity term (4,4) of the matrix in 2.32, despite the fact that in zed members the warping constant is null (i.e.  $I_w = 0$ ). Table 6 presents the  $\varphi_6/\varphi_7$  ratio: in particular, it can be noted that increasing the cross-section slenderness, the ratio also increases and, as in case of lipped channels, maximum values are associated with 2-bay beams. Furthermore, independent of the eccentricity value, the use of formulations neglecting warping leads to values of the  $\varphi_6$  rotation significantly greater than  $\varphi_7$ , from 1.7 to 3.9 times, approximately.

**Table 4-6. Values of the ratio  $\varphi_6/\varphi_7$  for zed profiles.**

	h/b = 2	h/b = 2.5	h/b = 3
1 bay	1.67	2.01	2.39
2 bays	2.75	3.55	4.45
3 bays	2.54	3.20	3.92

4.4.2 *Ultimate limit state*

As an example of the normal stress distribution due to bi-axial flexure ( $\sigma_F$ ), and to warping torsion ( $\sigma_w$ ) reference can be made to Figure 4-14 a, which also reports the total stress  $\sigma_{tot}$ . Also for the zed cross-section, the normalized stress is plotted in Figure 4-14 b with respect to the yielding stress, which is assumed to be achieved for pure bi-axial flexure in the most stressed point of the cross-section: warping stresses contribute significantly to the value of the total stress with reference to the bottom flange (element B'A'), where  $\sigma_w$  and  $\sigma_F$  have to be algebraically summed at the end point A'.

## Chapter 4

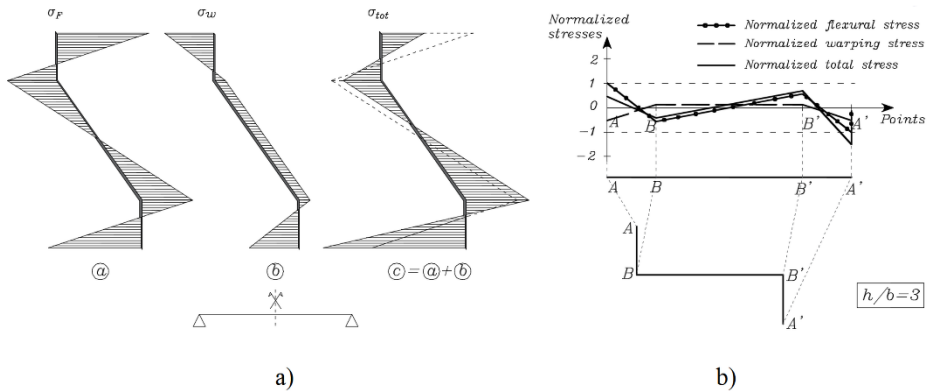


**Figure 4-14. Zed profiles mid-span stress distribution of a fixed end beam (a) and normalized stresses (b).**

As for lipped channels, the influence of  $\sigma_w$  can be evaluated with reference to the maximum flexural stress  $\sigma_F$  and Figure 4-15 refers to the cases of zed profiles restrained at each end by simple supports, presenting the ratio between the maximum of the total stress ( $\sigma_{tot}$ ) over the flexural stress ( $\sigma_F$ ) in selected beam cross-sections. Increasing the  $\bar{e}$  value, the  $\sigma_{tot}/\sigma_F$  ratio increases too and corresponds to the cross-sections governing design (identified by a circle), warping stresses contribute significantly to the total stress (from 17% to 71%).

Similar remarks arise with reference to members fixed at their ends. A more significant influence of the warping can be observed, as it appears from Figure 4-16. Ratio  $\sigma_{tot}/\sigma_F$  ranges from 1.00 up to 2.49 in cross-sections governing design, confirming once again the non-negligible rule played by warping torsion in resistance design.

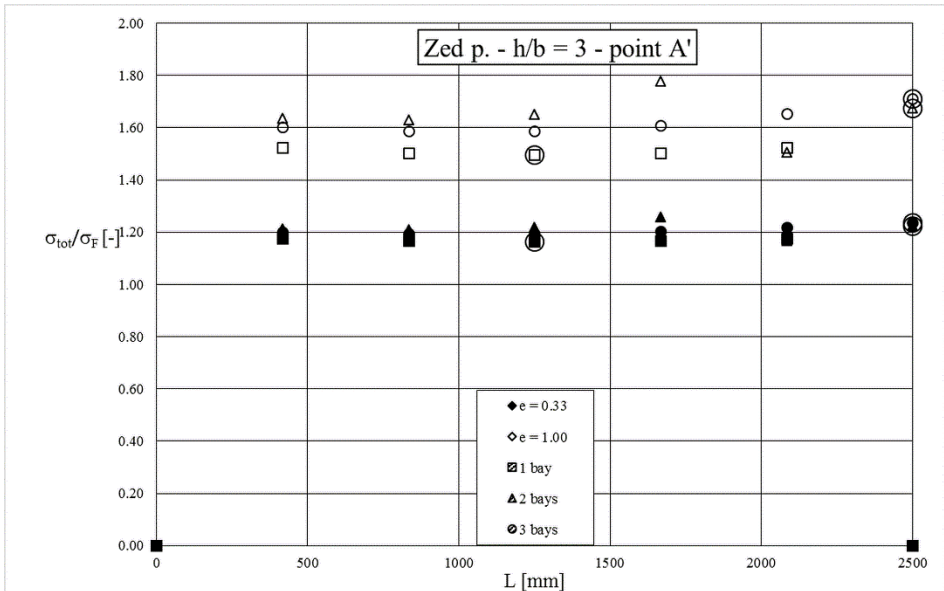


Figure 4-15. Distribution along the beam with simple end supports of  $\sigma_{tot}/\sigma_F$  for a zed profiles.

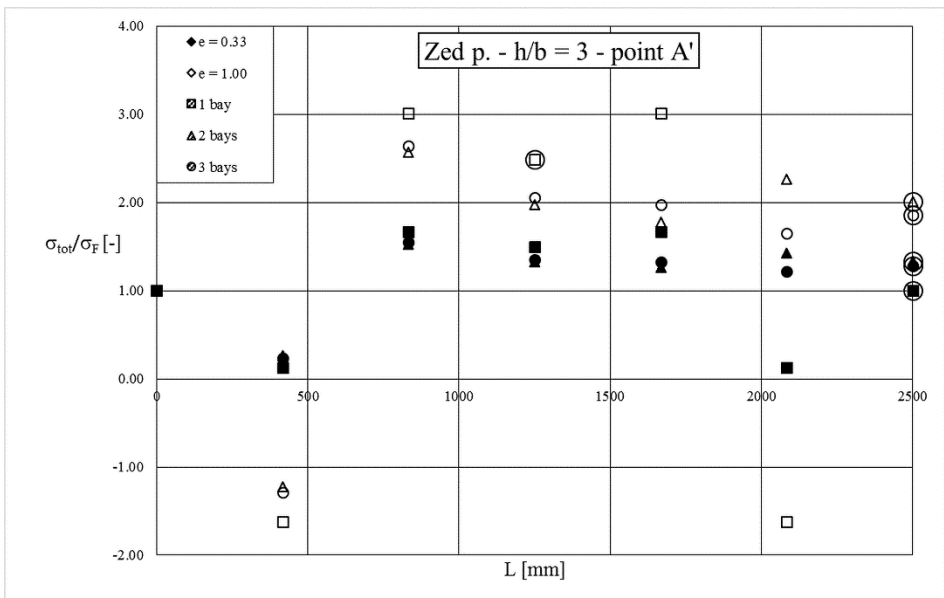


Figure 4-16. Distribution along the beam with fixed end of  $\sigma_{tot}/\sigma_F$  for a zed profiles.

A comparison between the influence of 6DOF and 7DOF design approaches on the member resistance is proposed in Figure 4-17 and Figure 4-18, presenting the ratio between the total stress on each longitudinal cross-section over the maximum bi-axial bending stress ( $\sigma_{F,max}$ ) in the whole member. For beams simply supported at the ends,

## Chapter 4

(Figure 4-17) and with reference to the cross-section of interest for design purposes (identified by a circle), a significant under-estimation of total stress occurs when warping effects are neglected: from 17% to 50% for mid-span sagging moments governing design and from 24% to 71% for cross-sections at the internal supports.

In the case of fixed ends, reference has to be made to Figure 4-18, where for a single bay the ratio  $\sigma_{tot}/\sigma_{F,max}$  is up to -0.75 and -1.24 for  $\bar{e}=0.33$  and  $\bar{e}=1$ , respectively. Otherwise, in case of continuous beams, the errors of a design procedure considering solely the flexural strength ranges between 28% and 34% for  $\bar{e}=0.33$  and 85% and 101% for  $\bar{e}=1$ .

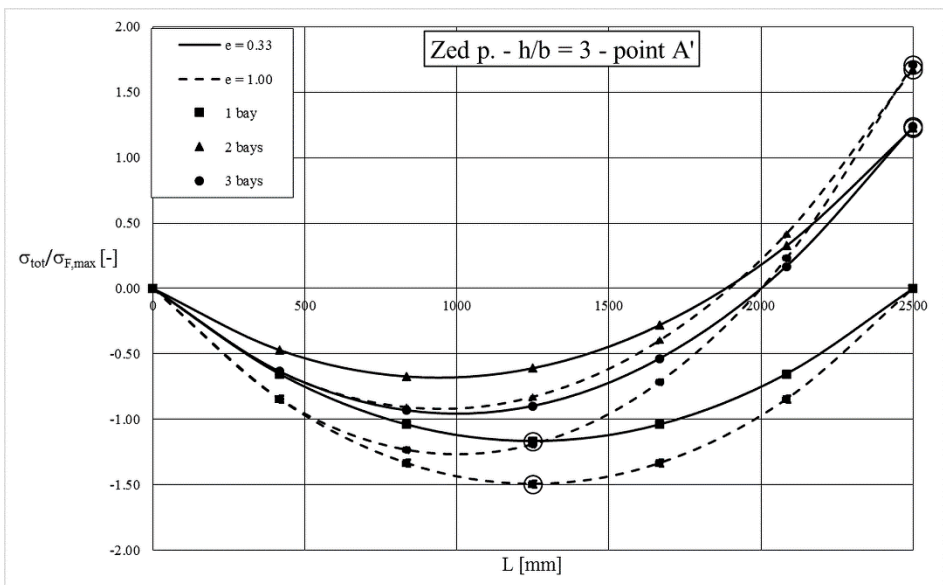


Figure 4-17. Distribution along the beam with simple end supports of  $\sigma_{tot}/\sigma_{F,max}$  for a zed profiles.

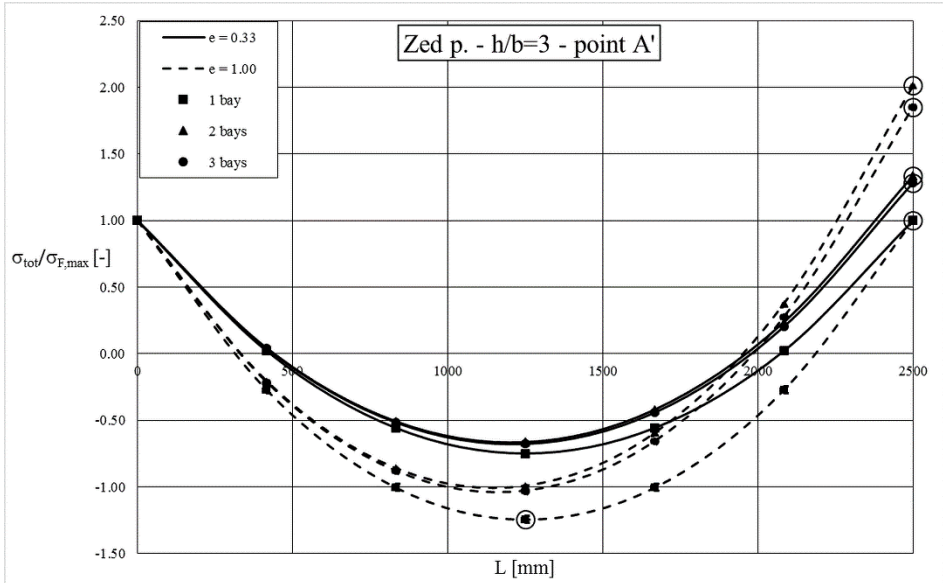


Figure 4-18. Distribution along the beam with fixed end of  $\sigma_{tot}/\sigma_{F,max}$  for a zed profiles.

#### 4.4.3 Load carrying capacity

For the rail beam design, the load carrying capacity has been evaluated by considering both serviceability and ultimate conditions, reference can be made to Table 4-7, where the ratio  $LCC^{6\varphi^F}/LCC^7$  is reported. The cases associated with  $\bar{e}=0$  have been neglected, owing to the absence of differences between the 6DOF and the 7DOF approaches when load is on the shear center. In the table, the condition governing the design is also specified between the round brackets: with reference to the kDOFs approach (with  $k=6$  or  $7$ ),  $\varphi_k$  and  $\delta_k$  are related to the rotation and displacement while  $B_w$  is related to resistance governing design.

Table 4-7. Warping influence on the zed beam performance: values of the  $LCC^{6\varphi^F}/LCC^7$  ratio.

		Simply supported ends			Fixed ends		
		$\bar{e}=0.33$	$\bar{e}=0.67$	$\bar{e}=1$	$\bar{e}=0.33$	$\bar{e}=0.67$	$\bar{e}=1$
h/b = 2	1 bay	1.00 ( $\delta_6/\delta_7$ )	1.00 ( $\delta_6/\delta_7$ )	0.88 ( $\varphi_6/\delta_7$ )	0.59 ( $\varphi_6/\varphi_7$ )	0.59 ( $\varphi_6/\varphi_7$ )	0.59 ( $\varphi_6/\varphi_7$ )
	2 bays	0.94 ( $\varphi_6/\delta_7$ )	0.49 ( $\varphi_6/B_w$ )	0.37 ( $\varphi_6/B_w$ )	0.68 ( $\varphi_6/B_w$ )	0.42 ( $\varphi_6/B_w$ )	0.35 ( $\varphi_6/\varphi_7$ )
	3 bays	1.00 ( $\delta_6/\delta_7$ )	0.68 ( $\varphi_6/\delta_7$ )	0.46 ( $\varphi_6/\delta_7$ )	0.66 ( $\varphi_6/B_w$ )	0.40 ( $\varphi_6/B_w$ )	0.38 ( $\varphi_6/\varphi_7$ )
h/b = 2.5	1 bay	1.00 ( $\delta_6/\delta_7$ )	1.00 ( $\delta_6/\delta_7$ )	0.73 ( $\varphi_6/\delta_7$ )	0.49 ( $\varphi_6/\varphi_7$ )	0.49 ( $\varphi_6/\varphi_7$ )	0.49 ( $\varphi_6/\varphi_7$ )
	2 bays	0.87 ( $\varphi_6/\delta_7$ )	0.49 ( $\varphi_6/\delta_7$ )	0.37 ( $\varphi_6/\delta_7$ )	0.60 ( $\varphi_6/B_w$ )	0.37 ( $\varphi_6/B_w$ )	0.30 ( $\varphi_6/B_w$ )

## Chapter 4

	3 bays	1.00 ( $\delta_6/\delta_7$ )	0.57 ( $\varphi_6/\delta_7$ )	0.38 ( $\varphi_6/\delta_7$ )	0.58 ( $\varphi_6/B_w$ )	0.35 ( $\varphi_6/B_w$ )	0.30 ( $\varphi_6/\varphi_7$ )
h/b = 3	1 bay	1.00 ( $\delta_6/\delta_7$ )	0.95 ( $\varphi_6/\delta_7$ )	0.63 ( $\varphi_6/\delta_7$ )	0.41 ( $\varphi_6/\varphi_7$ )	0.41 ( $\varphi_6/\varphi_7$ )	0.41 ( $\varphi_6/\varphi_7$ )
	2 bays	0.76 ( $\varphi_6/\delta_7$ )	0.45 ( $\varphi_6/B_w$ )	0.34 ( $\varphi_6/B_w$ )	0.55 ( $\varphi_6/B_w$ )	0.34 ( $\varphi_6/B_w$ )	0.27 ( $\varphi_6/B_w$ )
	3 bays	0.99 ( $\varphi_6/\delta_7$ )	0.49 ( $\varphi_6/\delta_7$ )	0.33 ( $\varphi_6/\delta_7$ )	0.53 ( $\varphi_6/B_w$ )	0.32 ( $\varphi_6/B_w$ )	0.25 ( $\varphi_6/B_w$ )

In general, the ratio is greater for simply supported ends and decreases with the increase of  $\bar{\epsilon}$ . It can be noted that the effective beam performance, identified by LCC<sup>7</sup>, is significantly lower than the one assessed via a design based on a 6DOF FE beam formulations. Only in a few cases, associated with lowest values of  $\bar{\epsilon}$  and for beam with fixed ends, there is no difference observed between the two approaches due to rotation governing design. Furthermore, in the case of refined design procedures, the great number of cases in which the load carrying capacity is governed by warping confirms, once again, the inadequacy of the 6DOF FE analysis packages currently adopted for routine design of industrial storage systems.

## **Chapter 5 Experimental pushover analysis on shelving racks**

### **5.1 Introduction**

Among the various types of cold-formed racks used to store goods and products nowadays offered from manufactures to the market [52], it is worth mentioning shelving rack storage systems, simply identified in the following as shelving racks or SRs. They represent a very popular solution, being commonly used for archive storage and domestic applications as well as for environments open to the public, such as shops, libraries, and superstores. Despite their limited height and the modest weight of what is stored, SR safety is extremely important. An eventual failure might result not only in the damage of stored goods, but also in severe injuries and loss of human life, with a potential consequence being the immediate and possibly long suspension of commercial activities.

The SR frames are composed of uprights, diagonals, and horizontal spacer bars, which are available on the market for varying depth and height. Furthermore, a key feature of modular SRs is that the number of loading levels and their spacing is highly customizable for any given frame height. Shelves are usually connected directly to the uprights by means of bolts, lugs, or clips, or may be supported directly on beams. Down-aisle (longitudinal) stability may be achieved by the action of semi-rigid joints between the beams and the uprights [53], which is the case of interest herein considered (Figure 5-1), or by bracing or sheeting in the spine of the rack. In the cross-aisle (transversal) direction, stability is provided by bracing or sheeting. A typical arrangement for SRs is presented in Figure 5-1. It appears that, from a structural point of view, SRs differ from selective pallet racks in terms of the small sizes and limited weight of the components and for the modest width and height of the storage system. Other key features of SRs are the weight of the stored units, which are always lower than those characterizing other storage systems, and the high percentage of the holes and their small pitch along the upright (Figure 5-2).

Several years ago SRs were traditionally considered by practitioners and engineers as secondary systems and therefore no specific design computations were required to be developed by rack manufacturing technical offices. Complete research can be found in [54].



Figure 5-1. Typical SR systems and key components.



Figure 5-2. Typical SR uprights with the regular perforation system.

Nowadays, due to the great presence of these ultra-light storage systems, as well as the increasing importance of their safe in-service use, a specific code has been developed for their design [55] but, like for provisions regarding other types of storage systems ([2], [43]), further improvements are urgently required. It is in fact necessary to increase the level of reliability of the design rules currently adopted, particularly the fact that in all the design phases some of the key features associated with the use of thin-walled cold-formed profiles with a mono-symmetric cross-section are being neglected or insufficiently considered. The Annex A of the SR provisions addresses design assisted by testing, in which it is stated that full-scale tests should be carried out to determine the load carrying capacity (strength test) or to verify a target performance (acceptance test) of the SR frame.

Experimental results should be used to extrapolate the design load carrying capacity of a family of structures similar to those tested but the test specimen itself should be the weakest configuration. It appears that the experimental assessment of the SR performance is undesirable for the following reasons: (i) excessive costs and (ii) extremely limited field of validity of the results. Full-scale tests are expensive because they require experienced technicians, suitable experimental equipment and refined measuring systems. The direct consequence is that, generally, the available manufacturing budget restraints allow manufactures to test only a very limited number of geometric layouts. Furthermore, the extrapolation of the experimental data to configurations differing in terms of geometry (story height and load levels configuration, upright frame width and bay length) and/or material components does not seem adequately reliable. On the other hand, the use of numerical approaches, based on experimental data regarding the performance of key components, seems a more efficient approach to achieving the goal of a safe design. However, this is only the case if advanced finite element (FE) beam formulations are available to capture the response of mono-symmetric cross-section members. Up until now, researchers have not paid adequate attention to SRs, except for [56] who tested under compression two different types of SR uprights by varying the specimen length and focusing attention on the combined effects of local and distortional buckling.

This paragraph presents the results of a combined experimental-numerical study performed by the Author and his research group in collaboration with a manufacturer on SRs that are unbraced in the longitudinal direction. In addition to component tests, eight representative configurations differing in terms of components (uprights and joints) and loads have been investigated by carrying out full-scale pushover and free vibration tests. The experimental results have then been simulated by means of advanced FE software, specifically developed for modelling industrial storage systems with non-symmetric cross-section components.

## 5.2 Components tests

Component tests have been carried out on uprights and joints (beam-to-column and base-plate connections) with the goal of providing essential data for the design of complete framed systems. The well-established importance of these tests ([1], [2]) is fundamental not only for monotonic design but also in the case of structures subjected to earthquakes. As an example, if advanced FE analysis packages are available, the whole storage rack could be efficiently modelled to obtain the pushover curves numerically, instead of evaluating them experimentally, and thus significant costs could be avoided. Furthermore, if the model is able to reproduce the experimental response, extensive parametric analyses could be carried out with limited costs and cover a wide range of practical interest.

## Chapter 5

In the following, attention has been focused on two typologies of SRs, differing in terms of the thickness of the components (uprights, beams, battens, and lacings). Labels F1 and F3 identify the thinner and the thicker ones, respectively and the ratio between the F3 and the F1 thickness is 1.8. All the key data, from the cross-section geometry to the overall response, are herein presented in non-dimensional form for reasons of commercial sensitivity to avoid public disclosure of data related to the commercial products employed. Although the authors were required to maintain a certain level of confidentiality, the research outcomes still maintain their validity and interest for routine design. It is worth noting that the description of the experimental program comprises also of tests aimed at evaluating the effective cross-section parameters.

### 5.2.1 Upright tests

The considered uprights, as shown in Table 5-1, have an approximately tee-shaped cross-section, with flange stiffeners and perforation that are wide and long when compared with the pitch. The main geometric data of the cross-section of the two considered uprights are provided in the table, which are the ratios between the gross ( $A_g$ ) and the perforated ( $A_{\text{perff}}$ ) cross-section areas and the ratio between the second moment of area in the two principal direction ( $I_y/I_z$ ). In the table the value of the Saint Venant's torsional constant ( $I_t$ ), the warping constant ( $I_w$ ) and the ratio between the eccentricity of the shear center with respect to the centroid  $y_s$  and the coil thickness ( $t$ ) are also reported.

Owing to the scope of the study, which is to assess the accuracy in the numerical prediction of the experimental full-scale pushover relationships, attention has been focused on the tests necessary to characterize the response of the uprights.

Axial behavior has been investigated by means of stub column tests according to the requirements of Appendix A of the EN 15512 standard [2], in order to evaluate the effective area accounting for perforations, cold-manufacturing processes, connection points/zones, overlapping, and local and distortional buckling phenomena. The typical specimen is composed of a stub upright, at each end of which a thick steel plate is welded. On the basis of the failure load ( $R_d$ ), the effective area,  $A_{\text{eff}}$ , however limited to be not greater than the gross one ( $A_g$ ), is evaluated as:

$$A_{\text{eff}} = \frac{R_d}{f_y} = Q^N \cdot A_g \quad 5.1$$

**Table 5-1. Gross-section properties of the considered uprights.**

	F1	F3
$A_g / A_{perf}$	1.10	1.09
$I_y / I_z$	6.69	6.61
$I_t$ [mm <sup>4</sup> ]	42.12	245.62
$I_w$ [mm <sup>6</sup> ]	$0.49 \cdot 10^6$	$0.89 \cdot 10^6$
$y_s / t$	2.35	1.38

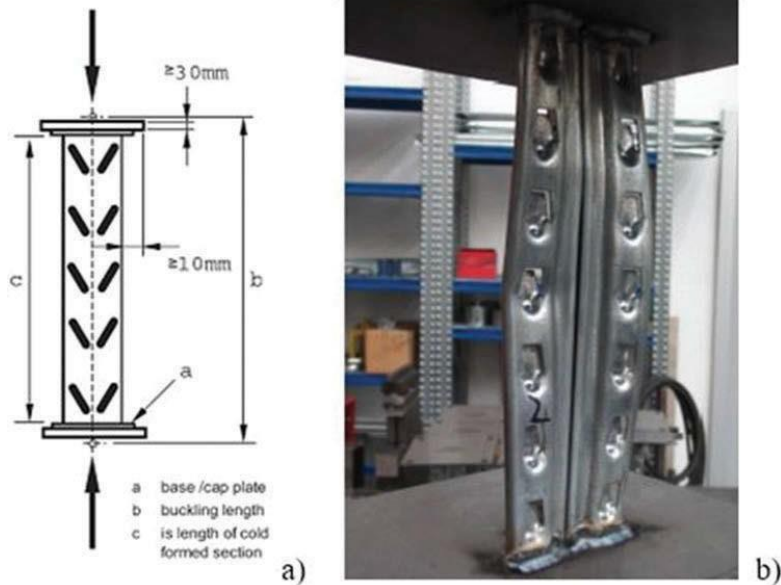


**Figure 5-3. Stub column test: (a) EN15512 and (b) test on F1 specimen.**

where  $f_y$  is the yielding strength of the base material before the cold working processes and  $Q^N$  is the reduction factor accounting for buckling on stocky thin-walled members.

In Figure 5-3 a typical layout of a stub-column test is depicted, together with a F1 specimen at collapse under the testing machine.

The reference values of the experimental reduction factors  $Q^N$  are 0.63 and 0.79 for F1 and F3 uprights, respectively, confirming the non-negligible influence of the extensive perforation system on this type of upright.

As to the bending behavior, the EN15512 provisions suggest bending beam tests for the prediction of the flexural performance of the uprights about the principal axes of flexure. In particular, from the experimental load vs. mid-span displacement curve, the values of the effective second moments of area and of the bending resistance can be directly assessed, which

are important design parameters that account for the presence of regular perforations in members. If attention is focused only on the upright flexural stiffness, owing to the fact that the resistance can be conservatively evaluated making reference to the perforated cross-section, a simple free vibration test coupled with numerical FE simulations should result in an efficient and inexpensive alternative, which has been used in the present study. In particular, it is worth noting that the experimental equipment and the measurement systems necessary for the free vibration tests are significantly cheaper and less complex than the ones recommended by standard provisions. Simply-supported beam specimens with a 2 m bay length have been suitably excited by means of a rubber hammer in order to capture the flexural behavior in all cross-section directions (Figure 5-4, a). A tri-axial accelerometer, MEMS microchip LIS344, fixed at the specimen mid-span and connected to an Arduino Uno acquisition data logger, has been used (Figure 5-4, b). In Figure 5-4 (c) a typical output in term of acceleration-time relationship is provided. Finally, the time history of accelerations acquired by the data logger has been converted in frequency domain via Fast Fourier Transform (FFT) functions, as shown in Figure 5-4 (d).

The value of the effective second moment of area,  $I_{eff,k}$ , has been evaluated by the assessment of the circular frequency,  $\omega_k$ , (with  $k$  indicating the  $y$  or  $z$  direction of vibration), or equivalently, of the natural frequency  $f_k$ , according to the well-established theory on dynamics of structures [57]:

$$\omega_k = \frac{2\pi}{f_k} = \pi^2 \sqrt{\frac{E_d I_{eff,k}}{mL^4}} \quad 5.2$$

where  $E_d$  is the dynamic Young's modulus,  $m$  is the specimen mass per unit length and  $L$  is the length between the supports.

During re-elaboration of test data, it has been noted that, due to the low energy dissipation capacity of uprights, damped and natural frequencies were very similar, with the assessed damping ratio always lower than 1%. In Table 5-2 the results in term of fundamental frequency ( $f$ ) are presented.

## Experimental pushover analysis on shelving racks

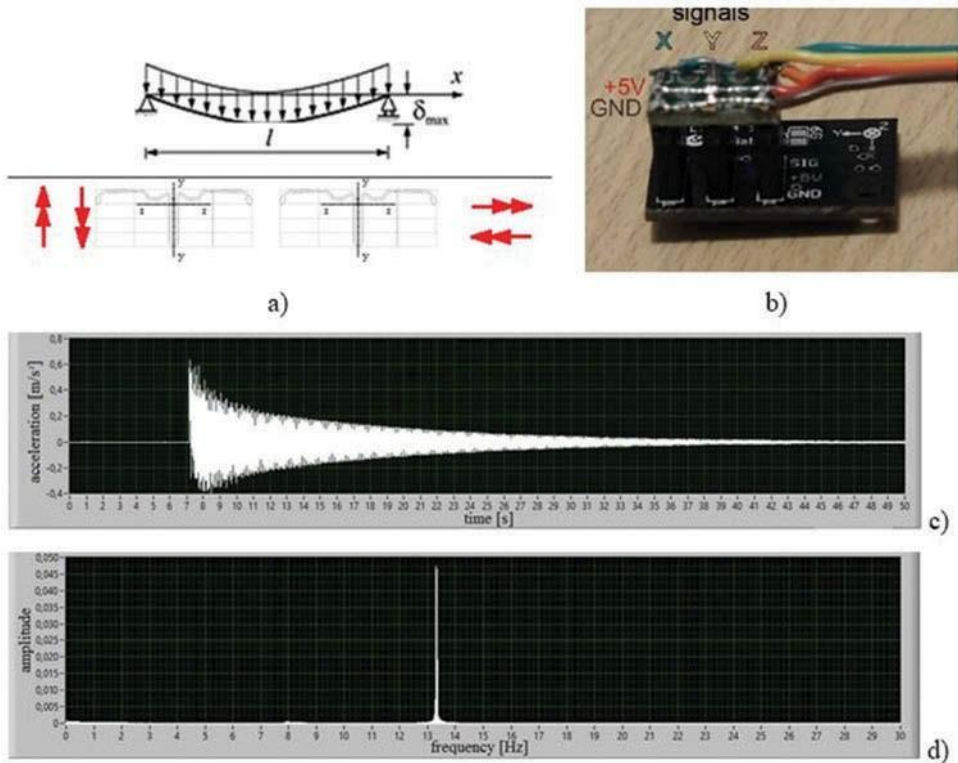


**Figure 5-4.** Vibration test on upright: (a) test scheme, (b) the MEMS accelerometer, (c) the response in term of acceleration and (d) the associated Fourier transform.

As shown in the table, the ratio  $\frac{f_y}{f_z}$  is significantly greater than unity: 2.18 and 2.27 for F1 and F3 uprights, respectively. Being  $\frac{\omega_y}{\omega_z} = \sqrt{\frac{I_{eff,y}}{I_{eff,z}}}$  according to 5.2 also in case of flexural performance, a remarkable influence of the direction of bending is expected owing to the great difference between  $I_{eff,y}$  and  $I_{eff,z}$ . The ratio of the second moments of area, which for the gross cross-section ranges from 6.6–6.7, reduces to 4.77 and 5.14 for F1 and F3 uprights, respectively.

**Table 5-2. Results from free vibrational test.**

Upright	Axes	Frequency [Hz]
F1	y-y	27.3
	z-z	12.5
F3	y-y	29.7
	z-z	13.1

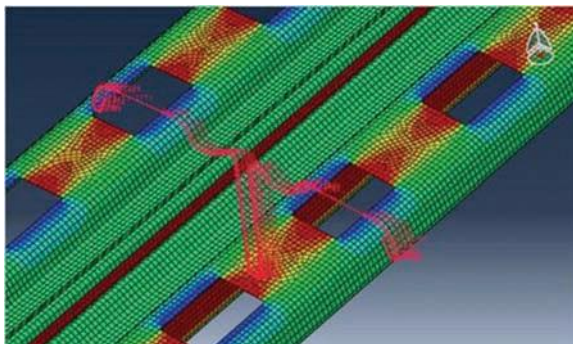


**Figure 5-5. Details of the finite element model of perforated upright.**

As the free vibration test is not yet standardized in design provisions, the authors decided to numerically validate experimental outcomes by means of the FE general purpose analysis package Abaqus [58]. Shell models with more than 10,000 S4R type elements have been used to accurately reproduce the sequence of gross- and perforated-sections, hence allowing the complex flexural behavior of the uprights to be captured (Figure 5-5). The effective second moments of area are evaluated on the basis of upright deflection under the considered load condition. The same finite element model has been used also for simulating the stub-column (compression) test in order to obtain the value of the effective area ( $A_{eff}$ ) as the ratio between the ultimate load and the virgin yielding strength of the material. It can be noted that a thick steel plates at both ends of the specimen have been added in the numerical models to simulate exactly the boundary conditions described in Figure 5-3.

Numerical (num) and experimental (exp) results are summarized in Table 3 in terms of the ratio between effective (subscript eff) and gross cross-section properties along both the principal axes. Effective area and second moment of area about the y-axis are predicted very accurately, while in case of bending along z-axis, the errors are lower than 10%, but on the safe side, confirming that the vibrational approach should be a very attractive alternative and more than adequate for practical design purposes.

**Table 5-3. Influence of perforations on the uprights.**

		F1_upright			F3_upright		
		Exp	Num	Exp/num	Exp	Num	
		Exp/num					
Area	$Q^N$	0.63	0.66	0.954	0.79	0.81	0.975
Second moment of area	$I_{y,eff} / I_y$	0.88	0.89	0.989	0.91	0.92	0.989
	$I_{z,eff} / I_z$	0.67	0.74	0.905	0.68	0.75	0.907

### 5.2.2 Tests on connections

Beam-to-column and base-plate joints have a great influence on the shelving rack response as well as on other types of industrial storage systems [59]. In the following the results associated with both types of tests are shortly summarized.

**Beam-to-column joints.** According to the requirements of Appendix A of EN15512, joint tests have been carried out on cantilever specimens that are composed of a one-way node (a short column connected to a beam) loaded by a shear force applied at the beam end, generating a bending moment on the joint. In Figure 5-6, the results in term of non-dimensional moment-rotation ( $\bar{m} - \bar{\phi}$ ) curves are reported.

The moment ( $M$ ) and the rotation angle ( $\phi$ ) have been proposed in dimensionless form by using the criterion reported in EC3-1-8 [38]:

$$\bar{m} = \frac{M}{W_{g,b} \cdot f_y}; \quad \bar{\phi} = \phi \frac{EI_b}{W_{g,b} \cdot f_y \cdot L_b} \quad 5.3$$

where  $I_b$  and  $W_{g,b}$  are, respectively, the second moment of area and the elastic section modulus of the gross cross-section of the beam with length  $L_b$ ,  $f_y$  is the yielding tension and  $E$  is the Young's modulus.

In the figure, two regions can be clearly identified: one for the hinges and the other for semi-rigid joints divided by a boundary that is represented as an elastic-perfectly plastic  $\bar{m} - \bar{\phi}$  relationship. It is characterized by a non-dimensional rotation and bending resistance values at the yielding point equal to 0.5 and to 0.25, respectively. Beam-to-column joint responses are always located in the hinge domain at significant distance from the semi-rigid domain. The initial branch of the  $\bar{m} - \bar{\phi}$  curves is always very close to the joint model boundary but as the bending moment increases, the flexural stiffness decreases owing to the spread of plasticity in the hooks of the connection details. Bending resistance is always very limited, but at the same time, non-negligible from the design point of view, corresponding to approximately 10% of the bending resistance of the beam. Dashed lines indicate the multi-linear relationships directly deduced from the experimental tests and used for the numerical simulation described in 5.5. These curves have been determined in order to best fit the moment-rotation curves obtained by tests.

**Base-plate connections.** Two different types of base restraints (Figure 5-7) are usually offered by the manufacturer, which can be identified as S-(support) and F-(fixed) restraints, independently on the thickness of the uprights. In the first case, the end of the upright is connected to a very thin plate simply supported on the floor that represents

Chapter 5

the common in-service situation and this is due to the need to change easily and rapidly the position of the shelving rack in the building during its life. In the second case, the end part of the upright is mechanically connected to the web of a T plate, whose flange is attached via two mechanical or chemical fasteners to the floor slab.

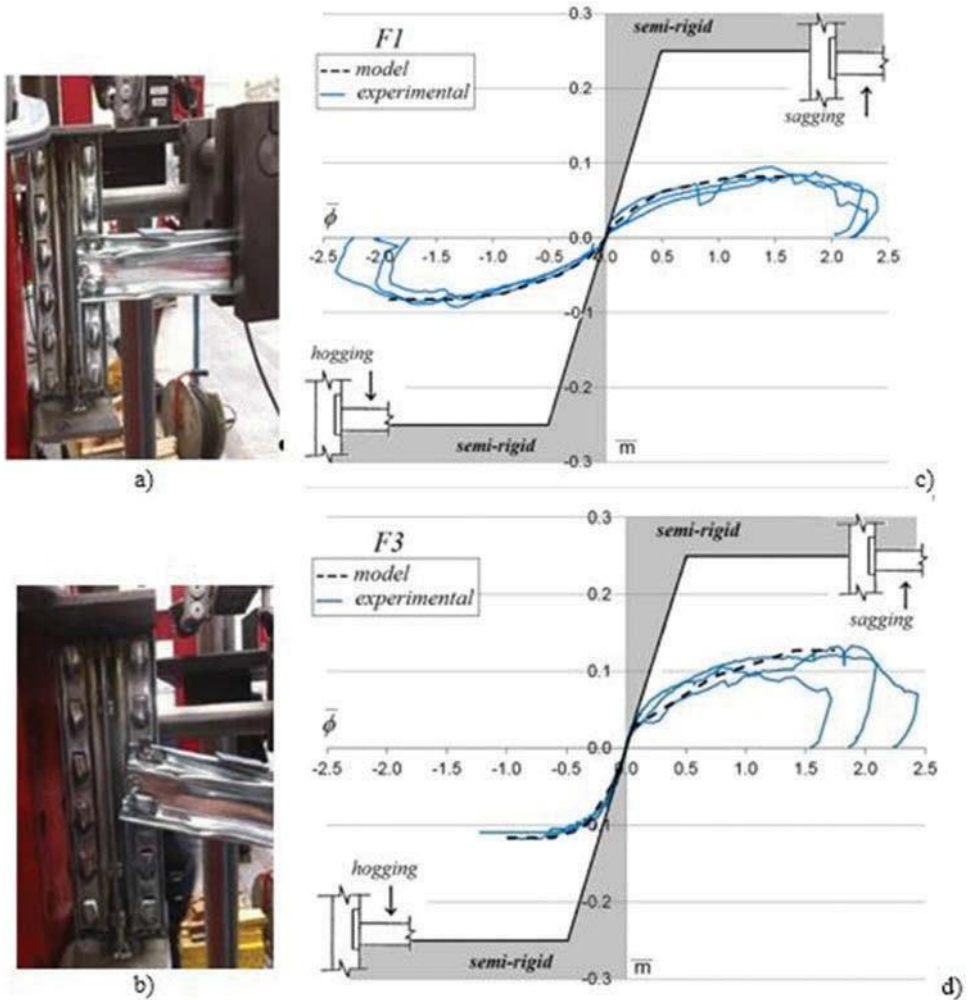


Figure 5-6. Beam-to-column joint experimental test: example of specimen (a, b) and curves associated with F1 (c) and F3 (d) specimens.

Base-plate connection tests according to the EN15512 code require complex testing equipment to evaluate the moment-rotation curves for different values of the axial force, which were not available for the present research. As an alternative the authors made reference to a simple portal frame test on a spatial specimen (Figure 5-8, a) composed of two short upright frames ( $h = 290$  mm) with the pallet unit hinged

to the uprights (Figure 5-8, b) and directly loaded by the sustained pallet unit load. A lateral force is increased from zero until collapse of the specimen or the achievement of a level of deformation that is beyond the range of engineering interest. The end restraint details for the S- and F- base joint types are presented in Figure 5-8 (c) and (d), respectively. The rigid floor condition has been achieved by bolting the base plate of each F-joint to a very stiff and thick steel plate. Otherwise, in case of S-joints, the thin plate at the upright end is simply supported on the floor plate.

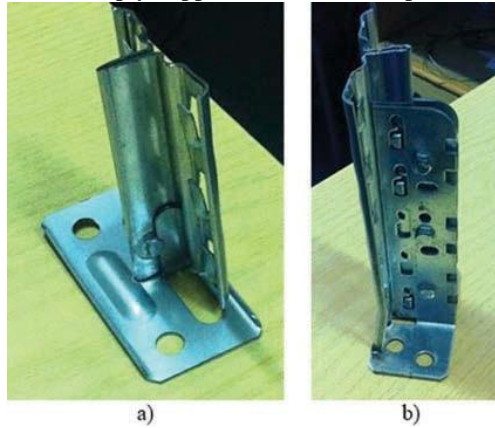
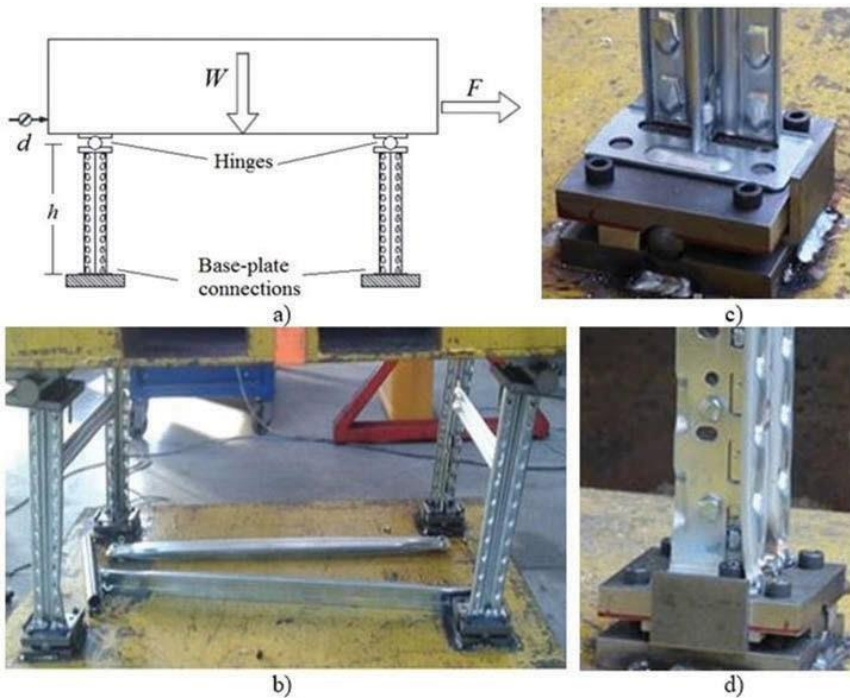


Figure 5-7. The support (a) and the fixed (b) restraints base-plate connections.



## Chapter 5

**Figure 5-8. Base-plate connection tests: scheme of the test (a), details of the specimen after test (b) and the S- (c) and F-restraint bases (d).**

The mass of pallet units (corresponding to a gravity load  $W$ ), was kept constant during the tests, which have been carried out by increasing the lateral push force ( $F$ ) and measuring the horizontal top displacement ( $d$ ) at the center of the bay. Owing to the high level of accuracy and precision of the geometry of the tested specimens, the vertical ( $N$ ) and horizontal ( $V$ ) load acting on each upright can be directly assumed to be equal to:

$$\begin{aligned} N &= \frac{W}{4} \\ V &= \frac{F}{4} \end{aligned} \tag{5.4}$$

Due to the circular bars (simulating cylindrical hinges) at the top end of upright frames, the response of each upright of the specimen is assumed to be that of a cantilever beam loaded on the top and with a rotational spring at the base. Therefore, the very limited contribution of shear deformations is neglected and the elastic top displacement ( $\delta_u$ ) is assessed as:

$$\delta_u = \frac{Vh^3}{3EI_u} \tag{5.5}$$

The upright axial deformations were considered negligible due to the very limited height of the specimen and hence the base plate rotation ( $\phi_{base}$ ) can be assessed as:

$$\phi_{base} = \arctan\left(\frac{d - \delta_u}{h}\right) \tag{5.6}$$

Bending moment acting on the base plate, considering both first and second-order effects is:

$$M_{base} = Vh + Nd \tag{5.7}$$

## Experimental pushover analysis on shelving racks

Also for base-plate connections, like for the beam-to-column joints, reference is made to the non-dimensional  $\bar{m} - \bar{\phi}$  curves, which are presented in Figure 5-9 and Figure 5-10, related to the F-and S-type bases, respectively. Dashed lines in Figure 5-9 and Figure 5-10 represent the multi-linear constitutive laws adopted to simulate the push-over responses. Also in this case, the curves used for numerical simulation (5.5) have been determined in order to best fit the experimental data. The straight line close to the moment axis is related to the boundary between semi-rigid and rigid base joints characterized by a stiffness and a strength equal to 30 times the flexural stiffness and to the bending resistance of the upright, respectively. With reference to the fixed bases (Figure 5-9), it appears that the base joint responses are typically semi-rigid and the limit resistance is approximately two times lower than the upright flexural resistance of the gross cross-section. Furthermore, it can be noted that there is a limited influence of the axial load on the fixed base restraints, which moderately increase the joint performance with the increase of the applied axial load. Failure was due to plasticity at the upright end and at the flange of the T plate.

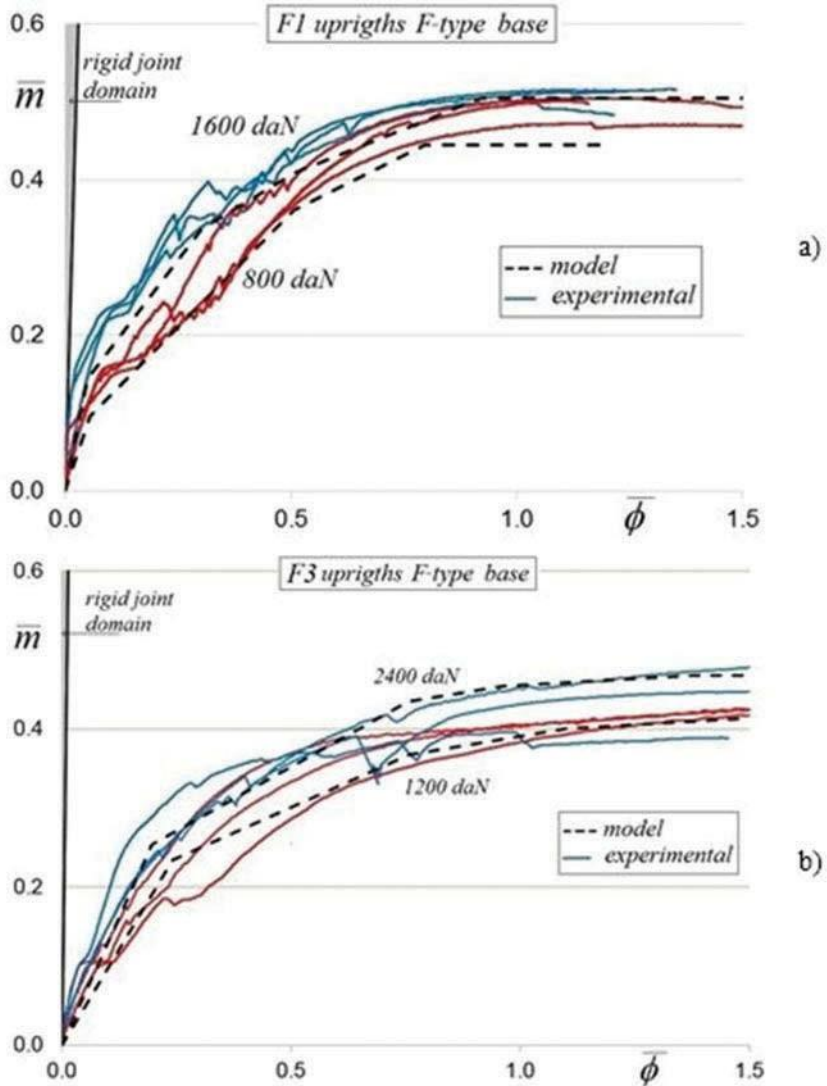


Figure 5-9. Base-plate experimental test: curves associated with F1 (a) and F3 (b) joints.

Similarly, the results related to the S-type connections are reported as non-dimensional  $\bar{m} - \bar{\phi}$  curves in Figure 5-10. As expected, the responses are remarkably more flexible than the response associated with the rigid bases, and for this restraint the curves are strongly influenced by the values of the axial load, as generally it appears in this type of tests [60] executed on behalf of rack manufactures. Flexural base strength is quite proportional to the level of axial force and ranges from approximately 5–25% of the upright bending resistance. Failure of the joints was due to the plasticity in the thin-end plate, equal for the S1 and S3 uprights, which remained elastic.

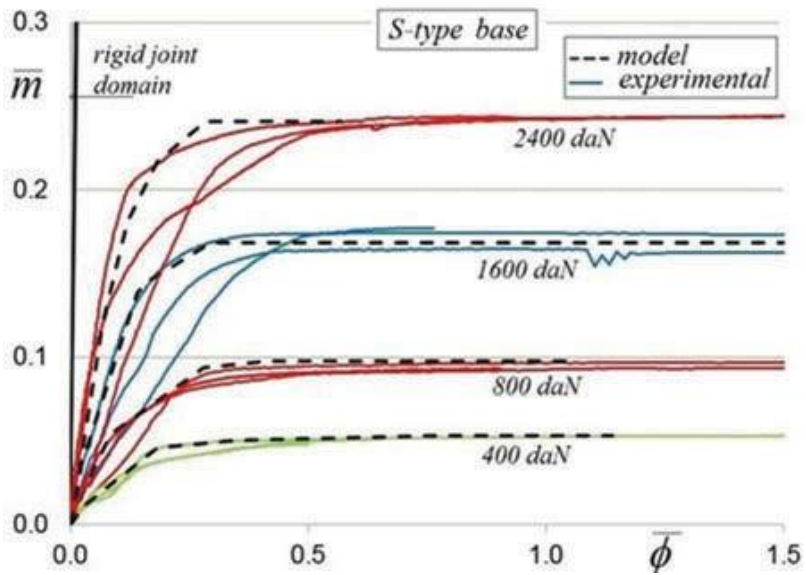


Figure 5-10. Base-plate experimental test: curves associated with S-type base-plate.



Figure 5-11. The typical full-scale tested SR configuration.

### 5.3 Full scale tests

The experimental program was comprised of 8 full-scale tests on specimens that all have the same geometric configuration, that is 2 bays and 4 stories (Figure 5-11). The length of the bay is 1210 mm and the inter-story height is approximately 500 mm, with a total height of 1972 mm.

The width of the upright frame is 500 mm, which is of a mixed type: near to the floor there is cross-bracing with lacings while in the remaining part battens connect the uprights. Differences among the specimens are mainly due to:

- components: two sets of components (beams, uprights, and lacings) have been considered for uprights and beams, which, as previously mentioned, are identified as F1 and F3 and differ for the thickness of the coils;
- base connection restraints: the supported (S-) and fixed (F-) bases, which represent the common solution for upright end connections, have been investigated together with ideal hinges (H-) at the upright bases. This limiting condition can very rarely be reached due to the presence of a continuous floor and to the benefits associated with the upright axial load. Like for the F-type bases the upright bottom end is strengthened by a T member, but no bolts were used to fix its flange to the thick supporting plate, which was free to rotate in the down-aisle rack direction (Figure 5-12); and
- vertical load: equal gravity loads were applied on each bay and different values have been selected to simulate the weight of the stored goods, depending on the rack types and on the base restraints.

Table 5-4 summarizes key features of the tested specimens in terms of components, base restraint, and value of the masses on each couple of pallet beams and presents the labels used for their identification. In the same table, the value of out-of-angle imperfections, which have been measured before each test in the fully loaded configuration, expressed in milliradians along the down- and cross-aisle direction are also reported and identified as Imp\_D and Imp\_C, respectively.

## Experimental pushover analysis on shelving racks



Figure 5-12. Details of the hinged base restraint.

Table 5-4. Key features of the full-scale specimens.

Name	Components		Base restraint			Masses [kg]			Out-of-plumb angle [mrad]	
	F1	F3	Hinge	Fixed	Support	100	200	300	Imp_D	Imp_C
F1-H	X		X			X			2.22	2.22
F1-F	X			X			X		2.67	2.67
F1-Sa	X				X		X		5.55	5.55
F1-Sb	X				X	X			1.11	6.67
F3-H		X	X				X		5.55	5.55
F3-F		X		X				X	5.55	1.67
F3-Sa		X			X			X	5.55	2.67
F3-Sb		X			X		X		5.55	5.55

Table 5-5. Values of the fundamental period of vibrations, expressed in seconds.

T <sub>1</sub> [s]	F1_specimens				F3_specimens			
	H	F	Sa	Sb	H	F	Sa	Sb
Unloaded	0.179	0.126	0.152	0.163	0.174	0.113	0.128	0.131
Loaded	1.232	1.274	1.442	1.114	1.237	1.015	1.051	0.938

## 5.4 Pushover tests

Overall frame tests have been carried out by pushing racks in the down-aisle direction using a hydraulic jack. Loads have been applied on each storage level in order to simulate an inverse triangular pattern [49], because it is able to reproduce the deformed modal shaper associated with the fundamental period of vibration [61], that increases from the bottom to the top via the load balancer indicated in Figure 5-13. Tests were carried out by increasing the value of the applied horizontal forces until collapse was achieved and/or the deformed shape of the rack was in the softening branch and beyond the range of interest for engineering purposes due to the large values of horizontal displacements.

The measuring system consists of a load cell used to monitor the total applied lateral load and inductive transducers to monitor the lateral displacements of each storage level. Top displacement was used as the control test parameter. A counter frame, approximately 3.0 m high, 5.0 m long, and 1.2 m wide, indicated in Figure 5-14, consisted of a spatial fully braced frame (trussed tower) constructed using bi-symmetric rectangular hollow section members and connected via a rigid and strong beam to an upright frame. The counter frame serves essentially to apply to the specimen the lateral load and it has been rigidly fixed to an industrial foundation. In order to avoid possible damage due to a sudden and brittle collapse of the specimens, the masses simulating the effects of gravity loads have been attached to a crane by means of steel cables.



Figure 5-15 and Figure 5-16, which are related to the F1 and F3 frames, respectively, present the experimental  $\bar{v}^{exp} - \delta^{exp}$  relationships, where  $\bar{v}^{exp}$  is the non-dimensional base shear and  $\delta^{exp}$  is the horizontal displacement at the top of the rack. The term  $\bar{v}^{exp}$  has been

expressed as the ratio between the total base shear applied to the frame ( $V_b^{exp}$ ) over the maximum base shear reached on the Sa specimens, i.e.  $\bar{v}^{exp} = \frac{V_b^{exp}}{V_{b,max}^{Sa}}$ .

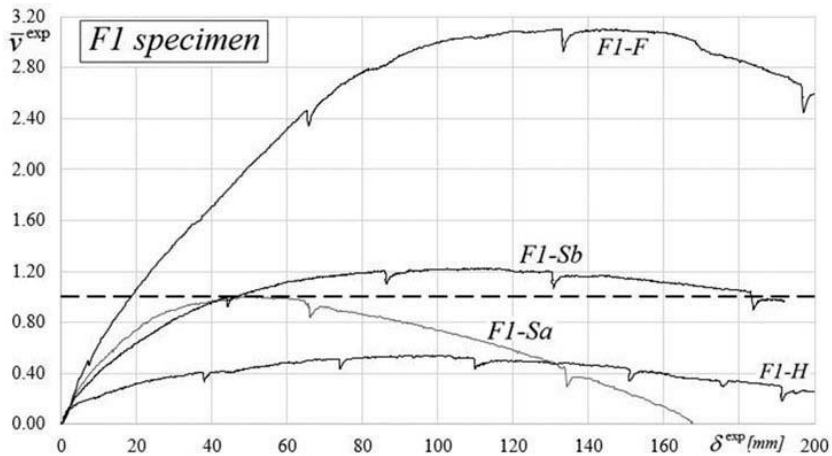


Figure 5-15. Pushover experimental curves on F1 specimens.

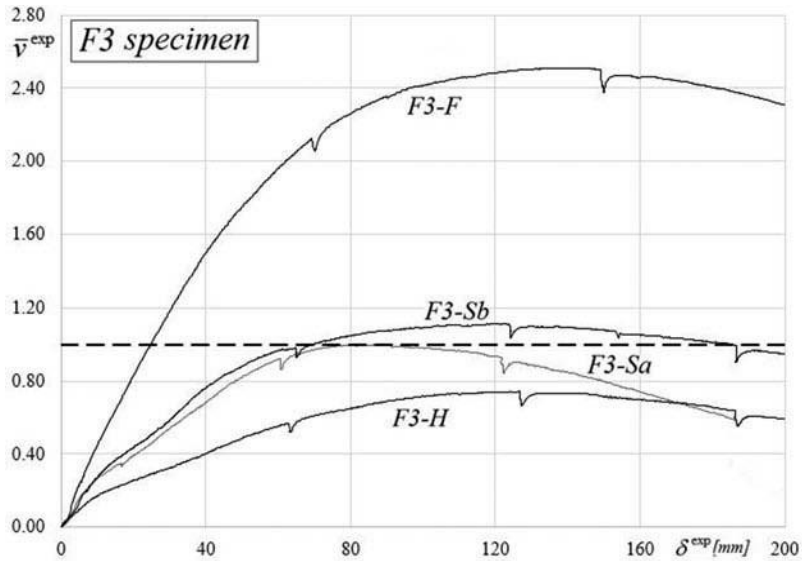
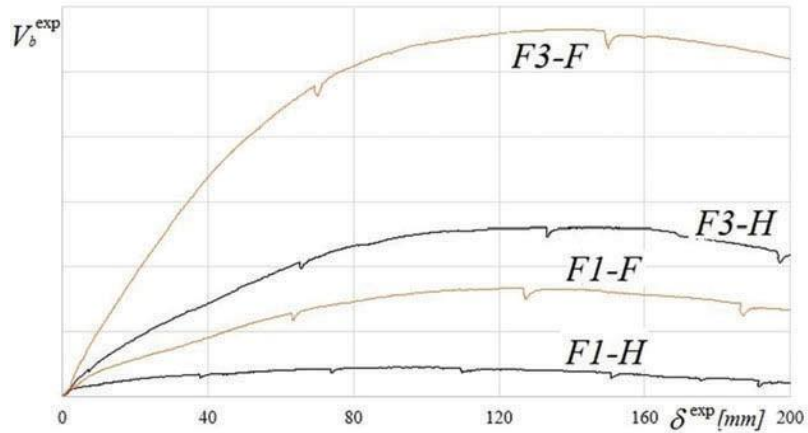


Figure 5-16. Pushover experimental curves on F3 specimens.



**Figure 5-17. Direct comparison between F1 and F3 specimens with hinged and fixed upright bases.**

Both figures present similarities in all the pushover curves. The initial stiffness depends only on the type of rack and due to the stabilizing action of the gravity loads is not strongly influenced by the efficiency of the base restraints. Increasing the applied lateral loads, the stiffness of the specimen decreases until the maximum resistance is reached and then a softening branch can be observed. The best and worst performances are associated, as expected, to the F- and H-cases, respectively, and the responses of the S-specimens are in between but closer to H specimens. The influence of the vertical loads can be directly observed by comparing the Sa and Sb specimens, which are loaded with the heaviest and lightest masses, respectively. No great differences can be observed in the value of the stiffness, while the maximum applied lateral force is greater in the case Sb, up to 1.2 times larger than for the Sa specimens. To evaluate the influence of the thickness of the material of the specimen performance, Figure 5-17 can be considered, where the pushover curves for the F1 and F3 specimens are presented in dimensional form for the cases of F- and H-base restraints. Despite the absence of the values on the ordinate axis scale which have been omitted for reasons of commercial sensitivity, it can be noted that an increase of 80% of the thickness lead to a maximum shear for F3 specimens that was more than 3 (F bases) and 6 (S bases) times greater than the corresponding F1 values. Tests were stopped when the end stroke of the hydraulic jack was reached and brittle failures were never observed.

All the specimens sustained a large global deformation in the plastic range, between the yield and ultimate collapse loads (Figure 5-18), mainly provided by the inelastic deformations of beam-end connectors as shown in Figure 5-19.

A relevant contribution in terms of ductility was due to the type of the base restraints and Figure 5-20 show the typical deformed shapes of the restraints for the F-, S-, and H- framed systems. As to the hinged bases, it can be noted that the plastic deformation of the thin plate is similar to that observed during base-plate connection tests.

A summary of the test data related to the maximum base shear and the associated level of lateral displacements is reported in Table 5-6, for each specimen.



Figure 5-18. Large deformation on the specimen under testing.



Figure 5-19. Details of the beam-to-column joints after tests.

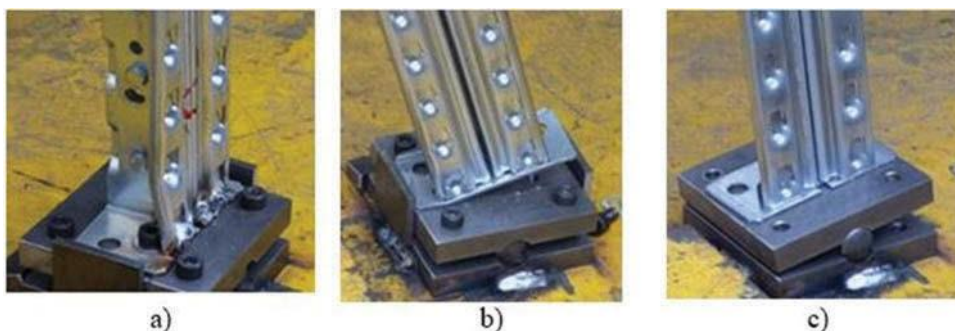


Figure 5-20. Base-plate connection after the test: the typical deformed shape of the F-(a), S-(b), and H-(c) restraints.

Also reported are the non-dimensional values of the shear force ( $\bar{v}_{max}^{exp}$ ) and displacement value ( $\delta_{max}^{exp}$ ), the values of the inter-story drift,  $\Delta_j$ , and the inter-story drift ratio,  $\Delta_j/h_i$

Independent of the type of bases, a non-negligible level of lateral displacement was reached in each specimen.

The lowest values are associated with the F1-Sa and F3-Sa specimens and using  $H_{tot}$  to indicate total height, the values of the ratio  $\frac{\delta_{max}^{exp}}{H_{tot}}$  are 1/39 and 1/23, respectively. The largest value of  $\frac{\delta_{max}^{exp}}{H_{tot}}$  is approximately 1/14, which was reached both for F1-F and F3-F specimens. The deformed shape of each specimen is of the panel mechanism type, which is always governed by the rotation of the joints with all the uprights only inclined, as confirmed from movies taken during the tests. Similar remarks can be made based on Figure 5-21, where lateral displacements are plotted versus the storage level.

**Table 5-6. Key data of the deformed shape in correspondence of the maximum lateral load.**

	$\bar{v}_{max}^{exp}$	$\delta_{max}^{exp} [mm]$	$\Delta_1/h_1$ [%]	$\Delta_2/h_2$ [%]	$\Delta_3/h_3$ [%]	$\Delta_4/h_4$ [%]
F1-H	0.54	96.7	5.12	4.74	5.12	4.55
F1-F	3.11	143.99	5.53	7.05	8.31	8.21
F1-Sa	1	50.64	2.25	2.52	2.77	2.69
F1-Sb	1.22	112.47	5.34	5.62	5.95	5.81
F3-H	0.75	126.63	7.04	6.01	6.54	5.98
F3-F	2.51	139.83	5.49	6.94	7.57	8.25
F3-Sa	1	86.41	4.32	4.12	4.83	4.2
F3-Sb	1.12	120.14	6.5	5.46	6.37	5.95

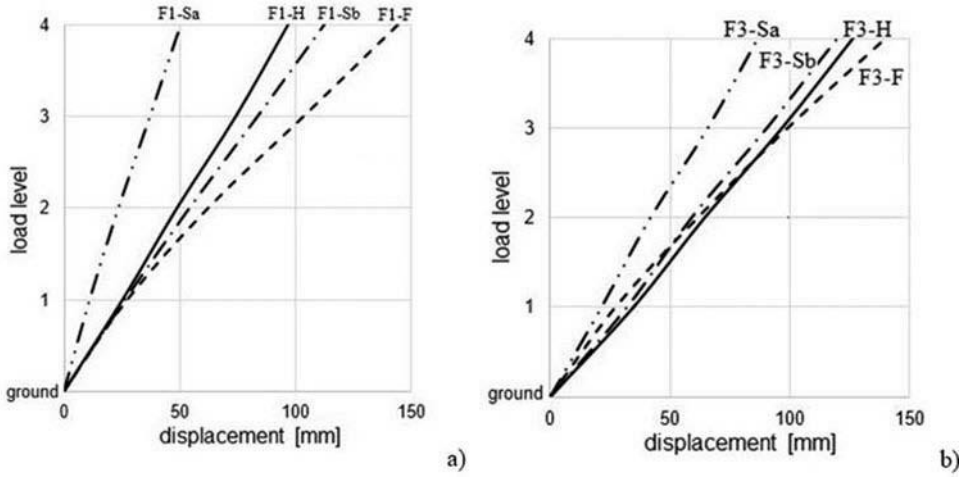
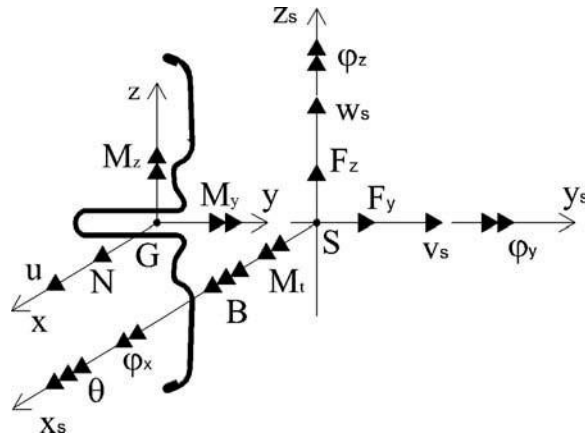


Figure 5-21. Displacements along elevation for (a) F1 and (b) F3 specimens.

## 5.5 Numerical simulations with Śiva software

As already observed in previous research on rack performance ([37], [10]) under static loads, the influence of warping effects must always be accounted for when mono-symmetric open thin-walled members are used as uprights. As a consequence, independent of the complexity and extension of the geometric layout, refined FE analysis packages are also required in routine design. Owing to the non-coincidence between the shear center  $S$  and the centroid  $G$ , in the case of mono-symmetric cross-sections, reference is generally made to point  $S$  for the definition of the sets of generalized displacements, except for the axial displacement  $u$ , which is assumed to coincide with point  $G$ . The shear forces ( $F_y$  and  $F_z$ ), uniform torsional moment ( $M_t$ ), and bimoment ( $B$ ) are referred to point  $S$ , whereas bending moments ( $M_y$  and  $M_z$ ) and axial force ( $N$ ) are defined with respect to the centroid, as depicted in Figure 5-22. Cross-section warping  $\theta$ , which is the 7<sup>th</sup> DOF, is essential to correctly model open singly-symmetric cross section members and is defined as:

$$\theta = \theta(x) = -\frac{d\varphi_x}{dx} \quad 5.8$$



**Figure 5-22. Sets of displacements and generalized forces at the node location for FE beam formulations with 7DOFs.**

Only the presence of  $\theta$  guarantees that the rack design is developed using appropriate analysis tools and adequately considering the key features of rack upright cross-sections, the geometry of which is accurately described by the Wagner constants and the eccentricity between points  $G$  and  $S$ .

In the context of the present research, the experimental behavior of the tested SRs has been reproduced by using the Šiva FE analysis program, which is based on the Fortran code NONSAP but suitably modified. Non-linear springs are implemented to reproduce the behavior of connections and hence it is possible to simulate the behavior of moment-resisting frames, where plasticity can be concentrated in correspondence of the beam-to-column joints and at the base of the columns (at the base-plate connections). As to the details related to the rack modeling:

- both beam-to-column joints and base-plate connections have been simulated via a mono-dimensional rotational spring element. The multi-linear (5 branches) moment-rotation relationships are represented by the dashed lines in Figure 5-6 (beam-to-column joints), Figure 5-9 (F1-bases), and Figure 5-10 (F3-bases);
- members have been modeled via a 7 DOFs beam elements and the geometric properties refer to the gross cross-section, according to the requirements of common design codes; and
- the vertical loads simulating the presence of pallet units have been modeled as uniform distributed loads on the pallet beams.

Initially the free vibration tests were simulated and Table 5-7. Prediction of the dynamic SR properties. presents the ratio between the experimental and numerical fundamental period of vibration ( $T_1$ ) for the loaded and unloaded racks and the percentage of the participating mass associated with the first mode of vibration

(evaluated numerically). From the data, it appears that the accuracy of  $\acute{S}iva$  in the prediction of the fundamental period of vibration is more than satisfactory. Errors range from 2–25% and should be easily reduced by increasing the number of experimental tests. Furthermore, owing to the absence of longitudinal bracing systems, the fundamental mode is always associated with a flexural cantilever deformed modal shape. The participating mass ranges between 75% and 85%. As a consequence, the common inverse triangular lateral force distribution can be adopted for pushover analysis.

**Table 5-7. Prediction of the dynamic SR properties.**

	Unloaded	Loaded	
	$T_1^{exp} / T_1^{\acute{S}iva}$	$T_1^{exp} / T_1^{\acute{S}iva}$	mp [%]
F1-H	1.122	1.152	80.81
F1-F	1.154	1.121	74.81
F1-Sa	1.212	1.112	77.62
F1-Sb	1.225	1.111	79.51
F3-H	1.124	1.258	84.78
F3-F	1.025	1.251	78.56
F3-Sa	1.051	1.213	79.26
F3-Sb	1.238	1.111	80.8

Eigenvectors associated with the dynamic eigenvalues are similar for all the considered specimens and, as an example, in Figure 5-23 the first and second mode shapes for the F1-F frame are depicted, which are always related to the longitudinal and transversal directions of vibration, respectively.

The numerical pushover curves  $\bar{v}^{num} - \delta^{num}$  are compared with the  $\bar{v}^{exp} - \delta^{exp}$  experimental ones in Figure 5-24 and Figure 5-25, which are related to the F1 and F3 specimens, respectively. In the figures, which are divided into four parts, each associated with one of the four tested specimens, the degree of utilization (DUJ) is presented for each joint. It is expressed as the ratio between the bending moment at the joint over its flexural resistance evaluated with reference to the maximum applied base shear.

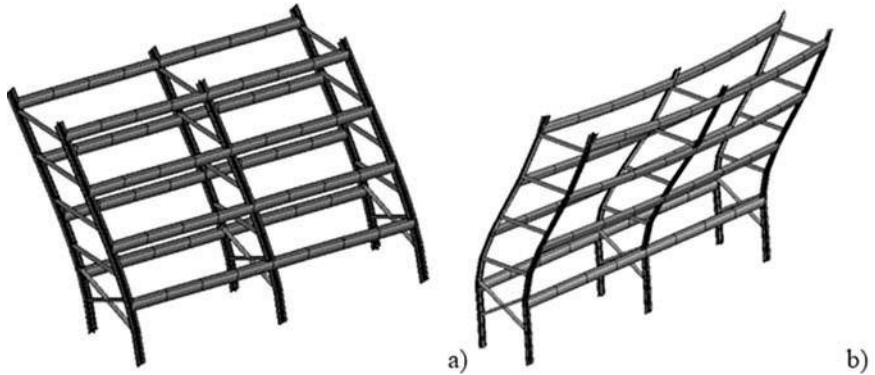


Figure 5-23. Example of the 1st (a) and 2nd (b) mode shape obtained by Síva software.

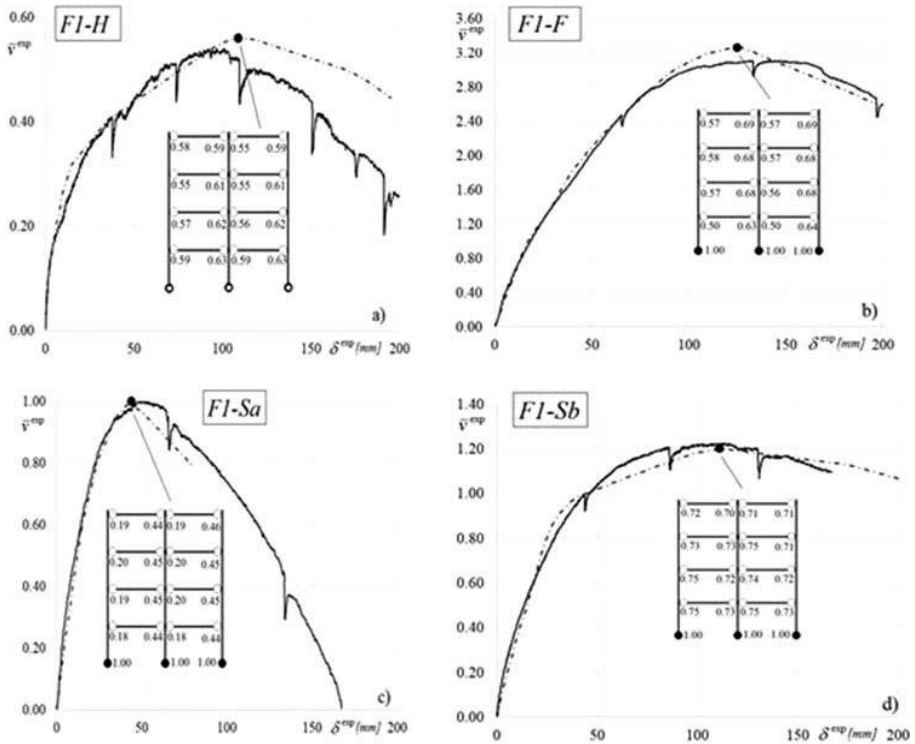


Figure 5-24. Experimental vs. numerical pushover curves for the F1-SRs.

It can be noted that, at first, the degree of accuracy of the numerical simulation is more than satisfactory for design purposes. The initial branch of the pushover curves is accurately reproduced, as well as the trend of the experimental curve, including also the softening branch.

Differences in components, base-plate joints and load conditions with the numerical approach are reflected in different pushover curves, as experimentally observed. A check of the coefficient of utilization of the uprights shows that they are in elastic range during the pushover analysis, confirming the key role played by the ductility of connections. The failure condition of the specimens, which can be associated with the maximum lateral load applied, is due to interaction between plasticity and instability: in particular, plasticity at both beam-to-column joints and base-plate connections and overall instability of the rack frame. For the sake of simplicity, in the following the labels PBH and PBS are introduced to indicate the beam-to-column joints subjected to hogging and sagging moments, respectively, under lateral load. In particular, it can be noted that:

- base-plate connections are always in the plastic range (DUJ=1);
- the values of DUJ for PBH and PBS are independent of the bay and load level, with the exception of the PBS joints at the first load level in the F1-F specimen, characterized by a DUJ slightly lower than at the other levels; and all beam-to-column joints are in elastic range, with the exception of the PBH joints of the F3-F specimen, with DUJ=1 for each level.

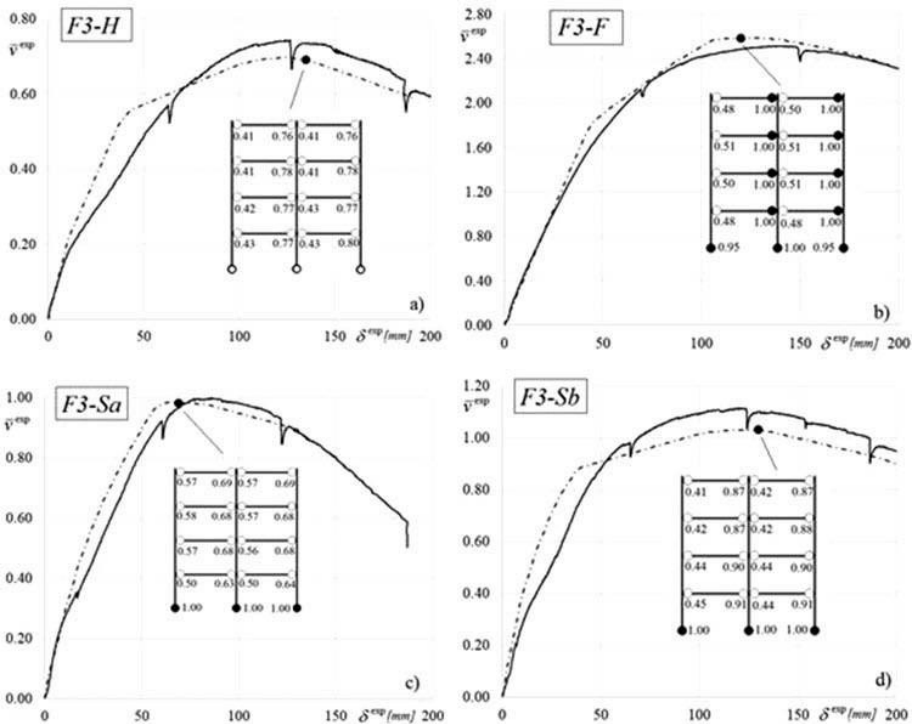


Figure 5-25. Experimental vs. numerical pushover curves for the F3-SRs.

**Table 5-8. Key data related to the accuracy of the 7DOFs FE simulations.**

	F1_specimens				F3_specimens			
	H	F	Sa	Sb	H	F	Sa	Sb
$k^{num}/k^{exp}$	1.035	1.054	0.989	0.979	0.937	1.03	0.985	0.925
$V_{b,max}^{num}/V_{b,max}^{exp}$	1.148	0.951	0.873	0.987	0.963	0.903	0.868	1.024

Table 5-8 summarizes the key data required for an appraisal of the accuracy of the 7DOFs simulations, with results expressed in terms of the numerical values (subscript num) over the experimental values (subscript exp). In particular, reference is made to the accuracy in the prediction of the initial stiffness (k), which has been evaluated by interpolating via a straight line the sets of numerical and experimental results according to the minimum square root method. A regression coefficient not lower than 0.95 has been imposed. It can be observed that the errors are always very limited, in particular the overestimation is not greater than 5%. The ratios related to the numerical versus the experimental maximum shear base are also reported in the table. The  $\frac{V_{b,max}^{num}}{V_{b,max}^{exp}}$  ratio ranges between 0.87 and 1.14, confirming that the degree of accuracy is more than adequate for design purposes.



## Chapter 6 Conclusion

After a briefly introduction to the steel storage pallet racks in Chapter 1, the thesis presents in Chapter 2 a beam element which is able to take in account the warping effects: it is an influential phenomenon which is generally present in thin-walled open cross-sections. Furthermore, the geometric stiffness matrix is deduced; through this it is possible to perform both buckling and second-order analysis. The formulation is developed by the total equilibrium equations, adopting the principle of virtual work and it is applicable in problems involving arbitrary thin-walled open section. The main characteristic of the developed formulation is the existence of 7DOFs per node, whereas the seventh is related to the warping displacements. The introduction of this additional degree of freedom also allows to correctly consider the coupling between the flexure and torsion in buckling analysis. After the development of the software and an accurate phase of validation, the new tool has been adopted for the study of steel storage pallet racks, which are strongly influenced by warping and flexural-torsional buckling. Different articles have been published and then summarized in the thesis; as they are an outcome of the research work.

The results proposed in Chapter 3 deal with medium-rise racks, and attention has been paid on the effects of the warping on the resistance checks. The response of several geometric configurations of interest for rack practice has been considered; a parametric study has been carried out by using two FE beam formulations differing in the number of nodal degrees of freedom considered, both implemented in *Śiva*. With a reference to the worldwide used resistance check approaches, design results of a traditional 6DOFs analysis have been compared with those from a more refined formulation, considering warping effects, i.e. characterized by 7DOFs per node. It has been demonstrated that warping plays a very important role on the rack response and this directly reflects on the safety level of design, in fact if warping is neglected safety level is significantly overestimated, especially for external uprights.

A research on non-bisymmetric cross-section members has been developed in Chapter 4. The design is complex and steel provisions for industrial racks currently neglect key features of these types of elements, especially when used as pallet and rail beams. Furthermore, FE analysis packages adopted for routine design are inadequate in simulating the response of non bi-symmetric cross-section members.

The presented study reports the results of a study regarding the comparison between the effective member performances and those estimated by means of traditional FE software

## Conclusion

which only offers 6DOFs beam formulation. It has been demonstrated that a safe and optimal design can be achieved only if the cross-section warping is adequately accounted for in structural analysis. All in all, in the case of pallet beams, the errors associated with the adoption of design procedures, which neglect the key features of non bi-symmetric cross-section members are absolutely non negligible and significantly more substantial than the those discussed by referring to the uprights of selective pallet racks [37]. It is hence expected that both pallet and drive-rack design codes will be urgently improved, including clear and correct indications for the design of horizontal members in industrial storage rack systems.

Chapter 5 presents a study which involves shelving racks. This type of structure represents the lowest level of storage systems in terms of dimensions, costs and weight of the stored goods and products. They are commonly and extensively used worldwide, despite the fact that they are designed neglecting some key features of the structural behavior. Current design approaches are, in fact, based on extremely poor rules and standard codes are in need of urgent improvements, especially to adequately account for earthquake excitation. The research summarizes a combined experimental and advanced numerical analysis. In particular, the experimental phase, which was briefly summarized, allows the evaluation of the key features of the response of isolated components as well as of the whole set of different specimens tested under push-over loads. The more than satisfactory agreement observed in the numerical simulations of test data confirms the adequacy of the Śiva FE software in modelling racks. In wider terms, the ways to the extensive numerical simulations, which are necessary to improve the seismic design rules for industrial storage racks, are opened by the evidence of the accuracy in the simulation of experimental overall behavior, based on single component test results.

## Chapter 7 References

- [1] N. Baldassino and R. Zandonini, "Design by testing of industrial racks," *Advanced Steel Construction*, vol. 7, no. 1, pp. 27-47, 2011.
- [2] EN15512 - Steel static storage systems - Adjustable pallet racking systems - Principles for structural design, Brussels: CEN, European Committee for Standardization, 2009.
- [3] FEM 10.2.08 - Recommendations for the design of static steel storage pallet racks in seismic conditions, Brussels: Federation Européenne de Manutention, 2010.
- [4] RMI MH16.1 - Specification for the Design, Testing and Utilization of Industrial Steel Storage Racks, Charlotte: Rack Manufactures Institute, 2008.
- [5] AS 4084 - Steel Storage Racking, Sydney: Australian Standards, 2012.
- [6] K. J. R. Rasmussen and B. P. Gilbert, "Analysis-based design provisions for steel storage racks," *Journal of Structural Engineering, ASCE*, vol. 139, pp. 849-859, 2013.
- [7] L. H. Teh, G. J. Hancock and M. J. Clarke, "Analysis and design of double sided high-rise steel pallet rack frames," *Journal of Structural Engineering*, vol. 130, pp. 1011-1021, 2004.
- [8] C. Bernuzzi, A. Gobetti, G. Gabbianelli and M. Simoncelli, "Unbraced pallet rack design in accordance with European practice. Part 1: selection of the method of analysis," *Thin-Walled Structures*, vol. 86, pp. 185-207, 2015.
- [9] C. Bernuzzi, A. Gobetti, G. Gabbianelli and M. Simoncelli, "Unbraced pallet rack design in accordance with European practice. Part 2: essential verification checks," *Thin-Walled Structures*, vol. 86, pp. 208-229, 2015.
- [10] C. Bernuzzi, A. Gobetti, G. Gabbianelli and M. Simoncelli, "Simplified approaches to design medium-rise unbraced steel storage pallet racks. I: elastic buckling analysis," *Journal of Structural Engineering (United States)*, vol. 141, no. 11, 2015.

## References

- [11] C. Bernuzzi, A. Gobetti, G. Gabbianelli and M. Simoncelli, "Simplified approaches to design medium-rise unbraced steel storage pallet racks. II: fundamental period estimates," *Journal of Structural Engineering (United States)*, vol. 141, no. 11, 2015.
- [12] EN16681 - Steel static storage systems - Adjustable pallet racking systems - Principles for seismic design, Brussels: CEN, European Committee for Standardization, 2016.
- [13] Eurocode 8 - Design of structures for earthquake resistance, Brussels: CEN, European Committee for Standardization, 2004.
- [14] Eurocode 3 - Design of steel structures - Part 1-1: general rules and rules for buildings, Brussels: CEN, European Committee for Standardization, 2004.
- [15] P. Fajfar, "A nonlinear analysis method for performance-based seismic design," *Earthquake Spectra*, vol. 16, no. 3, pp. 573-592, 2000.
- [16] Eurocode 3 - Design of steel structures - Part 1-3: general rules - supplementary rules for cold-formed members and sheeting, Brussels: CEN, Committee for Standardization, 2004.
- [17] C. Bernuzzi and C. A. Castiglioni, "Experimental analysis on the cyclic behaviour of beam-to-column joints in steel storage pallet racks," *Thin-Walled Structures*, vol. 39, no. 10, pp. 841-859, 2001.
- [18] A. Castellani and E. Faccioli, *Costruzioni in zona sismica*, Milano: Hoepli, 2007.
- [19] K. Adamakos and I. Vayas, "Estimation of the behavior factor of steel storage pallet racks," in *4th ECCOMAS thematic conference on computational methods in structural dynamics and earthquake engineering*, Kos Island, 2013.
- [20] C. A. Castiglioni, *Seisracks 2 - Seismic behavior of steel storage pallet racking systems*, Berlin: Springer, 2016.
- [21] A. Kanyilmaz, G. Brambilla, G. P. Chiarelli and C. A. Castiglioni, "Assessment of the seismic behaviour of braced steel storage racking systems by means of full scale pushover tests," *Thin-Walled Structures*, vol. 107, pp. 138-155, 2016.
- [22] C. Braham and H. Degèe, "Characterization of the seismic behavior of steel storage pallet racks in cross-aisle direction," in *Proceedings of the 9th international conference on structural dynamics, EURO DYN 2014*, Porto, Portugal, 2014.

- [23] W. McGuire, R. H. Gallagher and R. D. Ziemian, *Matrix Structural Analysis*, 2nd edition, Faculty Books, 2000.
- [24] J. S. Przemieniecki, *Theory of Matrix Structural Analysis*, New York: Dover Publications, INC, 1968.
- [25] W.-F. Chen and T. Atsuta, *Theory of Beam-Columns Volume 2: Space Behavior and Design*, New York: J. Ross Publishing, 2008.
- [26] S. P. Timoshenko and J. M. Gere, *Theory of elastic stability*, 2nd edition, New York: McGraw Hill, 1961.
- [27] V. Z. Vlasov, *Thin-walled elastic beams*, 2nd edition, Jerusalem: Israel program for scientific transactions, 1961.
- [28] H. Wagner, "Verdrehung und knickung von offenen profilen (Torsion and buckling of open sections)," *NACA Technical Memorandum No. 807*, Washington, DC, 1936.
- [29] S. Rajasekaran, *Finite element analysis of thin-walled members of open section*, Edmonton: PhD thesis, Department of Civil Engineering, University of Alberta, 1971.
- [30] G. Turkalj, J. Brnic and P.-O. Jasna, "Large rotation analysis of elastic thin-walled beam-type structures using ESA approach," *Computers and Structures*, vol. 81, pp. 1851-1864, 2003.
- [31] J.-M. Battini and C. Pacoste, "Co-rotational beam elements with warping effects in instability problems," *Computer methods in applied mechanics and engineering*, vol. 191, pp. 1755-1789, 2002.
- [32] J. M. Battini, "Co-rotational beam elements in instability problems," Technical report from Royal Institute of Technology Department of Mechanics, Stockholm, 2002.
- [33] G. M. Voros, "Free vibration of thin walled beams," *Periodica Polytechnica*, vol. 48, pp. 99-110, 2004.
- [34] B. W. Shafer, "Cold-formed steel structures around the world - A review of recent advances in applications, analysis and design," *Steel Construction*, vol. 4, no. 3, pp. 141-149, 2011.
- [35] W.-W. Yu and R. A. LaBoube, *Cold-formed steel design*, 4th Edition, New Jersey: John Wiley & Sons, 2010.

## References

- [36] A. Ghersi, R. Landolfo and F. M. Mazzolani, Design of metallic cold-formed thin-walled members, Milton Park: Spon Press, 2002.
- [37] C. Bernuzzi, A. Gobetti, G. Gabbianelli and M. Simoncelli, "Warping influence on the resistance of uprights on steel storage pallet racks," *Journal of Constructional Steel Research*, vol. 101, pp. 234-241, 2014.
- [38] Eurocode 3 - Design of steel structures - Part 1-8: design of joints, Brussels: CEN, Committee for Standardization, 2004.
- [39] K. Bathe and E. L. Wilson, Numerical methods in finite element analysis, New Jersey: Prentice-Hall, 1976.
- [40] D. Dubina, V. Ungureanu and R. Landolfo, Eurocode 3: Design of Steel Structures, Part 1-3 - Design of Cold-formed Steel Structures, Hoboken, NJ: Wiley-Blackwell, 2012.
- [41] T. Pekoz and G. Winter, "Cold-formed Steel Racks Structures," in *2nd International Specialty Conference on Cold-Formed Steel Structures*, St. Louis, MO, 1973.
- [42] C. Bernuzzi, G. Gabbianelli, A. Gobetti and A. Rosti, "Beam design for steel storage racks," *Journal of Constructional Steel Research*, vol. 116, pp. 156-172, 2016.
- [43] FEM 10.2.07 - The design of drive-in and drive-through racking, Hitchin, UK: FEM racking and shelving product group, 2011.
- [44] M. H. R. Godley, "The behavior of drive-in storage structures," in *16th International Specialty Conference on Cold-Formed Steel Structures*, Orlando, 2002.
- [45] A. M. S. Freitas, F. T. Souza and M. S. R. Freitas, "Analysis and behavior of steel storage drive-in racks," *Thin-Walled Structures*, vol. 48, no. 2, pp. 110-117, 2010.
- [46] B. P. Gilbert and K. J. R. Rasmussen, "Determination of accidental forklift truck impact forces on drive-in steel rack structures," *Engineering Structures*, vol. 33, no. 5, pp. 1403-1409, 2011.
- [47] B. P. Gilbert and K. J. R. Rasmussen, "Drive-in steel storage racks. I: stiffness tests and 3D load-transfer mechanisms," *Journal of Structural Engineering*, vol. 138, no. 2, pp. 135-147, 2012.

- [48] K. J. Bathe and E. L. Wilson, "NONSAP - Finite Element Calculation for Nonlinear Static and Dynamic Analysis of Complex Structures," Structural Engineering Laboratory, University of California, Berkeley, 1978.
- [49] Eurocode - Basis of structural design, Brussels: CEN, Committee for Standardization, 2008.
- [50] UNI EN 15620 - Steel static storage systems - Adjustable pallet racking - Tolerances, deformations and clearances, 2009.
- [51] F. D. Markazi, R. G. Beale and M. H. R. Godley, "Experimental analysis of semi-rigid boltless connectors," *Thin-Walled Structures*, vol. 138, no. 2, pp. 135-147, 1997.
- [52] K. Tilburgs, "Those peculiar structures in cold formed steel: racking and shelving," *Steel Construction*, vol. 6, no. 2, pp. 95-106, 2013.
- [53] Analysis and design of steel frames with semi-rigid joints, European Convention of Constructional Steelwork. Doc. n. 67, 1992.
- [54] C. Bernuzzi, A. Di Gioia, G. Gabbianelli and M. Simoncelli, "Pushover analyses of hand-loaded steel storage shelving racks," *Journal of Earthquake Engineering*, 2016.
- [55] FEM 10.2.06 - The design of hand loaded low rise steel static shelving, Hitchin, UK: FEM racking and shelving product group, 2012.
- [56] A. N. Trouncern and K. J. R. Rasmussen, "Flexural-torsional buckling of ultra light-gauge steel storage rack uprights," *Thin-Walled Structures*, vol. 81, pp. 159-174, 2014.
- [57] M. Paz, Structural dynamics, New York: Springer, 1985.
- [58] Abaqus FEA, Dassault Systemes, November 2014. [Online]. Available: [www.simulia.com](http://www.simulia.com).
- [59] N. Baldassino and C. Bernuzzi, "Analysis and behaviour of steel storage pallet racks," *Thin-Walled Structures*, vol. 37, no. 4, pp. 277-304, 2000.
- [60] N. Baldassino and R. Zandonini, "Numerical and experimental analysis on base-plate connections of steel storage pallet racks," in *XVIII Congress C.T.A.*, Venice, 2001.

## References

- [61] G. Gabbianelli, A. Kanyilmaz, C. Bernuzzi and C. A. Castiglioni, "A combined experimental-numerical study on unbraced pallet rack under pushover loads," *International Journal of Earthquake Engineering*, submitted.
- [62] F. Mohri, L. Azrar and M. Potier-Ferry, "Lateral post-buckling analysis of thin-walled open section beams," *Thin-Walled Structures*, vol. 40, pp. 1013-1036, 2002.
- [63] A. Prokic, R. Mandic and M. Vojnic-Purcar, "Influence of bimoment on the torsional and flexural-torsional elastic stability of thin-walled beams," *Thin-Walled Structures*, vol. 89, pp. 25-30, 2015.

## A. Appendix – Tests and Validations

The following tests have the aim to validate the developed software. Herein are reported simple cases, which are easily reproducible by the reader adopting both hand calculations and matrices exposed in 0. The following cases have been carry out with a lipped channel cross-section. All the properties are reported in the following table. For what concern the material properties has been choice an orthotropic elastic material with the following value: elastic modulus,  $E = 210000$  MPa, Poisson coefficient,  $\nu = 0.3$ .

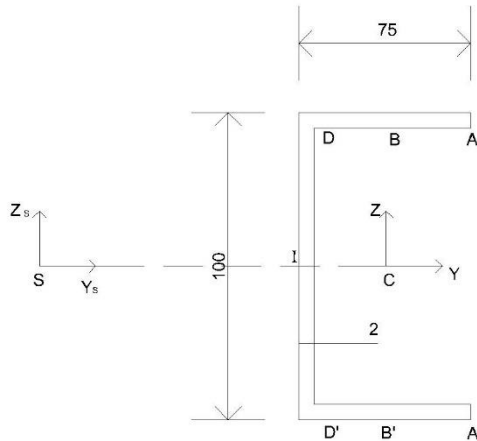


Figure 7-1. Section 1, C-section.

Geometric characteristic	
Height [mm], h:	100
Base [mm], b:	75
Thickness [mm], t:	2
Area [mm <sup>2</sup> ], A:	492
Moment of Inertia, [mm <sup>4</sup> ], I <sub>y</sub> :	867561.33
Moment of Inertia, [mm <sup>4</sup> ], I <sub>z</sub> :	296505.37

Torsional Constant, [mm <sup>4</sup> ], $I_x$ :	656
Warping Constant [mm <sup>6</sup> ], $I_w$ :	500233825.87
Shear center, y axis [mm], $y_s$ :	-52.57
Shear center, z axis [mm], $z_s$ :	0.0
Wagner coefficient, [mm <sup>2</sup> ], $\alpha_x$ :	5129.61
Wagner coefficient, [mm], $\alpha_y$ :	0.0
Wagner coefficient, [mm], $\alpha_z$ :	-144.74
Wagner coefficient, [mm <sup>-2</sup> ], $\alpha_\omega$ :	0.0

## A.1 Static analysis

The first step of the validation of the software concerns the static analysis. It is very easy to check the results because if the geometry of the structure is simple, it is possible to use theoretical formulas:

### Case 1: Torsion and distributed torsion

The key parameter governing the torsional member response is the torsional rotation  $\varphi_x(x)$ , which can be determined by solving a differential equation of the fourth order. In particular, the general solution is given by:

$$\varphi_x(x) = C_1 + C_2 \frac{x}{L} + C_3 \sinh \frac{\bar{k}}{L} x + C_4 \cosh \frac{\bar{k}}{L} x + \bar{\varphi}_x(x)$$

where the constants  $C_1 - C_4$  depend on the boundary conditions, meanwhile  $\bar{\varphi}_x(x)$  is related to the load condition and expresses the rotation due to uniformly distributed applied torsion and  $\bar{k}$  is the relative torsional rigidity defined as  $\bar{k} = L\sqrt{GI_t/EI_w}$ . It should be noted that other parameters governing design are obtained from the derivatives of the torsion angle  $\varphi_x(x)$  and, in particular:

- the pure torsion moment,  $T_t(x) = GI_t \dot{\varphi}_x(x)$ , where  $\dot{\varphi}_x(x)$  is defined as:

$$\dot{\varphi}_x(x) = -\theta(x) = \frac{C_2}{L} + C_3 \frac{\bar{k}}{L} \cosh \frac{\bar{k}}{L} x + C_4 \frac{\bar{k}}{L} \sinh \frac{\bar{k}}{L} x + \dot{\bar{\varphi}}_x(x)$$

- the bimoment  $B(x) = EI_w \ddot{\varphi}_x(x)$ , where  $\ddot{\varphi}_x(x)$  is defined as:

$$\ddot{\varphi}_x(x) = C_3 \sinh \frac{\bar{k}}{L} x + C_4 \cosh \frac{\bar{k}}{L} x + \frac{L^2}{\bar{k}^2} \ddot{\bar{\varphi}}_x(x)$$

- the warping (non-uniform torsion) moment  $T_w(x) = -EI_w\ddot{\varphi}_x(x)$ , where  $\ddot{\varphi}_x(x)$  is expressed as:

$$\ddot{\varphi}_x(x) = C_3 \frac{\bar{k}}{L} \cosh \frac{\bar{k}}{L} x + C_4 \frac{\bar{k}}{L} \sinh \frac{\bar{k}}{L} x + \frac{L^2}{\bar{k}^2} \ddot{\varphi}_x(x)$$

In the following, the main results of hand calculations are provided schematically.

*Cantilever in beam torsion:*

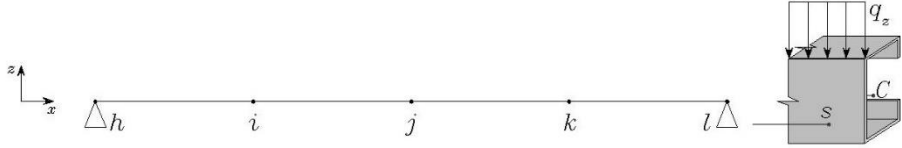


The torsional moment applied at the free end is  $\bar{M}_t = 0.01 \text{ kNm} = 10000 \text{ Nm}$ . The boundary condition associated with the applied loads are:  $\bar{\varphi}_x(x) = 0$ ,  $\varphi_x(0) = 0$ ,  $\dot{\varphi}_x(0) = 0$ ,  $B(L) = 0$  and  $M_t(L) = 10000 \text{ Nm}$ . Main numerical values are reported in the following table.

	L=0.75m	L=1.00m	L=1.25m
$\bar{\varphi}_x(x) = -\frac{\bar{m}_t z^2}{2 GI_t}$	0	0	0
$\bar{k} = L \sqrt{\frac{GI_t}{EI_w}}$	0.533	0.710	0.888
$C_2 = \frac{\bar{M}_t}{GI_t} L$	0.142	0.189	0.236
$C_3 = -\frac{C_2}{\bar{k}}$	-0.266	-0.266	-2.266
$C_4 = -C_3 \frac{\sinh \bar{k}}{\cosh \bar{k}}$	0.130	0.162	0.189
$C_1 = -C_4$	-0.130	-0.162	-0.189
$\varphi_x$ at the free end	0.69°	1.51°	2.70°
$\delta_z = y_G \varphi_x$	0.63 mm	1.39 mm	2.48 mm
Value obtained via 7DOFs FEM formulation			
$\varphi_x^{FEM} \left( \frac{\varphi_x}{\varphi_x^{FEM}} \right)$ at the free end	0.69° (1.00)	1.51° (1.00)	2.70° (1.00)
$\delta_z^{FEM} \left( \frac{\delta_z}{\delta_z^{FEM}} \right)$ at the free end	0.63 mm (1.00)	1.39 mm (1.00)	2.48 mm (1.00)

## Appendix – Tests and Validations

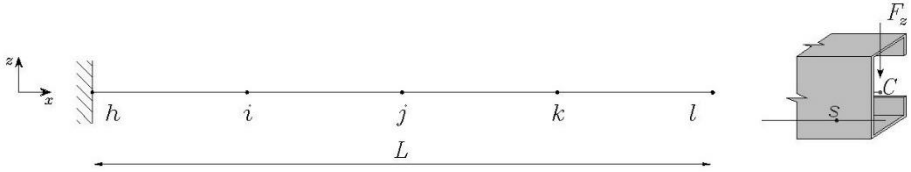
Simply supported beam under gravity loads:



A distributed load equal to  $q_z = -15$  N/mm is applied in the centroid, then we obtain a distributed torsional moment equal to  $\bar{m}_t = -788.6$  Nmm/mm. In the following table, key data are reported related to the hand calculations and finite element analysis.

	L=0.75m	L=1.00m	L=1.25m
$\bar{\varphi}_x(x) = -\frac{\bar{m}_t z^2}{2 GI_t}$	1.046	1.860	2.907
$\bar{k} = L \sqrt{\frac{GI_t}{EI_w}}$	0.533	0.710	0.888
$C_2 = \frac{\bar{m}_t L^2}{2GI_t}$	-4.186	-7.441	-11.627
$C_3 = \frac{\bar{m}_t L^2}{GI_t \bar{k}^2} \left( \frac{1}{\sinh \bar{k}} - \frac{\cosh \bar{k}}{\sinh \bar{k}} \right)$	7.678	10.059	12.300
$C_4 = \frac{\bar{m}_t L^2}{GI_t \bar{k}^2}$	-29.507	-29.507	-29.507
$C_1 = -C_4$	29.507	29.507	29.507
$\varphi_x$ at the mid-span	-1.72°	-5.33°	-12.66°
$\delta_z = \frac{5q_z L^4}{384EI_y} + y_o \varphi_x$	-1.92 mm	-5.96 mm	-14.23 mm
Value obtained via 7DOFs FEM formulation			
$\varphi_x^{FEM} \left( \frac{\varphi_x}{\varphi_x^{FEM}} \right)$ at the mid span	-1.72° (1.00)	-5.33°(1.00)	-12.66°(1.00)
$\delta_z^{FEM} \left( \frac{\delta_z}{\delta_z^{FEM}} \right)$ at the mid span	-1.92 mm (1.00)	-5.96 mm (1.00)	-14.23 mm (1.00)

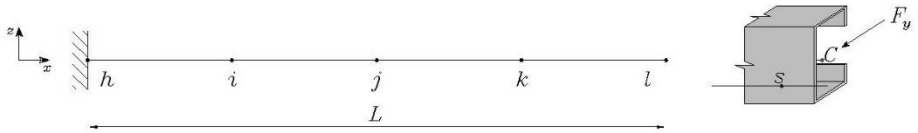
**Case 2: Cantilever with a shear force (along z)**



	L=0.75m	L=1.00m	L=1.25m
$F_z$ [N]	-1000	-1000	-1000
$\bar{\varphi}_x(x) = -\frac{\bar{m}_t z^2}{2 GI_t}$	0	0	0
$\bar{k} = L \sqrt{\frac{GI_t}{EI_w}}$	0.533	0.710	0.888
$C_2 = \frac{\bar{M}_t}{GI_t} L$	-0.744	-0.992	-1.240
$C_3 = -\frac{C_2}{\bar{k}}$	1.397	1.397	1.397
$C_4 = -C_3 \frac{\sinh \bar{k}}{\cosh \bar{k}}$	-0.681	-0.853	-0.992
$C_1 = -C_4$	0.681	0.853	0.992
$\varphi_x$ at the free end	-3.62°	-7.96°	-14.21°
$\delta_z = \frac{F_z L^3}{3EI_y} - y_S \varphi_x$	-4.09 mm	-9.13 mm	-16.61 mm
Value obtained via 7DOFs FEM formulation			
$\varphi_x^{FEM} \left( \frac{\varphi_x}{\varphi_x^{FEM}} \right)$ at the free end	-3.62° (1.00)	-7.96° (1.00)	-14.21° (1.00)
$\delta_z^{FEM} \left( \frac{\delta_z}{\delta_z^{FEM}} \right)$ at the free end	-4.09 mm (1.00)	-9.13 mm (1.00)	-16.61 mm (1.00)

Appendix – Tests and Validations

**Case 3: Cantilever with a shear force (along y)**



	L=0.75m	L=1.00m	L=1.25m
$F_y$ [N]	-1000	-1000	-1000
$\delta_y = \frac{F_y L^3}{3EI_z}$	-2.26 mm	-5.35 mm	-10.46 mm
Value obtained via 7DOFs FEM formulation			
$\delta_y^{FEM} \left( \frac{\delta_y}{\delta_y^{FEM}} \right)$ at the free end	-2.26 mm (1.00)	-5.35 mm (1.00)	-10.46 mm (1.00)

## A.2 Buckling analysis

### Case 1: Flexural-torsional buckling

Adopting the classic formulas of the instability theory, for a beam-column under compression and fixed at one end, we have:

$$N_{cr,y} = \frac{\pi^2 \cdot E \cdot I_y}{L_0^2}; \quad N_{cr,z} = \frac{\pi^2 \cdot E \cdot I_z}{L_0^2}; \quad N_{cr,x} = \frac{A \cdot G \cdot I_x}{I_c} \cdot \left( 1 + \pi^2 \cdot \frac{G \cdot I_x}{E \cdot I_w \cdot L_0^2} \right);$$

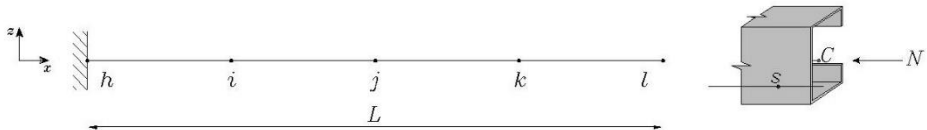
$$N_{cr,FT} = \frac{K}{2} \cdot \left[ N_{cr,y} + N_{cr,x} - \sqrt{(N_{cr,y} + N_{cr,x})^2 - 4 \cdot \frac{N_{cr,y} \cdot N_{cr,x}}{K}} \right]$$

Where:

$$I_G = I_y + I_z; \quad I_C = I_G + A \cdot y_S^2; \quad K = \frac{I_C}{I_G}$$

And for this particular case (cantilever):

$$L_0 = 2L$$

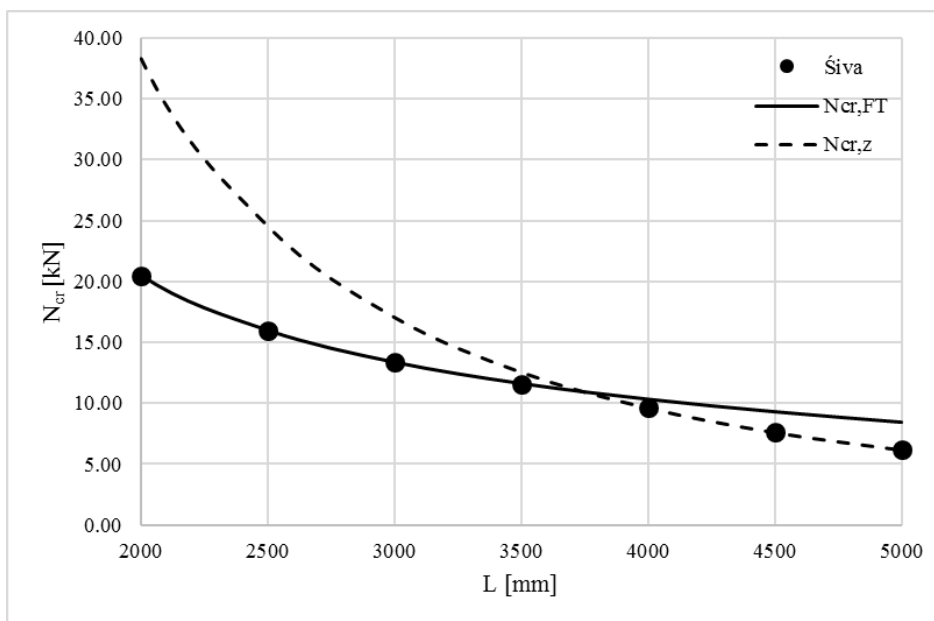


L [mm]	Theory [kN]		Siva [kN]	
500	$N_{cr,FT}$	199.09	1 <sup>st</sup> eigenvalue	199.09
	$N_{cr,z}$	614.54	2 <sup>nd</sup> eigenvalue	614.54
1000	$N_{cr,FT}$	56.49	1 <sup>st</sup> eigenvalue	56.49
	$N_{cr,z}$	153.64	2 <sup>nd</sup> eigenvalue	153.64
2500	$N_{cr,FT}$	15.96	1 <sup>st</sup> eigenvalue	15.96

## Appendix – Tests and Validations

	$N_{cr,z}$	24.58	2 <sup>nd</sup> eigenvalue	24.58
5000	$N_{cr,z}$	6.15	1 <sup>st</sup> eigenvalue	8.39
	$N_{cr,FT}$	8.39	2 <sup>nd</sup> eigenvalue	6.15

In the following figure a comparison of the flexural-torsional buckling and the flexural buckling between the first eigenvalue calculated from Šiva.



**Case 2: Elastic critical moment (about y)**

Herein the elastic critical moment formula, where  $C_1 - C_3$  are coefficients depending from the boundary and load conditions,  $k_x$  and  $k_w$  are the coefficients of effective length,  $z_g$  is the distance between the load location and the shear center,  $z_j$  is a Wagner coefficient and  $L_{0,z}$  is the effective length.

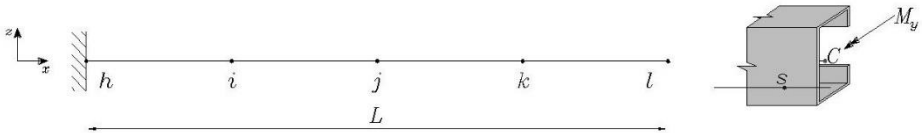
$$M_{cr} = C_1 \cdot \frac{\pi^2 \cdot E \cdot I_z}{(k_z \cdot L_{0,z})^2} \cdot \left[ \sqrt{\left(\frac{k_x}{k_w}\right)^2 \cdot \frac{I_w}{I_z} + \frac{(k_x \cdot L_{0,z})^2 \cdot G \cdot I_x}{\pi^2 \cdot E \cdot I_z} + (C_2 \cdot z_g - C_3 \cdot z_j)^2} - (C_2 \cdot z_g - C_3 \cdot z_j) \right]$$

Where:

$$C_1 = 1; \quad C_2 = 0; \quad C_3 = 1; \quad k_x = 1; \quad k_w = 1; \quad z_g = 0; \quad z_j = 0; \quad L_{0,z} = 2L$$

With:

$$z_j = z_s - 0.5 \frac{\int_A (y^2 + z^2) z dA}{I_y}$$



L [mm]	Theory [kNm]	Šiva [kNm]
500	25.88	25.88
1000	6.93	6.93
2500	1.52	1.52
5000	0.62	0.62

For symmetry, applying the moment in the positive direction we will have the same results.

Appendix – Tests and Validations

**Case 3: Elastic critical moment (about z) – Negative moment**

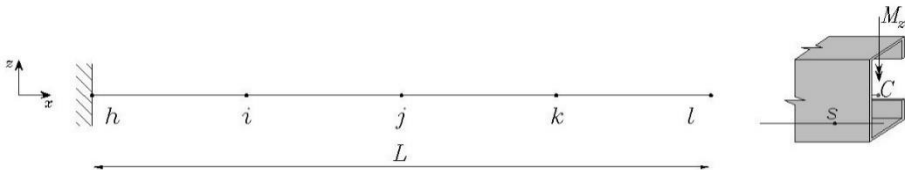
$$M_{cr} = C_1 \cdot \frac{\pi^2 \cdot E \cdot I_y}{(k_z \cdot L_{0,z})^2} \cdot \left[ \sqrt{\left(\frac{k_x}{k_w}\right)^2 \cdot \frac{I_w}{I_y} + \frac{(k_x \cdot L_{0,y})^2 \cdot G \cdot I_x}{\pi^2 \cdot E \cdot I_y} + (C_2 \cdot y_g - C_3 \cdot y_j)^2} - (C_2 \cdot y_g - C_3 \cdot y_j) \right]$$

Where:

$$C_1 = 1; \quad C_2 = 0; \quad C_3 = 1; \quad k_x = 1; \quad k_w = 1; \quad y_g = 0; \quad y_j = 72.37; \quad L_{0,y} = 2L$$

With:

$$y_j = 0.5 \frac{\int_A (y^2 + z^2) y dA}{I_z} - y_s$$



L [mm]	Theory [kNm]	Śiva [kNm]
500	267.58	267.59
1000	67.15	67.16
2500	11.03	11.06
5000	2.98	2.98

**Case 4: Elastic critical moment (about z) – Positive moment**

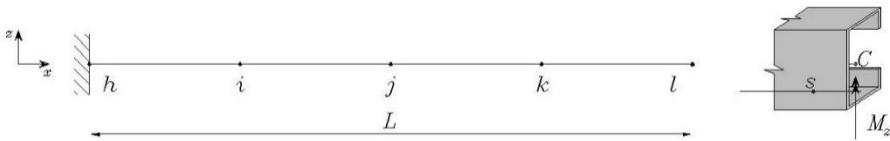
$$M_{cr} = C_1 \cdot \frac{\pi^2 \cdot E \cdot I_y}{(k_z \cdot L_{0,z})^2} \cdot \left[ \sqrt{\left(\frac{k_x}{k_w}\right)^2 \cdot \frac{I_w}{I_y} + \frac{(k_x \cdot L_{0,y})^2 \cdot G \cdot I_x}{\pi^2 \cdot E \cdot I_y} + (C_2 \cdot y_g - C_3 \cdot y_j)^2} - (C_2 \cdot y_g - C_3 \cdot y_j) \right]$$

Where:

$$C_1 = 1; \quad C_2 = 0; \quad C_3 = 1; \quad k_x = 1; \quad k_w = 1; \quad y_g = 0; \quad y_j = -72.37; \quad L_{0,y} = 2L$$

With:

$$y_j = y_s - 0.5 \frac{\int_A (y^2 + z^2) y dA}{I_z}$$

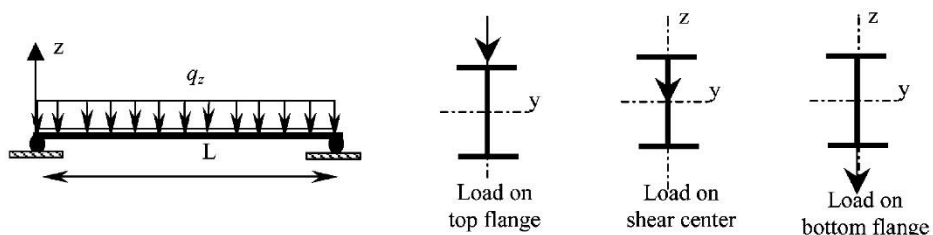


L [mm]	Theory [kNm]	Śiva [kNm]
500	7.32	7.32
1000	2.09	2.09
2500	0.62	0.62
5000	0.38	0.38

## Appendix – Tests and Validations

### *Mohri et al.*

Reference to [62] can be made. The paper aim to the study of the nonlinear behavior of thin-walled beam with open sections. The authors developed a nonlinear model where the governing coupled equilibrium equations obtained from Galerkin's method are solved by a Newthon-Raphson iterative process. They performed also some comparisons with the solutions commonly used in linear stability, which is the same performed by *Śiva* software.



IPE300		Mohri et al.		
	Numeric	Analytic (66)	Analytic (EC3)	Śiva
Load on top flange	73.0	72.82	70.75	71.35
Load on shear center	98.2	97.82	94.07	94.81
Load on bottom flange	132.2	131.42	125.06	125.87

HEA200		Mohri et al.		
	Numeric	Analytic (66)	Analytic (EC3)	Śiva
Load on top flange	119.5	119.5	101.77	103.61
Load on shear center	169.6	170.09	134.47	135.12
Load on bottom flange	240.5	241.33	177.68	176.07

Śiva perfectly match the linear elastic results. As already mentioned, to match the numeric and analytic results from the article, it is necessary to develop a formulation able to predict large displacements and rotations.

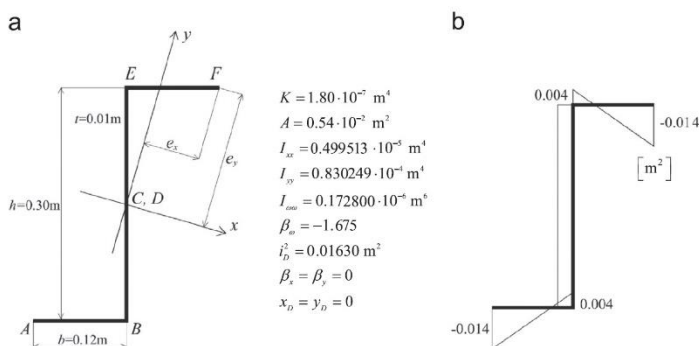
## Appendix – Tests and Validations

### Prokic

Reference to [63] can be made. The article studies the influence of the bimoment on the buckling of thin-walled beams with open cross-section subjected to axial load. In the case of thin-walled Z-section beam, it is shown that influence of the bimoment could be of importance in the assessment of buckling loads. In order to verify the accuracy and validity of the analysis, the obtained results are compared with those calculated by ANSYS software.

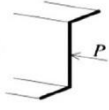
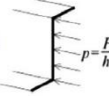
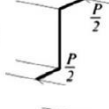
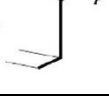
The example reported is a simply supported beam subjected to an eccentric compressive force  $N = -P$  at both ends. The internal forces produced by the axial force are:  $M_y = -Ne_z$ ,  $M_z = -Ne_y$  and  $B = -N\omega_p$ , where  $e_y$  and  $e_z$  are the eccentricities of the loading point and  $\omega_p$  is the value of the sectorial coordinates in the loading point.

The article proposes four different case, comparing a FE solution from ANSYS, adopting shell elements (4-node SHELL181), and a closed form solution, obtained approximating the bimoment distribution  $\lambda(x)$  with a constant value  $\lambda_m$ . As a consequence, the solutions proposed by Prokic et al. will be a little different from the real solution. In Siva is possible to apply at the ends of the beam a bimoment, which for each case will be calculated in order to repeat the examples proposed in the article. In the following figure (from [63]) we can find the section adopted for the example with his properties (a), and also the value of the sectorial coordinates in each point (b).



In the first three load cases, the beam is subjected to a centric compression force and a pure torsional buckling may occur, but the different bimoments are generated depending on the end load distributions. In the following table, the critical loads for the first torsional (load cases 1 to 3) and lowest flexural-torsional (load case 4) buckling modes are calculated.

Appendix – Tests and Validations

Case	L = 4.0 m			L = 6.0 m			L = 8.0 m		
	Ansys	Theory $\lambda = \lambda_m$ $\lambda = 0$	Śiva	Ansys	Theory $\lambda = \lambda_m$ $\lambda = 0$	Śiva	Ansys	Theory $\lambda = \lambda_m$ $\lambda = 0$	Śiva
1 	3.5366	3.1320 2.2652	3.307	2.1214	1.8939 1.5023	2.032	1.6273	1.4711 1.2352	1.583
2 	3.4203	3.1320 2.2652	3.307	2.0733	1.8939 1.5023	2.032	1.6010	1.4711 1.2352	1.583
3 	1.0513	1.1504 2.2652	1.074	0.7661	0.8712 1.5023	0.776	0.6718	0.7912 1.2352	0.677
4 	0.3987	0.4162 0.4414	0.411	0.2039	0.2119 0.2172	0.209	0.1257	0.1304 0.1318	0.129

As we can see, Śiva is more accurate than the theory proposed by Prokic et al. accomplishing better the results from Ansys. Because it is not possible to apply a distributed load in beam element, the load P is always applied in the centroid, meanwhile the value of bimoment is different for each case, being a function of the position of the load P. As a consequence, the analyses in Śiva for the first and second case are the same.

Case	$P$ [kN]	$\omega_p$ [m <sup>2</sup> ]	$M_y$ [kNm]	$M_z$ [kNm]	$B$ [kNm <sup>2</sup> ]
1	-1000	0.004	0	0	-4
2	-1000	0.004	0	0	-4
3	-1000	-0.0014	0	0	1.4
4	-1000	-0.0014	-178.3	71.5	1.4